Mississippi State University
Scholars Junction

Theses and Dissertations | Theses and Dissertations

1-1-2013

Conventional Pavements and Perpetual Pavements: A Rational and Empirical Approach

Wenqi Wang

Follow this and additional works at: https://scholarsjunction.msstate.edu/td

Recommended Citation
Wang, Wenqi, "Conventional Pavements and Perpetual Pavements: A Rational and Empirical Approach" (2013). *Theses and Dissertations*. 1183.
https://scholarsjunction.msstate.edu/td/1183

This Dissertation - Open Access is brought to you for free and open access by the Theses and Dissertations at Scholars Junction. It has been accepted for inclusion in Theses and Dissertations by an authorized administrator of Scholars Junction. For more information, please contact scholcomm@msstate.libanswers.com.

www.manaraa.com

Conventional pavements and perpetual pavements: a rational and empirical approach

By

Wenqi Wang

A Dissertation
Submitted to the Faculty of
Mississippi State University
in Partial Fulfillment of the Requirements
for the Degree of Doctor of Philosophy
in Civil and Environmental Engineering
in the Department of Civil and Environmental Engineering

Mississippi State, Mississippi

December 2013

www.manaraa.com

Copyright by

Wenqi Wang

2013

www.manaraa.com

Conventional pavements and perpetual pavements: a rational and empirical approach

By

Wenqi Wang

Approved:

_____

Thomas D. White
(Major Professor)

_____

Edward B. Allen
(Minor Professor)

_____

Thomas E. Lacy
(Committee Member)

_____

William H. McAnally
(Committee Member)

_____

James L. Martin
(Graduate Coordinator)

_____

Achille Messac
Dean
James Worth Bagley College of Engineering

www.manaraa.com

Name: Wenqi Wang

Date of Degree: December 14, 2013

Institution: Mississippi State University

Major Field: Civil and Environmental Engineering

Major Professor: Thomas D. White

Title of Study: Conventional pavements and perpetual pavements: a rational and empirical approach

Pages in Study: 153

Candidate for Degree of Doctor of Philosophy

A study has been conducted to compare conventional pavements and perpetual pavements with a particular emphasis on perpetual pavements. One of the main drawbacks of conventional pavements and motivations for this work is the maintenance required for hot mix asphalt (HMA) pavements with sub-drainage systems. Perpetual pavements, as the name suggests, are designed with a long life. However, this is a relatively new concept and there are still many unknowns concerning their performance. This dissertation was written to answer some of the questions. The study examines structural response and performance of perpetual pavements. Also, deterioration and performance of perpetual pavements will be contrasted to conventional pavements.

Empirical data from the National Center of Asphalt Technology (NCAT) Test Track study was obtained, analyzed and used as a basis for evaluating theoretical models. Computational models for both conventional and perpetual pavements were constructed and analyzed using the general purpose finite element analysis software ABAQUS. Geometry, materials and loading are modeled with sufficient accuracy. This research examined several types of responses of perpetual pavements. It extends the traditional

www.manaraa.com

criteria of pavement distress by suggesting that longitudinal strain at the surface of a pavement HMA layer as an important criterion. Shear strain was studied and it provides a reasonable explanation of some distresses in pavements. By studying the FEA results from conventional and perpetual pavements and a thorough investigation of the thickness effects, it provides some rationale on why strain at the top of thick pavements is critical. The effects of dynamic wheel loadings are presented. Finally, the effect of environment, specifically temperature and moisture, on perpetual pavements are studied.

www.manaraa.com

DEDICATION

TO THE YEARS IN GRADUATE SCHOOL

Marooned,
At maroon and white?
Researched,
In the lab or labyrinth?

Materials and files,
Everything just piles.
Wood, gravel, asphalt,
Nature's gifts!

To build a house,
Enclosing our dream.
To construct a road,
Connecting to the sky!

Chapel, pond and lake,
Only appearances?
Yellow and green,
Ginkgo's falling leaves!

Fast, medium, slow,
A rhythmic moving.
Time and space,
Which one is dancing?

Spring, summer, fall,
Spring, summer, fall,
The truth, the good,
And the beautiful!

--Written in a midsummer night, August 2013

www.manaraa.com

ACKNOWLEDGEMENTS

Another Mississippi summer is quietly walking away. This one seems not so special when taking a quick look at heaven and earth. The Summer Triangle is still shining in the night sky. The squirrels are running on the ground. They still outnumber the people on campus. However, I definitely feel a little different inside because my graduate studies are close to the end of the *tunnel*. Although roads turned out to be my research topic in this study by pure accident, this also seems a kind of necessity. Roads, we all take them for granted and use them every day. There are really no mystic in them. But, the Chinese for "road" or "way" is "Dao (道)", which also means "the Eternal Truth" or "the Way", "the unnamable process of the universe" in Chinese philosophy (as shown in the book Daodejing). Therefore, I would also like to view the studies as a *path* toward Dao. I remember over this long process what I've asked myself the most is what do I *know?* What did I learn? These questions are quite silly because I finally found I could not give a satisfactory answer. But I feel an urge to give an answer so that my studying ends well. "All is well that ends well."

One thing I learned and felt strongly is Pascal's thought that "Man is but a reed, the weakest thing in nature." Although he didn't forget to make it more optimistic and added "but he is a thinking reed," this "thinking" part sometimes does not help much. So many thinking reeds and also the manmade structures (buildings, bridges, roads, etc) created by thinking reeds have been destroyed by major natural disasters in recent years.

www.manaraa.com

The earthquakes in Sichuan (08), Sumatra (09), Haiti (10), Chile (10), Yushu (10), Tohoku (11), Lushan (13) were all so powerful, with magnitudes from 6.9-9.0 and numbers of deaths from hundreds to hundreds of thousands. During the above events, I only shed some *alligator* tears because they are too far removed from me. However, everyone gets a *probability*. The super powerful tornado outbreak in April 2011 really "struck home." I experienced the primitive state of nature where there was no electricity and internet. Also, people all fought for food in grocery stores. Nobody knew what happened. Many hours later, it turned out that in the towns nearby many houses and people were flattened in a second.

Just so simple, we are quite vulnerable. A graduate student is as vulnerable as everyone else, if not more so. However, another thing I learned is that some reeds are *thicker* and therefore *stiffer.* We cannot control the vulnerability, but we can grow our *strength and flexibility.* As a student, one of the obligations is to become a better reed. I just feel that although I am still a quite feeble reed, I am *stronger, stiffer* and hopefully also have better *plasticity* under extreme winds.

Despite this vulnerability and growing strong, I feel blessed that I can manage to finish my studies under many people's kind help.

First, I would like to thank my thesis advisor Dr. Thomas White's trust, guidance, and support in many aspects both in and out of the research. His patience, confidence and expertise all left a good impression on me.

Next, my committee members Dr. McAnally, Dr. Lacy, Dr. Allen have all been quite helpful. I thank you all for your support in my research.

www.manaraa.com

At the beginning of the research, I also received much valuable assistance on modeling from David, Clemence, and Youssef from CAVS.

Special thanks go to Dr. Truax's kind support and also to many other friends, professors and staff in and out of the Department of Civil and Environmental Engineering.

Last but not least, I am indebted to my parents who always show the greatest love and encouragement.

www.manaraa.com

TABLE OF CONTENTS

www.manaraa.com

www.manaraa.com

www.manaraa.com

LIST OF TABLES

www.manaraa.com

LIST OF FIGURES

www.manaraa.com

www.manaraa.com

www.manaraa.com

www.manaraa.com

www.manaraa.com

www.manaraa.com

www.manaraa.com

CHAPTER I

INTRODUCTION

1.1 Problem Statement

Around 95% of all the paved roads in the United States are surfaced with hot mixed asphalt (HMA). In the past 50 to 60 years, there has been a dramatic increase in traffic by all types of vehicles. The road network, which has not significantly expanded since 1960, is now carrying over four times the number of vehicles at the beginning of this period (WAPA 2010). See Figure 1.1.

Moreover, the traffic increase will be greater in cities or megacities due to the fast pace of urbanization in the United States and around the world. In 2010, 80.7% of Americans lived in urban areas (Lambert 2012). The world population hit 7 billion in 2011 and is likely to reach 9 billion by 2050. At that time, 70% of the world's population will be urban (Wilson 2012).

This large increase in traffic and heavy use of roads in urban areas remains a great challenge to pavement design practice in terms of sustainability and serviceability.

www.manaraa.com

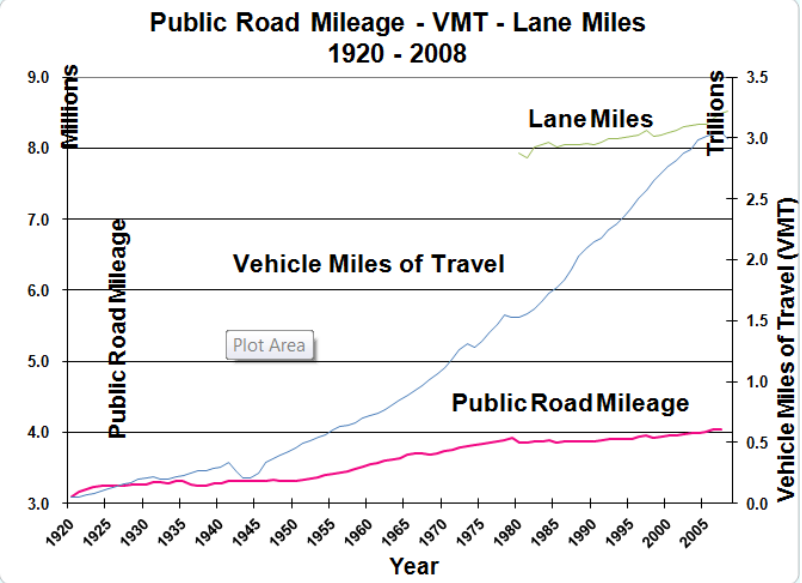

Figure 1.1 Public road mileage and the road use

Besides traffic load and volume, moisture is a major concern in flexible pavement design because moisture affects the strength of pavement layers and its foundation. In pavement design, there are two features that can reduce *water infiltration* and the level, extent and duration of *internal moisture* in pavement structures and their foundation. *Transverse pavement slope* is incorporated to ensure positive surface drainage and to minimize water infiltration. *Subsurface drainage systems* in conventional flexible pavements (abbreviated as "conventional pavements" herein) drains internal moisture accumulated by surface infiltration and migration from the sides and below. When internal moisture is reduced, the materials of the pavements layers and foundation are stiffer and have higher shear strength, thus enhancing pavement performance.

However, long term pavement system performance requires regular inspection and maintenance of subsurface drainage systems. The Mississippi Department of

www.manaraa.com

Transportation (MDOT) considers these activities to be time and cost consuming. As a result, consideration is being given to the concept of perpetual pavements (aka, long-life pavements, LLPs). A perpetual pavement is a full-depth pavement with layers designed to perform specific functions. A perpetual pavement usually has a larger total hot mix asphalt concrete (HMA, aka, asphalt concrete, AC) thickness. It is supposed that the bottom tensile strain is within an endurance limit so that bottom-up fatigue cracking is greatly mitigated. Instead, top-down cracking is expected to occur in perpetual pavements. This is considered an advantage because only surface maintenance is needed and it could be carried out in time to prevent major structural deterioration. No research has compared the performance of conventional pavements and perpetual pavements. A goal of this research is to conduct such analysis and facilitate a better understanding of the structural responses and performance of perpetual pavements. Also, the deformation mechanisms and critical locations for perpetual pavements might differ from those for conventional pavements. This research also intends to examine the response of perpetual pavements in detail and to provide insights into the concept of perpetual pavements.

1.2 Research Objectives and Methods

To realize the goal of gaining insights into the responses, performances and concept of perpetual pavements, specific objectives of this research include:

- Examine in detail the orientation and distribution of perpetual pavement responses under wheel loadings
- Identify the similarities and differences in the responses of conventional and perpetual pavements
- Investigate the effect of thickness, wheel paths, and dynamic loading

www.manaraa.com

- Investigate the climatic effects (temperature and moisture)

The research methods and tasks are listed below:

- Summarize current development in the research of perpetual pavement testing and modeling
- Study the NCAT Test Track and the experimental data of pavement structural responses collected
- Build finite element (FE) models for conventional pavements and perpetual pavements
- Validate the theoretical results with data from test sections at the NCAT that incorporate instrumentation to measure strains

1.3 Scope and Outlines

In Chapter 2, the evolution of roads and modern pavement design method are discussed in a historic point of view. The advantage of the finite element method for pavement analysis and also two approaches to pavement performance are discussed.

In Chapter 3, the mechanics and materials for flexible pavement are described in detail. This chapter provides a theoretical foundation for the pavement modeling and analysis.

Chapter 4 summarizes the NCAT Test Track structural study. The Phase III of the NCAT Test Track structural study is discussed in detail. Also the instrumentation, truck axial configuration and typical strain data are presented.

www.manaraa.com

FE models which include fair representations of pavement geometry, actual loads, and material models will be developed for both conventional and perpetual pavements in Chapter 5.

In Chapter 6, test section data will be used to validate the FE models. Subsequently, the models are used to extend the analyses. Theoretical pavement responses are studied in detail for perpetual pavements. The similarity and difference between two types of pavements are presented. In addition to the effects of thickness, wheel path, and dynamic loadings, temperature and moisture effects will be examined. Based on the research, recommendations will be made on the relative performance of conventional and perpetual pavements.

www.manaraa.com

CHAPTER II

LITERATURE REVIEW

2.1 The Evolution of Roads: Ancient to Modern

Roads are mainly built for military, trading and communication purposes. Built roads reflect the technology at a certain historic time. It is not exaggerated to say that the Romans already mastered the essentials of road building thousands of years ago. The roads in Rome were designed with many different layers and an efficient drainage system. Some have been used for thousands of years across medieval times all the way to today. The technology did not change much until the complex needs in modern ages produced new challenges to road design and construction.

2.1.1 Early Development of Road Network

"All roads lead to Rome." (de Lille 1175) This proverb indicates the focus of roads in the Roman Empire. Rome, once the capital (until 286 AD) of the empire, was the center of classical and Christian civilization. A map of the Roman road network and a cross section of a typical Roman road can be seen in Figure 2.1. Roman roads are a great example of engineered products in ancient times. After thousands of years, ancient Roman roads can still be seen nowadays in many countries, for example, the United Kingdom (UK), France, and German as well as Italy.

www.manaraa.com

Figure 2.1 The network and a section of Roman roads [1]

Ancient China also had large scale road construction and development. As early as the Zhou Dynasty (1046–256 BC), the imperial city's planning follow a certain rules. The roads were divided into urban and rural ones. Specifically, in the urban area (inner city), the roads have nine perfect north-south lines (nearly 50 feet wide for each line), nine west-east lines, and some "rings" to enclose these grids. In the rural areas, the roads were divided into five levels. Different levels of roads were maintained by different government entities. During the Qin Dynasty (221-206 BCE), the vehicle track width and road width were standardized. This facilitated a national road network. "Under Emperor Shihuangdi about 220 BC, China had a road system that paralleled the Persian Royal Road and the Roman road network in time and purpose. Many of the roads were wide, surfaced with stone, and lined with trees. Steep mountains were traversed by stone-paved stairways with broad treads and low steps." (Imperial 2012)

[1] http://historylink102.com/Rome/roman-roads.html

www.manaraa.com

The plank roads, which consisted of wooden planks supported on timbers inserted into the sides of cliffs, were also widely used in ancient China to travel through remote mountain areas. See Figure below.

Figure 2.2 The ancient plank roads in China [2]

According to the Greek Historian Herodotus, The Persian Empire's royal roads were constructed in the Achaemenid Dynasty (550-330 BC). It connected the capital of Lydia, Sardes (current Sart in Turkey), and the capitals of the Achaemenid empire, Susa and Persepolis (current Shush and Shiraz in Iran). See Figure below.

[2] http://www.bbkz.com/forum/gallery/index.php?n=57175

www.manaraa.com

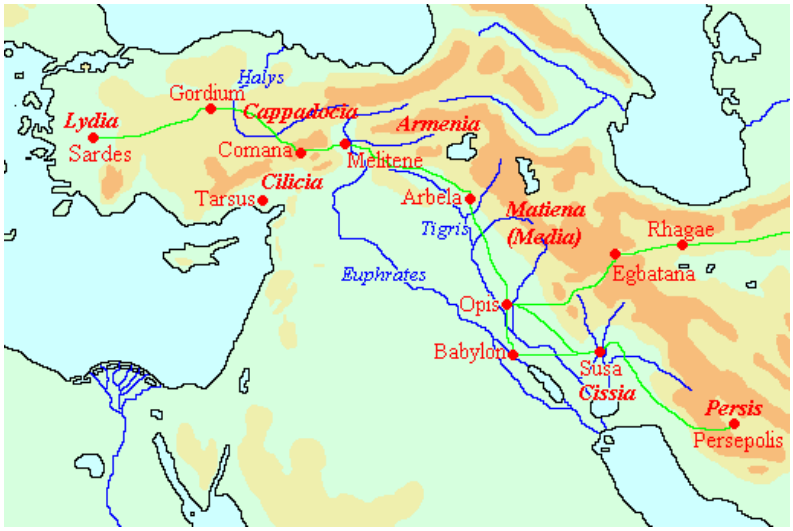

Figure 2.3 Persian's royal roads network [3]

Whereas the ancient Roman, Chinese and Persian roads were built partly for military purposes, the most important historical network of roads was the trade routes across the Afro-Eurasian landmass, i.e., the Silk Road. (Figure 2.4) This road network is a significant example of human drive to communicate and trade. "Along the Silk Road travelled the teachings of Buddha, Mohammed and Christ, and the caravans which exchanged precious metals for silks." (Hoppen 1997)

[3] http://www.livius.org/a/1/maps/royal_road_map2.gif

www.manaraa.com

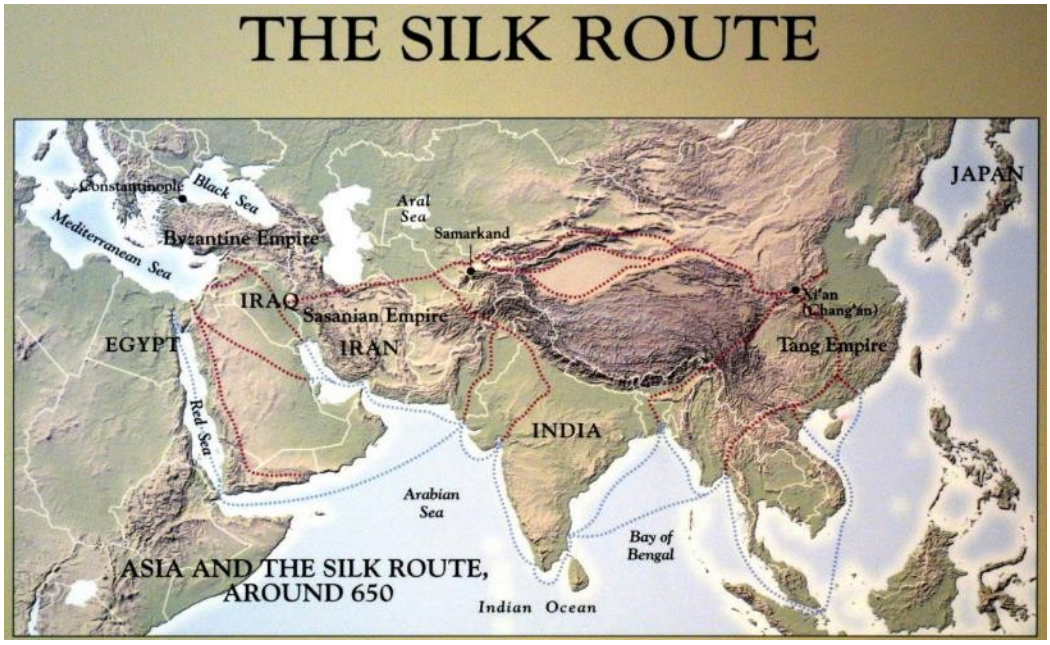

Figure 2.4 The network of silk route [4]

Road systems for similar purposes existed in other ancient civilizations. These roads were trafficked by humans on foot, horse and buggies (carriages), mules, camels, carts, and wagons. The travelling speed was slow and the capacity limited.

The industrial revolution in the 19th and 20th century changed many aspects of people's life, including their housing, food, and travel. The emergence and popularity of automobiles and trucks exerted new demands on the quantity and quality of roadways. This stimulated a revolution in pavement materials, structural design, and construction.

Moreover, fuel for the trains, automobiles and airplanes, integral to the modern transportation system, most often is produced by distillation of crude oil. This distillation

[4] http://www2.econ.iastate.edu/classes/econ355/choi/silkroad.htm

www.manaraa.com

process produces asphalt as a by-product. The asphalt by-product found ready use as a *binder* in asphalt pavements predominately used in many modern highways.

2.1.2 Modern Highways

Very often, the motivation for developing a transportation network (railway, roadway) is for military purposes, defense or offense. However, the existence of such transportation systems invites their use for economic purposes and they become the key to economic development. Modern examples are the German Autobahn and the US Interstate Highway System.

The "German Autobahn network" was conceived during the Weimar Republic in the early 20th century and was enthusiastically embraced and promoted by Adolph Hitler as a means of German economic development and also a means of moving the German military. After, WWII the Autobahn system was rebuilt and subsequently connected to similar roadway systems in other European countries. Currently, the interconnected European Autobahn/Motorway highway system extends into eastern European countries and along with the rail transportation system connects the economic fabric of Europe.

In the US, efforts to establish a nationwide highway system began in the 1920s. At that time it was difficult to drive across the country. The gravel surfaced Lincoln Highway connecting New York City and San Francisco was the first and only coast-to-coast highway for automobiles. Over the following years, the US Highway network was planned and built. After WWII, there was increased need for transportation of goods and services as well as personal travel. As a general in the US Army during WWII, Dwight D. Eisenhower had firsthand experience with logistics problems of the Allies and also observed the potential of the German Autobahn. After being elected President,

www.manaraa.com

Eisenhower strongly supported the Interstate highway system as a matter of the nation's defense. In 1956, he signed the Federal Highway Act, which established the Interstate Highway System. "It was the largest public works project in American history. It took longer than expected to build—35 years instead of 12—and it cost more than $100 billion, about three times the initial budget. But the first coast-to-coast interstate highway, Interstate 80, was completed in 1986, running from New York City to San Francisco." (APM 2012)

In China, the past 20 years has witnessed the rapid increase of modern highway construction, which is unprecedented in human history. The total distance increased from 357 miles in 1992 to 53,000 miles in 2012. The development of roads is playing an important role in economic growth and poverty reduction in China. Nowadays, growing attention is paid to the low-quality, rural roads that connect towns and villages. This approach will be more effective in reducing poverty of rural and urban poor than expressways (Fan and Kang 2005).

2.2 The Evolution of Modern Pavement Design Method

2.2.1 California Bearing Ratio (CBR) and US Army Corps of Engineers (USACE) Method

In the 1920s, the California Division of Highways developed the concept of CBR and used it for pavement design. This is an early empirical highway design method which strongly affected the method which the USACE used for heavier traffic and airfields. The empirical relation developed by the California Division of Highways related in situ CBR test values to thickness for loads and traffic at the time.

www.manaraa.com

The CBR test is used to evaluate the strength/stiffness of supporting soil and unbounded aggregate layers. In determining design CBR values, compacted soil samples are soaked in water for four days for a worst case condition. The test is then performed by measuring the load required to penetrate the soil sample. This load is compared with the one required to achieve an equal penetration on a standard limestone base. The standard crushed California limestone base was assigned a value of 100. Moist sand may have a CBR of 10.

$$CBR = \frac{p}{p_s} \times 100 \tag{2.1}$$

p = measured pressure for site soils [N/mm²]

p_s = pressure to achieve equal penetration on standard soil [N/mm²]

In 1940s, the Corps of Engineers was responsible for developing a pavement design method for airfield loadings. The CBR method was chosen mainly because it had proven a successful method. Also, the ease of use could satisfy the pressing short-term needs during WWII. It was first developed as single-wheel criteria. Later, multiple-wheel tests were performed and the Equivalent Single-Wheel Load (ESWL) method was developed. In application, the design criterion is based on a fixed traffic volume and the multi-wheel gear configuration is converted to single wheel loading (Ahlvin 1991). It is worth noting that this method only considers the soil properties when designing pavement structural layers. The material property and quality of the HMA layers are assumed to be unrelated to the stress distribution both in and under pavement layers.

The USACE method used the original empirical correlation of thickness and CBR value of supporting soil or unbounded aggregate layer. The curves for increasing airfield

www.manaraa.com

loads were extrapolated. The curves are then transformed to a unified design curves. Shear stresses were first calculated for the 12,000 lb case. These values were then used as allowed stress and kept constant for thickness adjustment of different loading values. Also, each shear stress corresponded to a certain CBR value of soil. CBR values of 3, 5, 7, and 10 percent correspond to shear stresses of 5, 8, 12, and 14 psi. Original CBR curves, the extrapolation curves for higher load and the final airport design curves are shown in Figure 2.5 and Figure 2.6 (Yoder and Witczak 1975).

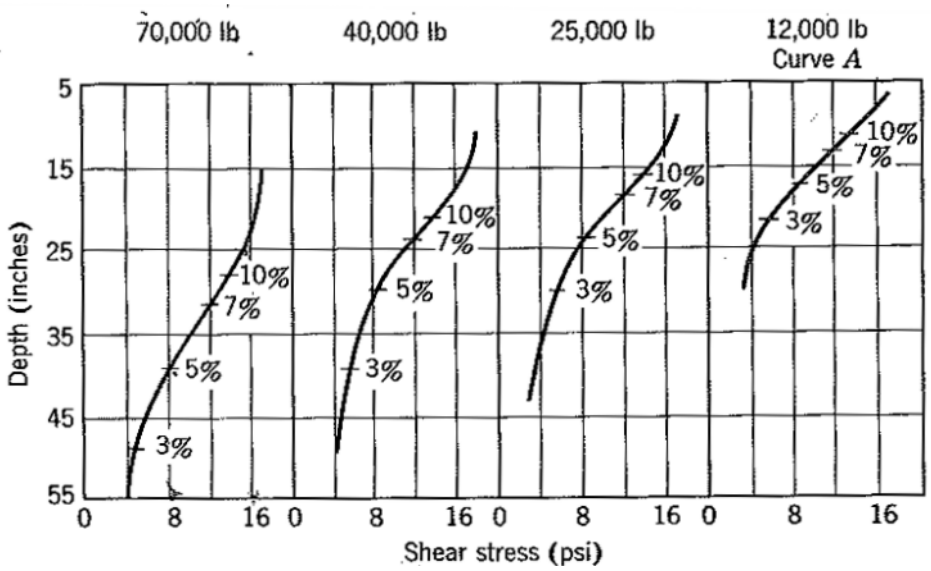

Figure 2.5 Extrapolation CBR curves for higher loads

www.manaraa.com

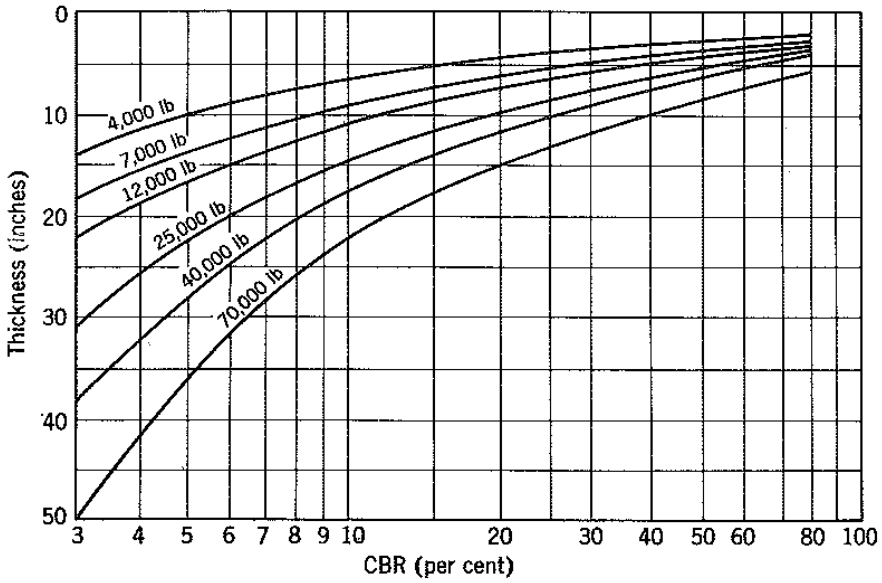

Figure 2.6 Design curves for airport pavements

2.2.2 American Association of State Highway and Transportation Officials (AASHTO) Method

The design of pavements and bridges on the Interstate Highway System is largely based on the results of the American Association of State Highway Officials (AASHO) Road Test. The major reason for the road test was to determine the performance relationships over a range of axle loads and pavement layer thicknesses for a subgrade with known characteristics. The road test site limited the results to one climate and required a way of extrapolating the performance results to other climate conditions. Construction began in August 1956 on seven miles of two-lane pavements in the form of six loops and a tangent, half concrete, and half asphalt. The 836 test sections employed a wide range of surface, base, and subbase thicknesses, and included 16 short-span bridges. Test traffic was inaugurated on October 15, 1958. The Department of Defense (DOD)

www.manaraa.com

provided heavy vehicles and drivers. The AASHO Road Test ended November 30, 1960. (FHWA 2011)

The road test flexible pavement sections were constructed with an asphalt mixture surface, a crushed limestone base, and a sand-gravel subbase. Three levels of surface thickness were used ranging from 1 to 6 inches. Three levels of base thickness ranging from 0 to 9 inches and three levels of subbase thickness ranging from 0 to 6 inches were combined for the experiment. The traffic consisted of single axle loads ranging from 2,000 to 30,000 pounds and tandem-axle loads ranging from 24,000 to 48,000 pounds.

The pavement performance was recorded in terms of roughness, cracking and rutting. Also stresses at the subgrade surface and temperature distribution were recorded and analyzed (AASHTO 1972). Results of the AASHTO road test provided the basis for development of the AASHTO pavement design guides. (1961, 1972, 1986, 1993) In the 1986 version, factors for the design include serviceability loss, design structural number (SN), equivalent single-axle load (ESAL), subgrade resilient modulus (Mr), drainage, and reliability level. The goal of the design is to make sure that the pavement structures perform well for the predicted number of ESALs.

Resilient modulus is assumed to represent the elastic modulus of soil and granular materials. In the laboratory, the resilient modulus is determined from a repeated triaxial test to simulate the repeated wheel loading.

For fine-grained, non-expansive soils with a soaked CBR of 10 or less, the correlation between the resilience modulus and CBR is (Heukelom and Klomp 1962) :

$$M_R = 1500\ (CBR) \qquad (2.2)$$

www.manaraa.com

Typical values of resilient/elastic modulus for geologic and other common civil engineering materials are summarized in the table below.

Table 2.1 Elastic modulus for some materials

Materials	E (Pascal)	E (ksi)
Steel	2×10^{11}	3×10^{4}
Reinforced Concrete / Glass	$3\sim5 \times 10^{10}$	$5\sim8 \times 10^{3}$
Wood (along grain)	$5\sim15 \times 10^{9}$	$8\sim25 \times 10^{2}$
Asphalt Concrete	$2\sim20 \times 10^{9}$	$3 \sim30 \times 10$
Gravel / Sand (depending on confining)	2×10^{8}	3×10
Silt and Clay / Rubber	2×10^{7}	3
Diamond	10^{12}	$5\sim8 \times 10^{5}$

As shown in Figure 2.7, resilient modulus for fine-grained soils depends on the applied axial deviator stress. The modulus decreases rapidly as the deviator stress increases. However, the resilient modulus for granular materials depends on the confining pressure. See Figure 2.8. A higher confining pressure can greatly raise the modulus for granular materials (Yoder and Witczak 1975).

www.manaraa.com

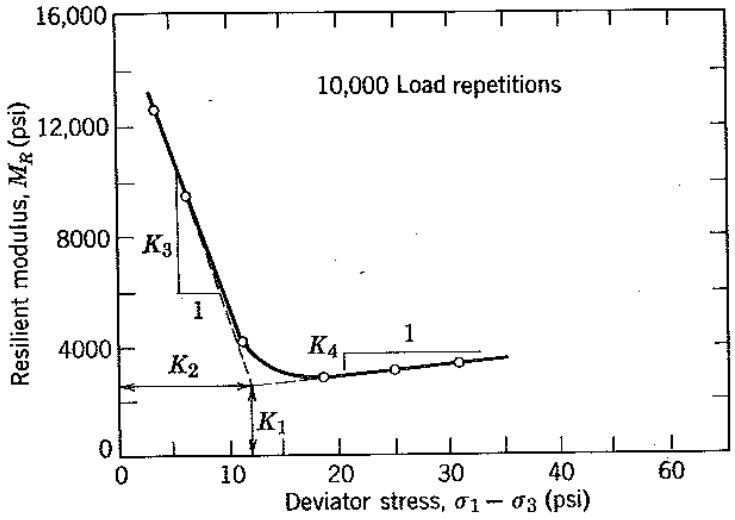

Figure 2.7 Resilient modulus and deviator stress for fine grained soils (Yoder and Witczak 1975).

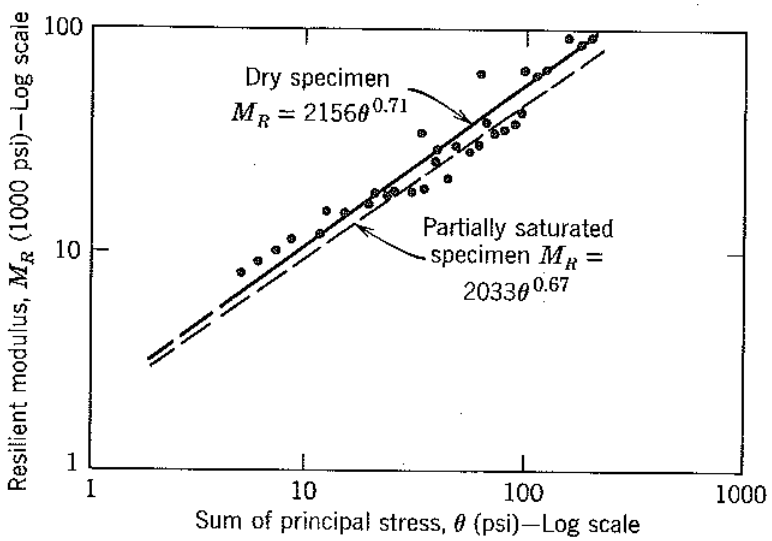

Figure 2.8 Resilience modulus and confining (bulk) pressure for granular materials (Yoder and Witczak 1975).

2.2.3 Mechanistic-Empirical Method

Mechanistic analysis can provide a rational basis for the pavement design. A true mechanistic analysis requires a good physical, material and load models. In 1977, the

www.manaraa.com

Asphalt Institute initiated an effort to explore the use of a mechanistic method for pavement design. The design criteria include two strains that were considered critical:

- The horizontal tensile strain at the bottom of the lowest asphalt-bound layer. This strain is considered to be related to fatigue cracking.
- The vertical compressive strain at the surface of the subgrade layer. This strain is considered to be linked to permanent or plastic deformation in the subgrade. The assumption is that plastic strains are proportional to elastic strains. And the elastic strain in the upper layers can be controlled by limiting the elastic strain in the subgrade.

Both strains values are connected to the number of load repetitions from empirical data. The Shell International Petroleum Company and Chevron Research Company developed their own elastic-layered pavement models for theoretical analysis. (Asphalt Institute 1982)

In the 1990s, the AASHTO Joint Force on Pavements, in cooperation with the National Cooperative Highway Research Program (NCHRP) and the Federal Highway Administration (FHWA) initiated study of a mechanistic-based design method. (I-37A 2004) However, the effort resulted in a hybrid mechanistic-empirical design procedure designated as the Mechanistic-Empirical Pavement Design Guide (MEPDG 2008). In MEPDG, the principles of mechanics are used to predict the responses of linear elastic models, which are correlated with empirical observational data as a basis of the design method. The design process has three elements:

1. The mechanistic element predicts critical pavement responses (strains, stresses, deflections, etc.)

www.manaraa.com

2. Material characterization used in the theory
3. Empirical correlation that defines the relationships between the critical pavement response parameter and field-observed distress.

The conceptual flow chart for MEPDG can be seen in Figure 2.9.

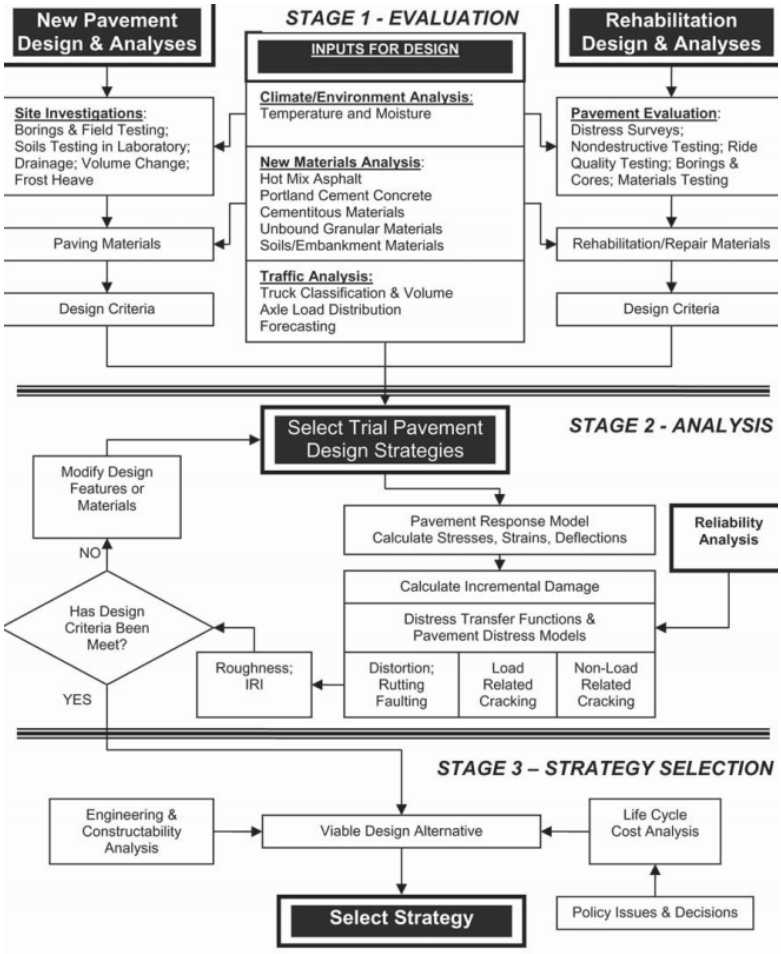

Figure 2.9 The conceptual flowchart of MEPDG

(Local 2010)

The conceptual differences between the new MEPDG and 1986/1993 AASHTO format is listed as follows: (Schwartz and Carvalho 2007)

www.manaraa.com

- Single performance criterion and multiple performance criteria. The 1986/1993 AASHTO use present serviceability index (PSI), while the MEPDG considers rutting, cracking, and roughness separately.
- Direct and iterative computation process. The 1986/1993 AASHTO format *determines* the layer thickness directly based on various inputs. MEPDG refines the trial section iteratively until an acceptable design is reached.
- Limited field test data and project-specific data. The 1986/1993AASHTO format is based on the AASHO road test, which is in Illinois. The MEPDG collects more site-specific data.
- ESALs and load spectra. The 1986/1993AASHTO format uses ESALs to represent traffic levels, while the MEPDG uses load spectra (percentage applications for different types of axles).

2.3 Finite Element Method (FEM) in Pavement Analysis and Design

As a numerical method to solve differential equations, FEM originated in the 1940s from the need to solve complex elasticity problems in civil and aerospace engineering. The estimation of the stiffness of beam-type structures (for example, rafters and purlins of a wooden roof, spars and ribs in an airplane's wing) are relative easy. However, the stiffness of shell type structures (for example, the metal skin of airplane's wing) is not easy to analyze. Hrennikoff invented a technique that can simulate a section of the metal skin with a lattice of bars of known stiffness (Hrennikoff 1941). This work is a prototype of the current version of FEM. Later, this technique was expanded by

www.manaraa.com

mathematician Courant and engineer Zienkiewicz to problems other than structures (Grandin 1986).

In FEM, field equations that describe the physics are approximated over simple regions and then assembled together. In this process, basic physical requirements are satisfied. For example, the forces applied on the nodes are in equilibrium and displacements at the common node of connecting elements are equal. Several important features when applying the method include meshing, i.e., dividing the whole problem domain into subdomains (finite elements), deriving approximation functions over each element, and assembling elements. Through these techniques, systems of algebraic equations are substituted for the complex partial differential equations that govern the physical problem with acceptable accuracy (Reddy 2006).

With the development of mainframe computers in the 1950s and personal computers in the 1980s, the solution of large scale matrix equations becomes possible. Therefore, FEM grew more popular and widely used in various engineering disciplines. Before FEM, finite difference method (FDM) was used to solve similar problems. But FEM has several advantageous such as solving problems with more complex geometries.

Historically, mechanistic based design methods including the MEPDG include layered elastic analysis (Boussinesq's single layer theory and Burmister's multi-layer theory.) The layered elastic models are based on idealized conditions such as the materials are homogeneous and isotropic elastic. In addition, the layers are considered to be infinite horizontally. Also, loads are static and assumed to be applied uniformly over a circular area. However, flexible pavement materials and foundation soils are inelastic.

www.manaraa.com

Also, the structural layers and foundation have boundaries. Loads are moving and dynamic.

FEM can better represent complex material properties, accurate pavement geometries, and moving, dynamic vehicle loadings (Zaghloul 1993, Hua 2000, Al-Qadi, Elseifi and Yoo 2004). In this research, FE models of conventional pavements and perpetual pavements will be constructed and their responses compared.

2.4 Conventional and Perpetual Pavements

Conventional flexible pavements usually consist of a surface course, a base course and an optional subbase. The surface course is usually composed of HMA. Base courses and subbase courses are constructed of crushed stones or gravels (aggregates). The pressure from wheel loadings decreases with depth from the surface of the pavement structure. For the sake of economy, material layers are usually arranged in order of descending stiffness and cost with the stiffest material (expensive) on the top and the lowest stiffness material (cheap) on the bottom. See Figure 2.10 .

The concept of a perpetual pavement is that all layers of the pavement structure are HMA. The surface HMA layer is a wear and rut resistant high quality HMA, the middle layer is a rut resistant stiff HMA, and bottom layer is fatigue resistant HMA (APA 2002). Also, the supporting surface is a stiff subgrade and may include stabilization. The design of perpetual pavement is still evolving. The current US approach to design is shown in Figure 2.11.

www.manaraa.com

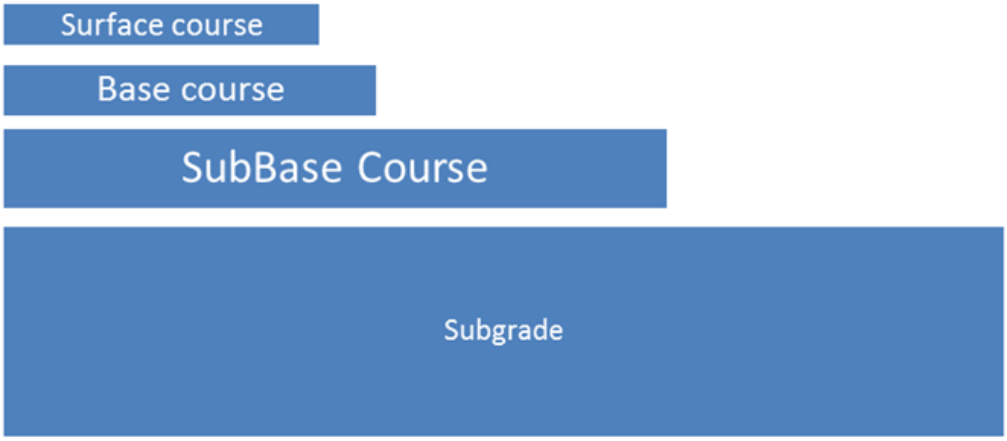

Figure 2.10 Pavement courses of a typical flexible pavement structure.

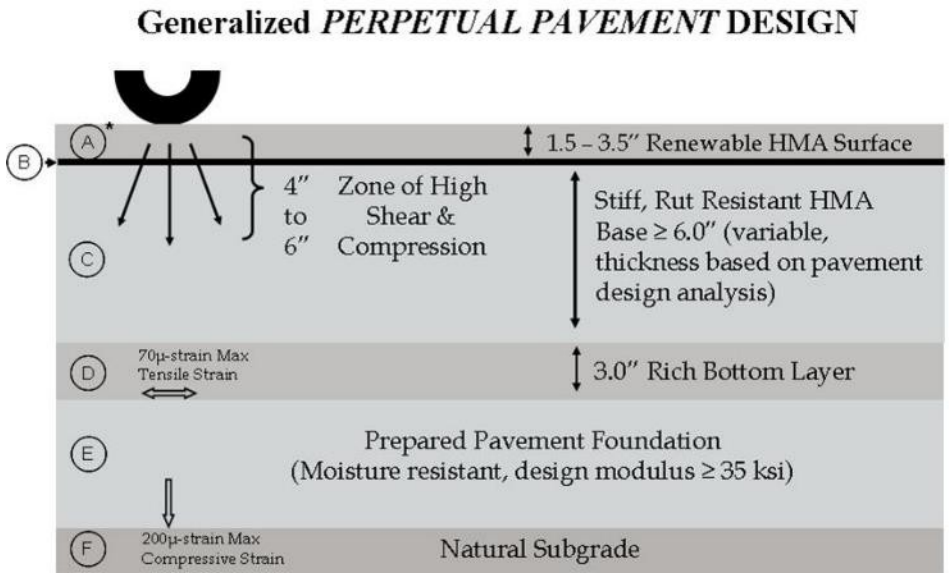

Figure 2.11 Pavement courses of a perpetual pavement structure. [5]

[5] http://onlinemanuals.txdot.gov/txdotmanuals/pdm/pavement_types.htm

www.manaraa.com

2.5 Pavement Performance

Generally speaking, pavement performance is affected by many factors, including structure, environment, construction, maintenance, and traffic as shown in Figure 2.12 (Haas 2001).

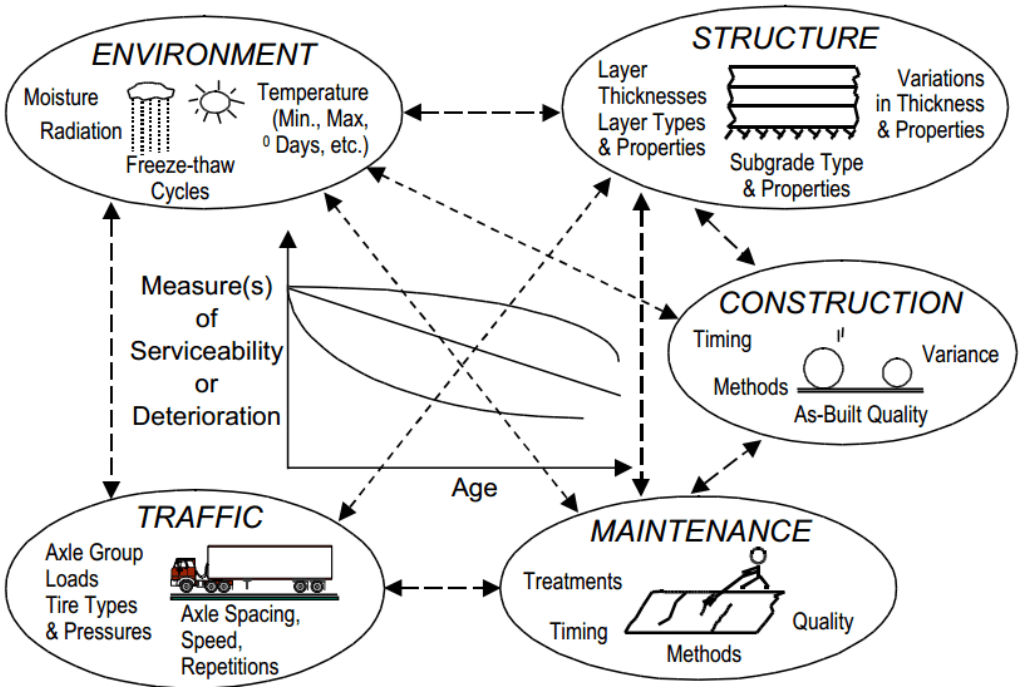

Figure 2.12 Factors affecting pavement performance (Haas 2001)

The ways to account for the pavement performance in design are slightly different in Europe and the US.

2.5.1 European Approach

In Europe, flexible pavement performance is associated with (Ferne 2006):

- Permanent deformation leading to surface rutting.

www.manaraa.com

- Full depth cracks through which surface water reaches and weakens any unbound layers and the pavement subgrade.
- The surface rutting is a result of accumulation of deformation in all layers of the pavement. On the other hand, the full depth cracking is assumed to start at the bottom of the bound layers and progress upwards to the surface.

Over the past three decades, observations were made in France (Dauzats and Linder 1982), the Netherlands (Pronk and Buiter 1982), and South Africa (Strauss, Servas and Marais 1984) of top-down cracking. More recently, Nunn, et al. (Nunn, et al. 1997) reported observations of cracking initiated from the surface (top-down cracking).

The significance of "top-down cracking" visible at the surface is minimal if the cracking does not extend to the bottom of the pavement. The result is surface water will not have access to any unbound layers or subgrade as with surface visible bottom-up cracking. Only periodical replacement or treatment of the wearing surface is needed to maintain smoothness. This is the original European concept of "long-life pavements." As a consequence of the above observations, the concept evolved that there is a threshold thickness beyond which additional thickness is not beneficial.

In 2000, the European Long-life Pavement Group (ELLPAG) was formed by the Forum of European National Highway Research Laboratories (FEHRL) to identify the state of the art in the pavement design. The group defined long-life pavement as "a well designed and constructed pavement that could last indefinitely without deterioration in the structural elements provided it is not overloaded and the appropriate surface maintenance is carried out." (Ferne 2006)

www.manaraa.com

2.5.2 The US Approach

In the US, pavement structural performance is assumed to be based on accumulation of fatigue cracking from repetitive traffic tensile strains at the bottom of the lowest asphalt layer. The cracking is assumed to be bottom-up cracking. In practice, the limit of fatigue cracking for design is based on load repetitions to produce a level of cracking severity and extent.

Based on the AASHTO design guide, pavements with higher traffic volumes and heavier loads require thicker pavements. However, many pavements of heavily trafficked roads have exceeded a 20-year design life. These include I-90 in Washington State, I-80 in Iowa, and the Kansas Turnpike (Timm and Newcomb 2006).

Based on the performance of these roads, a fatigue endurance limit for bottom-up cracking was introduced for HMA. More details on this subject are covered in section 3.2.4 about fatigue in HMA.

www.manaraa.com

CHAPTER III

MATERIALS AND MECHANICS FOR FLEXIBLE PAVEMENTS

3.1 Soils

3.1.1 Definition

In engineering, soil is considered a three phase material containing solid particles and voids. However, the voids could be filled with water and air. The solid particles evolve from either physical or chemical weathering of rocks. Soils particles evolve from three types of rocks. These rock types will be described in detail in the Aggregates section.

Soils can be classified as gravel, sand, silt or clay, etc. depending on the predominant particle size and the effect of water on its consistency. Soils can be cohesionless or cohesive. Generally speaking, the former contains gravel, sand, or silt. The latter contains silt and clay. Formed soils are often mixtures of the various sizes.

The soil grain size distribution affects its mechanical properties. To find a particle-size distribution curve for soil, sieve or hydrometer analysis can be used to find the percentage of soil particles smaller than a sieve size.

www.manaraa.com

3.1.2 Stresses in Soils

Stresses in soil strata due to self-weight are vertical in situ stresses. The vertical stresses in general follow the same rule as hydrostatic pressure. The difference is that the horizontal stresses are not equal to the vertical stresses.

Soils can be partially saturated or saturated. In saturated soils, effective vertical stresses (σ_v') account for the hydrostatic stress in the water and are calculated by (cannot be measured) (Terzaghi 1943):

$$\sigma_v' = \sigma_v - u \tag{3.1}$$

where σ_v is total vertical stress, u is pore water pressure

Pore water pressure has an important effect on the effective stress in soil. If loading on soil is fast and the pore water is not drained and, excess hydrostatic pressure can lead to soil failure.

3.1.3 Mechanics Background

Mechanics represents the behavior of physical bodies when subjected to forces or displacements. Nowadays, the study of material behavior as a continuum can be viewed as a branch of classical mechanics, in which Newton first stated his concepts of absolute time and space. The development of the theory evolved through a long historic time.

During the Age of Enlightenment, many people have explored the area of mechanics of materials with great interest. The Italian physicist Galileo, the founder of modern science, studied the failure of a cantilever beam. Swiss mathematician Euler investigated the elastic curve and bending of beams, and column buckling, etc. The

www.manaraa.com

French physicist Coulomb presented the first time an adequate stress analysis of a beam (Westergaard 1952).

The post-Enlightenment era saw three Frenchmen as the founders of the three dimensional theory of elasticity. The engineer Navier and two mathematicians, Cauchy and Poisson, are the most important contributors. Cauchy derived the differential equations for displacements in an elastic isotropic material in 1822 AD. In the equation, he used two constants of elasticity known today as Young's modulus and Poisson's ratio. The latter describes the ratio of transverse extension to axial contraction per unit length under uniaxial loading (a value of 0 in Poisson's ratio means almost no lateral expansion when compressed axially). Subsequent to Navier, Cauchy, and Poisson's work, the theories developed and continue today. Also, structural mechanics advanced as an individual subject after the 1850s. (Grattan-Guinness 1990, Westergaard 1952)

Continuum mechanics differs from the earlier Newtonian celestial mechanics in that the internal constitution of material plays an important role. The load-deformation (cause-effect) behavior depends on the internal constitution of matter (the nature of different materials).

Several important axioms guide the theory of continua (Desai 1984).

- Determinism: Past determines current. For example: the deformation in a body caused by an external force is dependent on the past loading history for the body.
- Causality: Cause and effect go together. The independent variables (cause, force) cause the dependent variables (effects, deformations).

www.manaraa.com

- Neighborhood: Local action only. The responses at a point are *not* affected by the conditions far away from that point. This can be seen in the domino effect in a chain reaction.
- Memorylessness: The present constitutive variables are *not* affected by the values in the *distant* past.

Rather than expressing the excitation and response explicitly, quantities relevant to internal reactions such as stress and strain are used as variables in constitutive equations in continuum mechanics (Desai 1984).

In the three dimensional (3-D) Cartesian coordinate system, the state of stress and strain at a material point associated with any infinitesimal planes could be described by Cauchy stress and strain tensors. They are widely used in the analysis of relatively stiff material, such as steel and concrete. These measures are considered to be very small in the elastic stage of the material deformation.

$$\begin{bmatrix} \sigma_{xx} & \sigma_{xy} & \sigma_{xz} \\ \sigma_{xy} & \sigma_{yy} & \sigma_{yz} \\ \sigma_{xz} & \sigma_{yz} & \sigma_{zz} \end{bmatrix} \tag{3.2}$$

$$\begin{bmatrix} \varepsilon_{xx} & \epsilon_{xy} & \epsilon_{xz} \\ \epsilon_{xy} & \epsilon_{yy} & \epsilon_{yz} \\ \epsilon_{xz} & \epsilon_{yz} & \epsilon_{zz} \end{bmatrix} \tag{3.3}$$

In the one dimensional (1-D) uniaxial case, the normal stress and the normal strain is linked only by the Young's modulus. However, in the 3-D case, the stress components at a point are linked to the strain components by a 6x6 matrix of elastic coefficients. For example, a normal stress could be affected by the strain in three directions.

www.manaraa.com

For homogeneous (the material has same properties at every point) and isotropic (the elastic properties are the same in every direction) materials, the matrix of elastic coefficients is a symmetric matrix as shown in Figure 3.1 (solid square means symmetric components). The components are all functions of young's modulus (E) and Poisson's ratio (υ). This matrix serves as the basis for the generalized Hook's law.

$$\begin{pmatrix} E_{11} & \blacksquare & \blacksquare & \blacksquare & \blacksquare & \blacksquare \\ E_{21} & E_{22} & \blacksquare & \blacksquare & \blacksquare & \blacksquare \\ E_{31} & E_{32} & E_{33} & \blacksquare & \blacksquare & \blacksquare \\ 0 & 0 & 0 & E_{44} & \blacksquare & \blacksquare \\ 0 & 0 & 0 & 0 & E_{55} & \blacksquare \\ 0 & 0 & 0 & 0 & 0 & E_{66} \end{pmatrix}$$

Figure 3.1 Matrix of elastic coefficients
(solid square means symmetric components)

It is worth saying that the development of the constitutive law (mathematical model) for a single material is very difficult. It can be achieved using either a macroscopic approach or a microscopic approach with experiments and observations playing an important part in the former approach.

If the force or displacement that the body is subject to exceeds a certain limit, plastic deformation will take place. The work done by applied loads in this stage is not stored as recoverable strain energy as in the elastic stage. In other words, plastic deformation absorbs (dissipates) energy and is not recoverable. This permanent deformation can be visualized by sliding a solid and a spring on a coarse surface as shown in Figure 3.2. Once the solid starts sliding (plastic deformation), the energy is

www.manaraa.com

dissipated by friction between solid and ground. When the load is removed, the spring will recover but the solid will not move back to its original location. Generally speaking, the total strain can be decomposed into elastic and plastic components. In the large strain case, the plastic strain can often be considered close to the total strain. See Figure 3.3 (Dunne and Petrinic 2005). The strain is usually represented by either the finite Lagrangian strain tensor (based on reference configuration) or Eulerian strain tensor (based on current configuration).

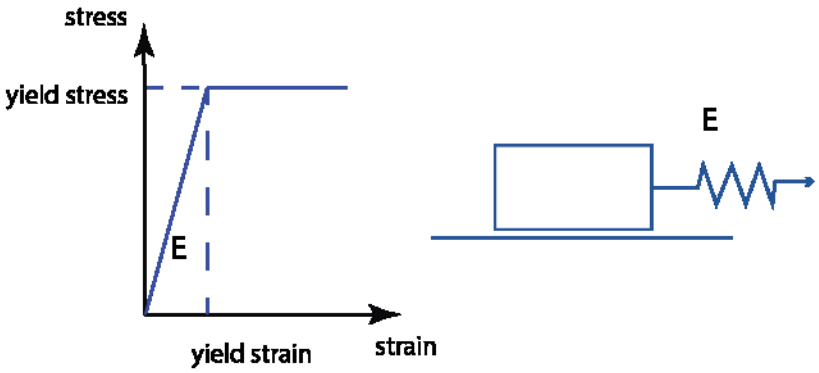

Figure 3.2 The analogy of plastic deformation

(E is the young's modulus of the spring/material)

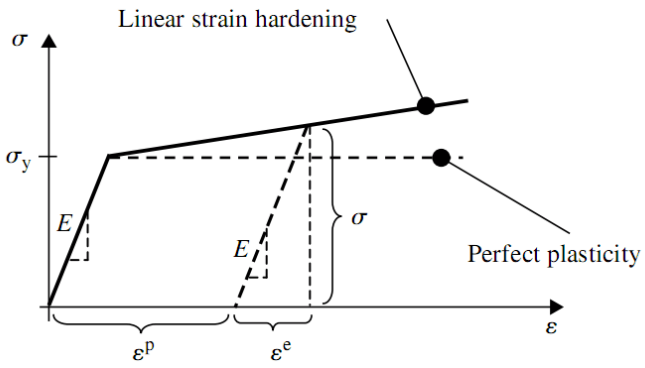

Figure 3.3 Decomposition of strain in a uniaxial tensile test

(Dunne and Petrinic 2005)

www.manaraa.com

In metals, crystal slip is considered origin of plasticity. In macroscopic plasticity, two rules usually apply (Dunne and Petrinic 2005):

- Plastic slip does not lead to volume change (incompressibility).
- Plastic slip is a shearing process. Hydrostatic stress doesn't contribute to slip.

However, in soils, plastic deformation could be due to the water expelled from the pores. If the soils are saturated with water, the volume of soil can change significantly due to the water draining. To simplify the problem, the plastic deformation due to drainage of water will not be considered in this research. This is reasonable because much of the time the soil is partially saturated.

Some important stress invariants are central to the models described in the next section. They are shown in the following equations (Abaqus, Abaqus 6.9 Analysis User's Manual 2009):

$$\mathrm{p} = \frac{1}{3}\mathrm{trace}\,(\sigma) \tag{3.4}$$

where p is mean stress (equivalent pressure stress)

$$\boldsymbol{S} = \boldsymbol{\sigma} - p\,\boldsymbol{I} \tag{3.5}$$

where S is deviatoric stress (also notated as $\boldsymbol{\sigma}'$)

$$q = \sqrt{\frac{3}{2}\,\boldsymbol{S} : \boldsymbol{S}} \tag{3.6}$$

where q is von Mises stress (also notated as σ_e)

$$t = \frac{1}{2}q\,[1 + \frac{1}{k} - (1 - \frac{1}{k})(\frac{r}{q})^3] \tag{3.7}$$

where t is a deviatoric measure**,** where r is the third stress invariant

www.manaraa.com

3.1.4 Mechanical Models for Soil

A number of models have been developed to describe the soils' elastic and plastic behavior. Usually, each model can be applied in a local realm. Despite many efforts by scientists, no universal model has yet been developed for all materials under all situations (Desai 1984). In other words, no models are omnipotent. In this section, several well-known and widely used models are summarized.

In 1700s, Coulomb developed a model to represent the shear failure of soil. A century later, Mohr expanded Coulomb's work and developed a general form, which is known as Mohr-Coulomb failure criterion (Terzaghi 1943). This model considers a soils cohesion and friction and normal stress. When taking into consideration of Terzaghi's effective stress concept, the model is written as:

$$\tau = c' + \sigma' tan\varphi' \tag{3.8}$$

where τ is the shear strength of soil, σ' is the effective normal stress at the failure surface, c' is the cohesion intercept and φ' is the internal friction angle.

Figure 3.4 illustrates the Mohr-Coulomb model. This model essentially says that the soil derives its strength from two sources. One is the cohesion between soil particles. The other is the frictional resistance between particles. The latter is stress dependent.

www.manaraa.com

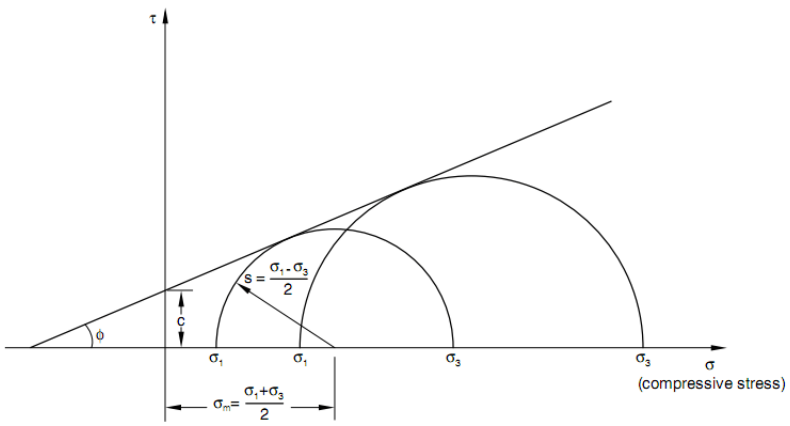

Figure 3.4 Mohr-Coulomb model

(Abaqus 2009)

Although soil contains discrete particles, models based on continuum media were developed to capture its mechanical properties. In these models, soil is treated as a continuous elastoplastic material. Some of the well-known models include the Drucker-Prager model and the Cam Clay model. These models differ in the yield criterion, strain hardening rule and plastic flow rule (Abaqus 2009).

The Mohr-Coulomb model assumes that failure is independent of the second principle stress σ_2. However, the Drucker-Prager model can be applied in a more general case. In most geotechnical applications, the Mohr-Coulomb model is accurate enough due to the failure of the materials has small dependence on the intermediate principle stress (Abaqus 2009). Figure 3.5 and Figure 3.6 show the yield surface of Drucker-Prager model in the p-t plane (p, t was defined in the last section) and deviatoric plane. Figure 3.7 compares the yield surfaces for Mohr-Coulomb and Drucker-Prager models.

www.manaraa.com

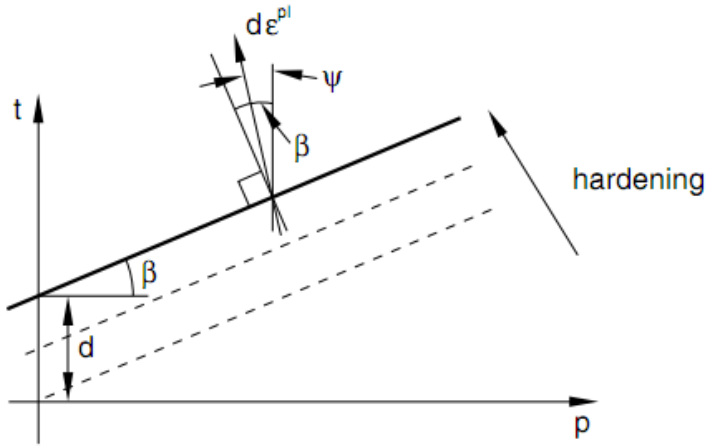

Figure 3.5 Yield surface for Ducker-Prager model in the p-t plane (Abaqus 2009)

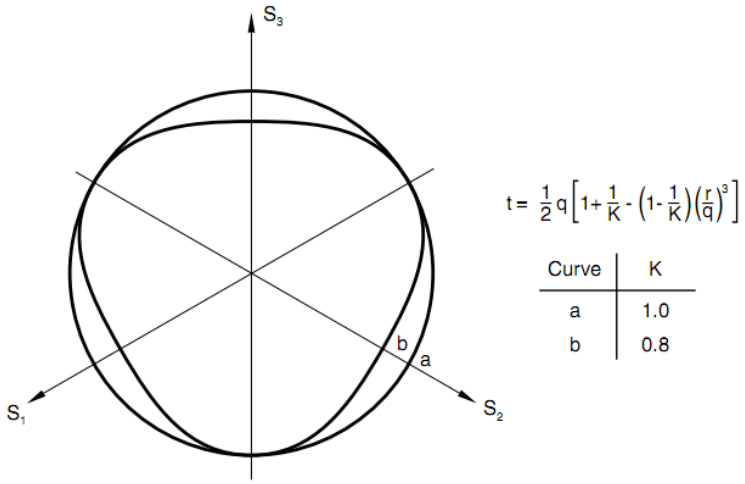

Figure 3.6 Yield surface for Ducker-Prager model in the deviatoric plane (Abaqus 2009)

www.manaraa.com

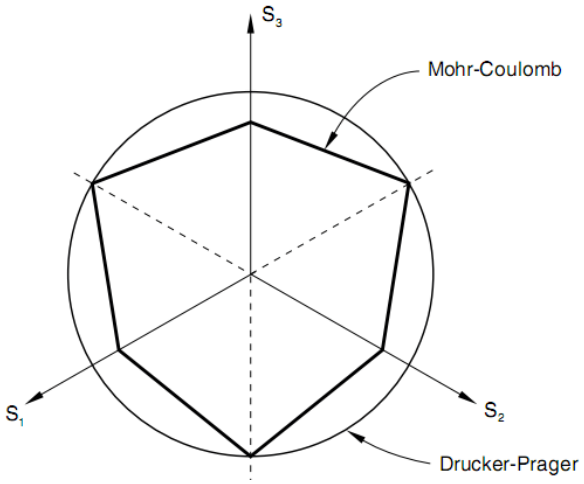

Figure 3.7 Yield surfaces for Mohr-Coulomb and Drucker-Prager model in the deviatoric plane

(Abaqus 2009)

The Cam clay model was developed by researchers in Cambridge University in the 1960s. It assumes that all the voids in soil are filled with water. Plastic volume change happens when the water is expelled from the voids due to an applied stress (Helwany 2007). Using the theory of plasticity, the state of soil is characterized by mean effective stress and the deviator stress. The yield surface for Cam clay model is shown in Figure 3.8 and Figure 3.9.

www.manaraa.com

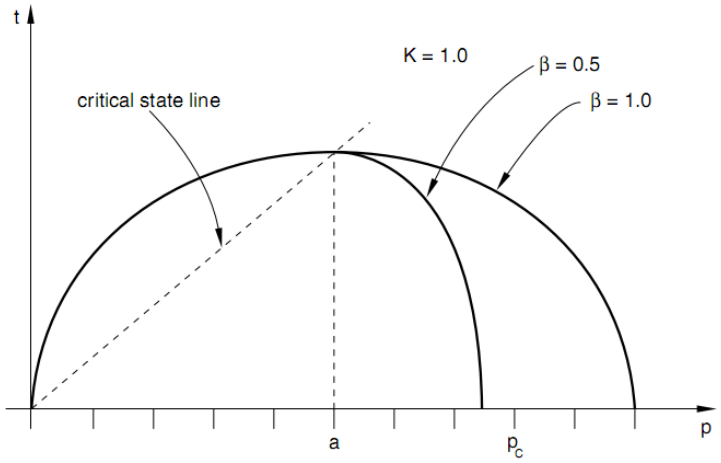

Figure 3.8 Yield surface for Cam Clay model in the p-t plane (Abaqus 2009)

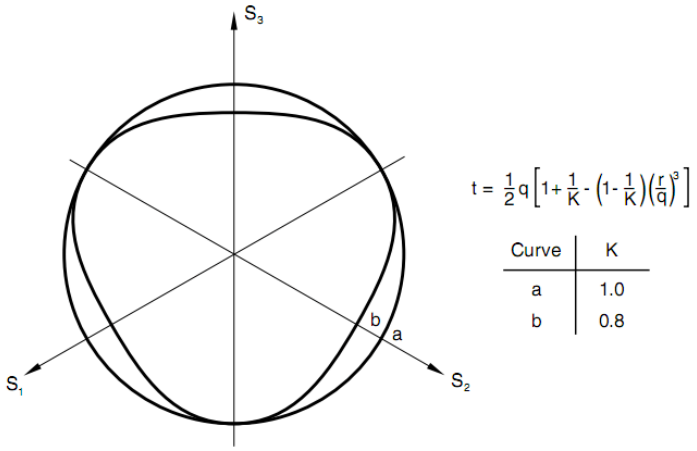

Figure 3.9 Yield surface for Cam Clay model in the deviatoric plane (Abaqus 2009)

Very recently, discrete element models (DEM) have been used to simulate the soil grain by grain. These models are complex and the volume of soil that can be reasonably modeled is limited. For this reason, continuum models that accounts for stiffness and strength are more efficient in modeling soil problems. It is worth saying that due to soil's

www.manaraa.com

complex components and physical behavior, both the continuum and particulate approach are only an approximation of soils' real behavior. (Gudehus 2011)

3.2 HMA

Asphalt concrete, or hot mixed asphalt (HMA) used in the pavement construction, is a combination of aggregate and asphalt cement (binder). It might seem simple, but the type of binder, the type of aggregate, aggregate gradation, and the production methods all affect the HMA properties.

For example, when the HMA aggregate contains particle sizes evenly distributed from the maximum size down to the smallest filler, it is designated as dense-graded. This type of HMA has a low void content (3-7%) and is more of a solid material. On the other hand, when small-size aggregates are limited or missing in the gradation, the HMA is designated as open-graded and has high void content (15-25%). The HMA with a dense-graded gradation usually produce pavements with higher stiffness than open-graded ones. (Young, et al. 1998) The gap-graded HMA usually contain small percentage of mid-size aggregates, resulting in a plot showing flat curve in the middle range. Also, gap-graded HMA has larger voids than dense-graded HMA but smaller voids than open-graded HMA.

Schematics showing the relative aggregate packing of three types of HMA mixes are shown in Figure 3.10. Gradation plots for three HMA mixes are shown in Figure 3.11 to Figure 3.13.

www.manaraa.com

Figure 3.10 The gradation of HMA

a) Dense-graded b) Open-graded c) Gap-graded (TXDOT 2013)

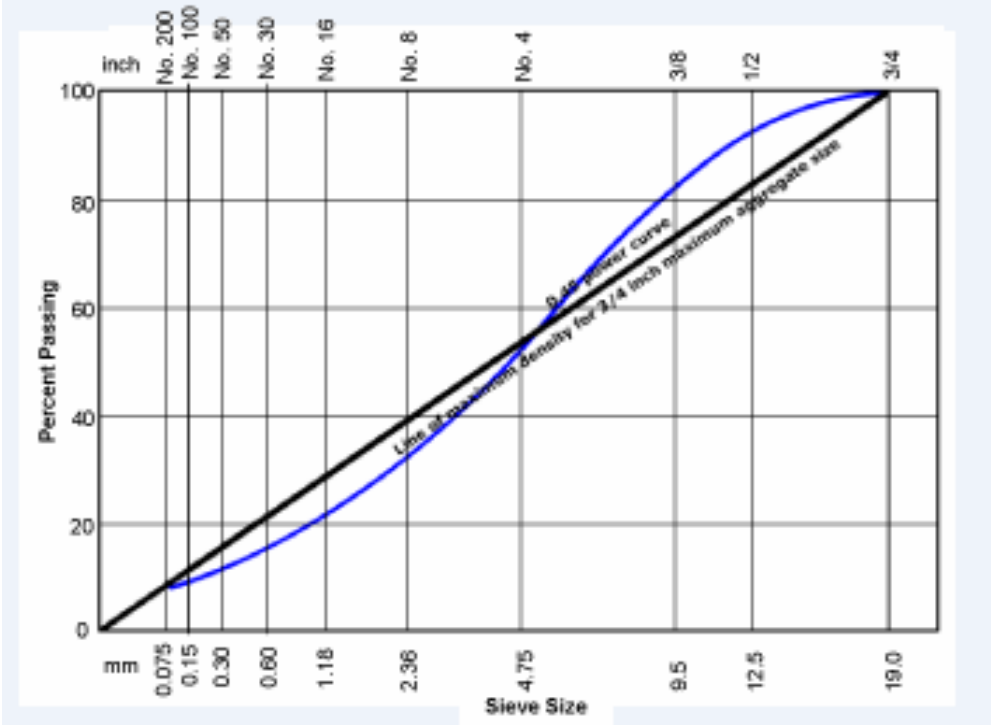

Figure 3.11 An example of gradation curve for dense-graded HMA

(TXDOT 2013)

www.manaraa.com

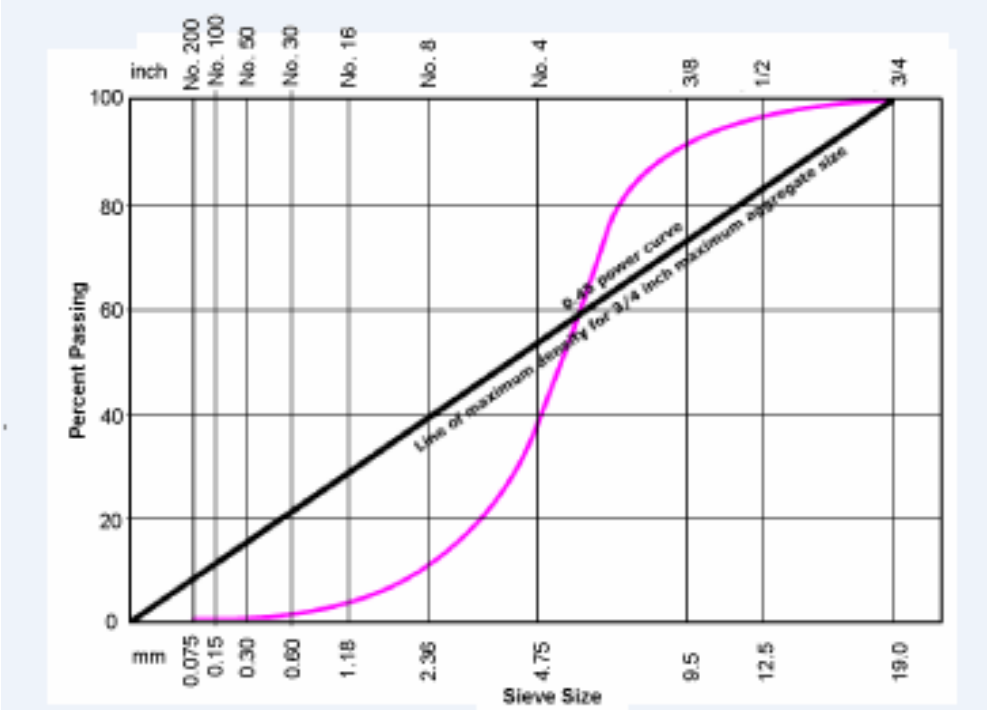

Figure 3.12 An example of gradation curve for open-graded HMA (TXDOT 2013)

www.manaraa.com

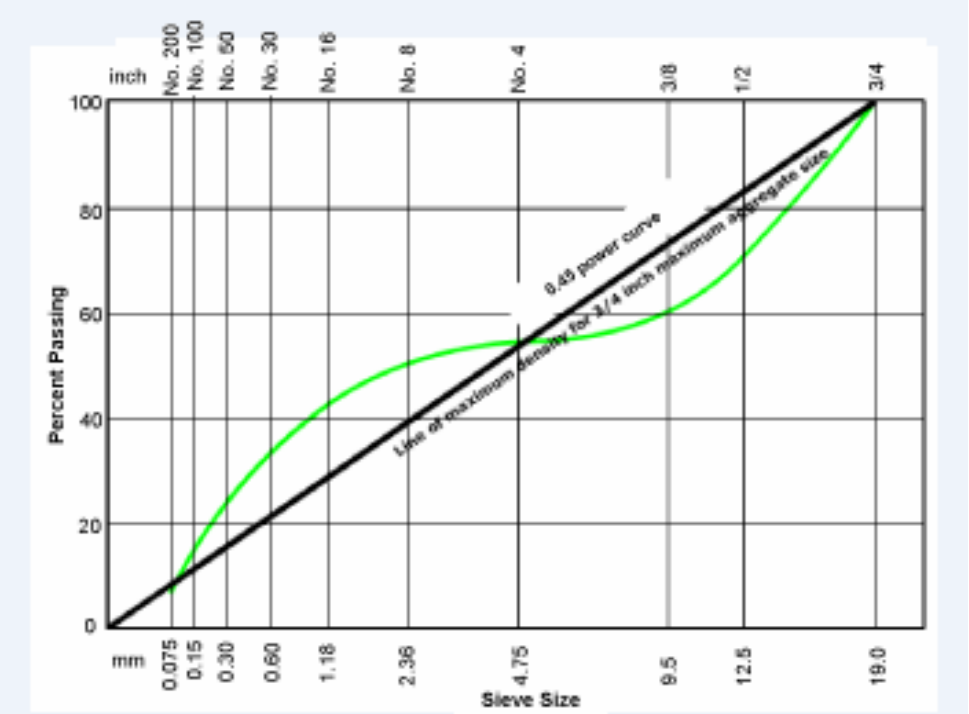

Figure 3.13 An example of gradation curve for gap-graded HMA (TXDOT 2013)

3.2.1 Aggregates

Aggregates are the mineral components in the pavement layers, either bounded or unbounded. Aggregates come from crushed rocks or natural occurring deposit. Granite, limestone and gravels are all common types of aggregates.

Rocks are classified as igneous, sedimentary, and metamorphic. Granite, limestone and marble are typical examples of each. It is worth noting that marble actually is formed from limestone (a sedimentary rock) under intense heat and pressure.

Igneous rocks can undergo weathering, erosion and deposition. The deposited layers could form *sedimentary rocks*. Under intense heat and pressure, *metamorphic rocks* are then created. Moreover, large amounts of dead organisms (algae) buried under sedimentary rocks could turn into different fossil fuels under intense heat and pressure.

www.manaraa.com

Petroleum (from Greek rock 'petro' + oil 'oleum'), as its name suggests, is one of the most important fossil fuels in modern society. Because asphalt cements, as discussed in the next section, also come from refining crude oil, it is interesting to see that all the components of the asphalt pavements are closely related to rocks.

Gravels can be from various parent rocks. Its component could be granite, limestone or sandstone. It consists of natural existing rock fractions usually found in a river bed. Particle size and moisture content can affect aggregates' physical properties.

3.2.2 Asphalt Cements, Bituminous Materials

As noted in the last section, asphalt (bitumen) largely comes from refinement of petroleum. It is used in cementing materials for waterproofing and as protection of surfaces. For example, asphalt is used in roofing (roof shingles) in North America. Also, it is widely used as binder in HMA for paving city streets and highway.

In the early1800s, macadam and tarmacadam were used for a period of time both in Europe and the USA. Tarmacadam uses tar as a binder. Tar is largely obtained from the pyrogenic distillation of coal in making coke for the steel industry. Like many scientific discoveries found by serendipity, the adoption of asphalt in paving a road is by pure accident. Natural asphalt can occur in lakes (La Brea Tar Pits), as solid hydrocarbon (Utah Gilsonite) and also as sedimentary rock (rock asphalt). In the mid-1800s, a Swiss engineer named Andre Merian observed that rock asphalt accidently dropped by *horse-drawn* carts on a bumpy road becomes a good wearing surface when crushed and compressed by traffic over time. He successfully paved a street in Val-de-Travers, Switzerland in 1849 duplicating this process. This technique was then used for paving streets in Paris, London, Berlin and later in the US (Brown 2013). For example, the

www.manaraa.com

Champs-Élysées (meaning Elysian Fields) was among the first that adopted this method (Lay 1992).

Figure 3.14 Natural asphalt rock and Champs-Élysées [6]

Belgian chemist DeSmedt modified the process and paved the first successful asphalt pavement in Newark, NJ in 1870. He used lake asphalt from Trinidad and heated it before mixing with sand. This is the origin of the HMA widely used today.

Petroleum-based asphalt, developed in the early 20th century as byproduct of crude oil refinery processes, quickly found a ready use in HMA. A diagram showing the process of crude oil distillation and the production of asphalt cements is shown in Figure 3.15 (Mamlouk and Zaniewski 1999). A summary of the bituminous material and the primary sub-categories, asphalt and tar is shown in Figure 3.16 (Mamlouk and Zaniewski 1999).

[6] http://geology.about.com/od/rocks/ig/sedrockindex/rocpicasphalt.htm

www.manaraa.com

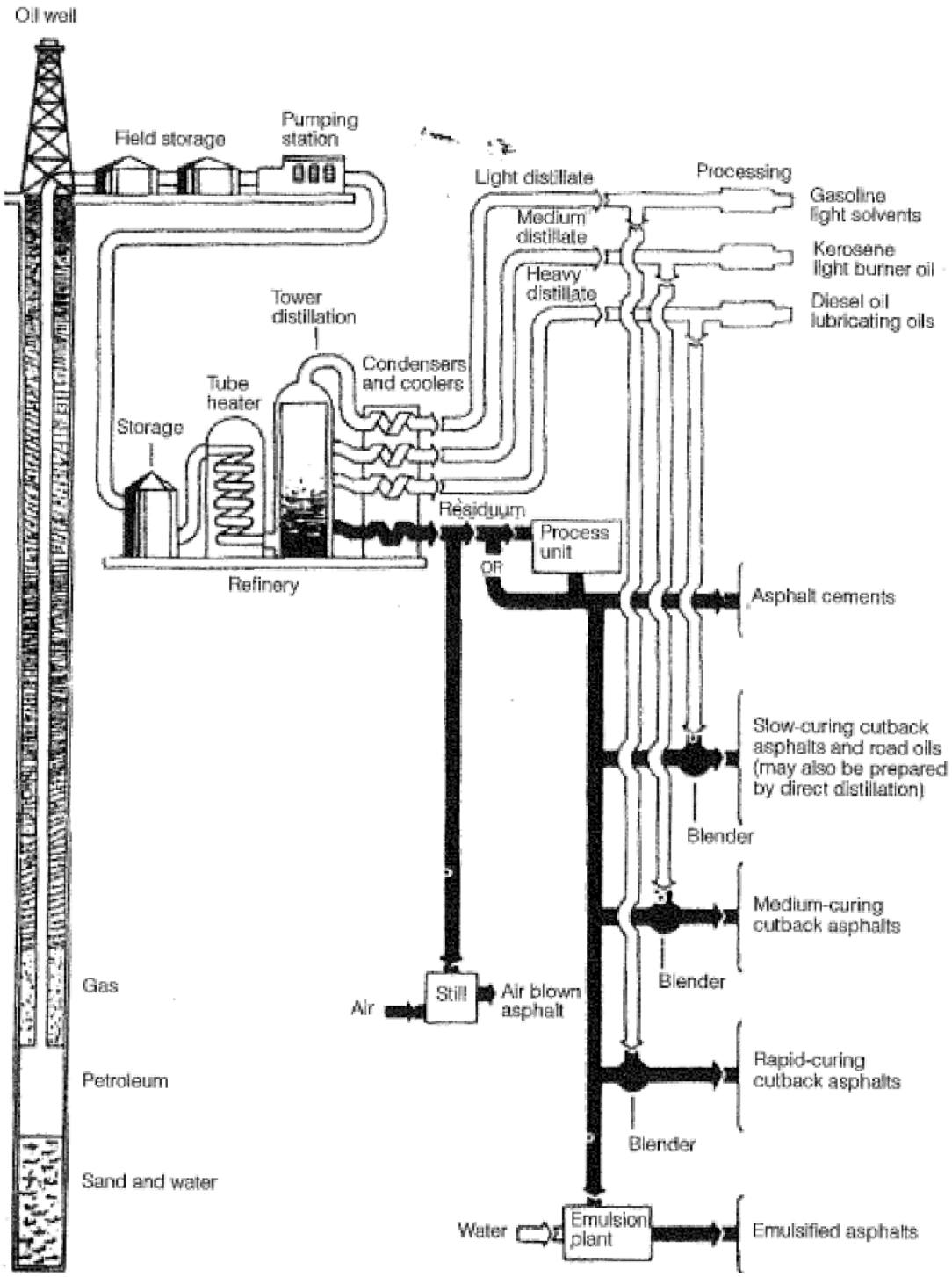

Figure 3.15 Distillation of crude oil

(Mamlouk and Zaniewski 1999)

www.manaraa.com

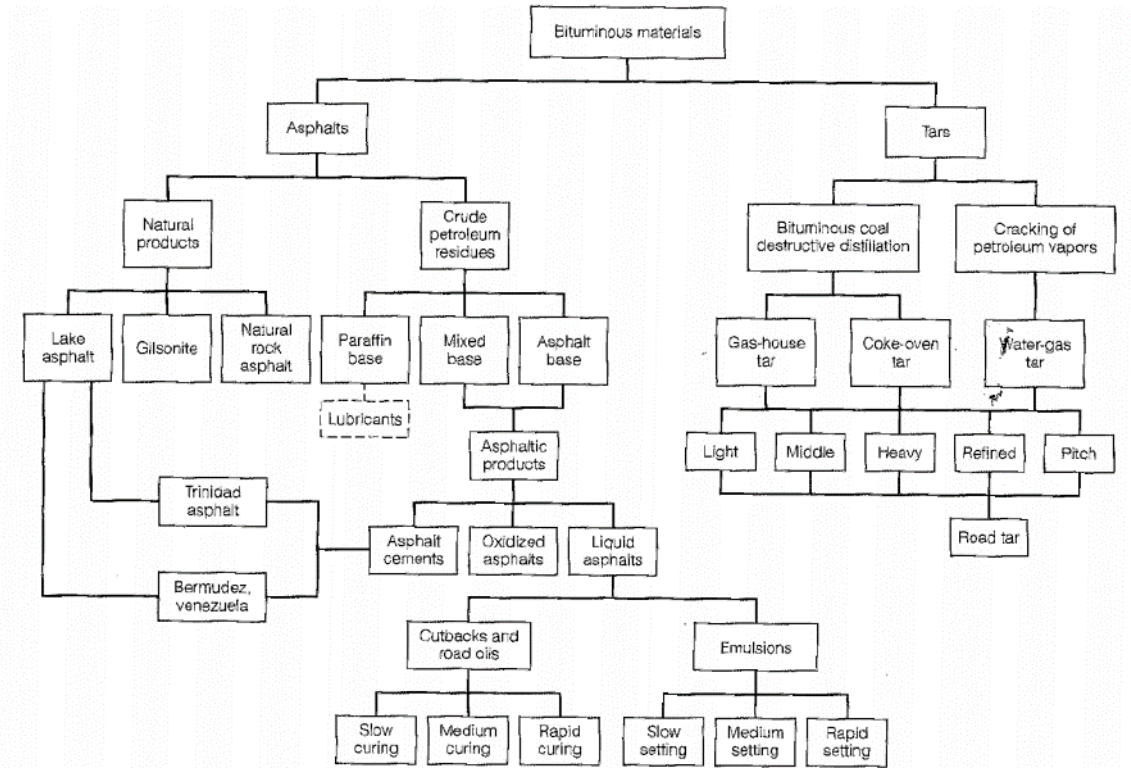

Figure 3.16 Classification of bituminous materials

(Mamlouk and Zaniewski 1999)

The chemical composition of asphalt is complex. Since asphalt has an organic origin, the asphalt cement contains mostly hydrocarbons. It consists of compounds of hydrogen and carbon with some proportions of oxygen, nitrogen, and sulfur.

The internal structure of asphalt has a continuous phase and a discontinuous phase. The different types of internal structural makeup contribute to asphalt's varying physical properties. Some asphalt displays Newtonian viscous fluid behavior. Others have more Hookeian elastic solid behavior, although showing inelastic and time-dependent deformational behavior (Young, et al. 1998).

www.manaraa.com

3.2.3 Creep in HMA

"Everything flows," (*panta rhei*) attributed to Greek philosopher Heraclitus (approximately 520 - 460 BC), describs his ideas that everything is in a constant flow and change. Materials such as asphalt and HMA fit this concept.

HMA, like many engineering materials, exhibits a time dependent viscous property in response to applied stress. As a viscoelastic material, HMA not only responds instantaneously to applied load as a perfect elastic solid but also shows substantial viscous characteristics with time. This makes the modeling of HMA very challenging.

The rheological models of viscoelastic materials are usually composed of combinations of several basic rheological models. Hookeian models and Newtonian models are widely used. While the Hookeian model is used to capture the essence of a perfect elastic solid using a spring element, the Newtonian model seeks to represent the typical viscous fluid using a dashpot element. These combinations can result in Maxwell or Kelvin models for viscoelastic materials (Figure 3.17 and Figure 3.18).

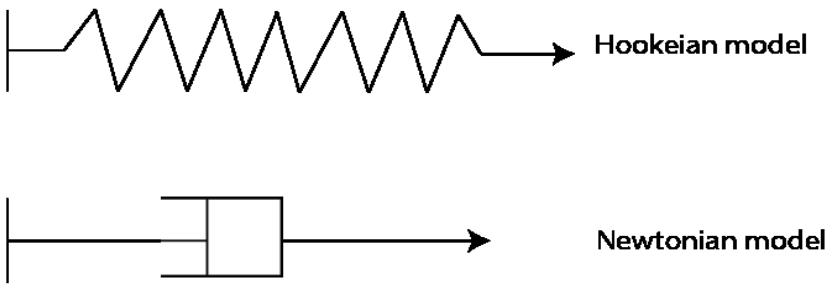

Figure 3.17 Hookeian and Newtonian models

www.manaraa.com

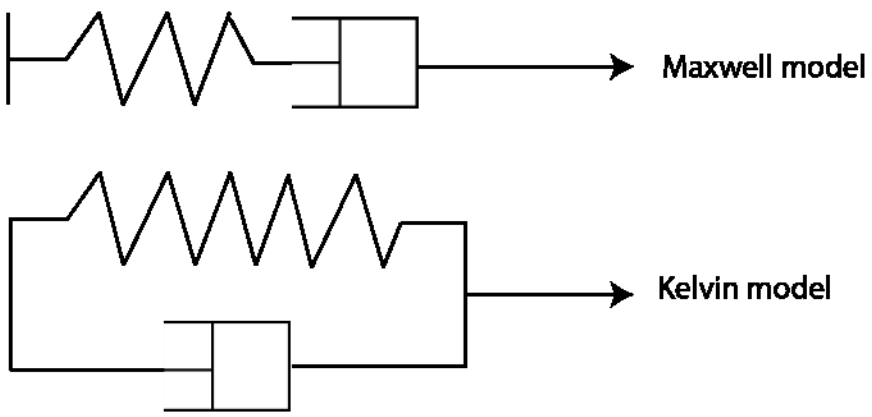

Figure 3.18 Maxwell and Kelvin models

When exposed to a long-term stress, viscoelastic materials can accumulate permanent deformation slowly. Creep is a term used in materials science that describes this phenomenon. The three stages of a typical empirical creep curve are shown in Figure 3.19. This curve can be modified to represent the effect of temperature.

www.manaraa.com

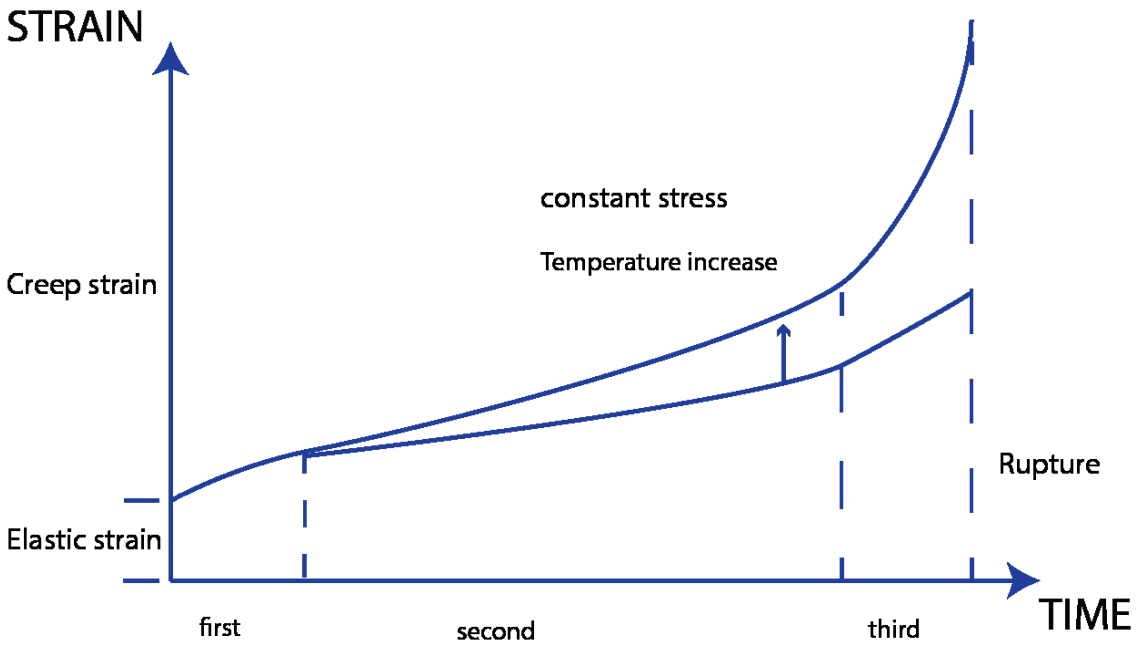

Figure 3.19 The three stages of creep strain and the temperature effect

Bailey-Norton law can capture the first and second stage of creep (Hua 2000):

$$\varepsilon = B\,\sigma^n t^{m+1} \tag{3.9}$$

Differentiating the Bailey-Norton model with time, we have:

$$\dot{\varepsilon} = A\,\sigma^n t^m \tag{3.10}$$

where $\dot{\varepsilon}$ is creep strain rate , σ is constant stress and A, m, n are empirical parameters changing with temperature (Note that $0<n<1$, and $-1<m<0$).

The creep model was successfully used in modeling HMA (Hua 2000). Hua identified two empirical creep models from the literature for modeling HMA. The models include two-term polynomial functions of stress. (Lai and Anderson 1973, Perl, Uzan and Sides 1983)

www.manaraa.com

After converting the two-term polynomial functions to single term algebraic functions using regression analysis, the two models can be expressed using the format below (Hua 2000):

$$\dot{\varepsilon} = A\,\sigma^{n} t^{m} \tag{3.11}$$

And the two models are

Lai: $$\dot{\varepsilon} = (1.03E-5)\,\sigma^{0.8477} t^{-0.75} \tag{3.12}$$

Perl: $$\dot{\varepsilon} = (0.47E-5)\,\sigma^{0.8159} t^{-0.78} \tag{3.13}$$

The A value ranges from 0.47E-5 to 1.03E-5 and n ranges from 0.82 to 0.85. m value ranges from -0.75 to -0.85.

3.2.4 Fatigue in HMA

Material fatigue occurs from repeated strain application. For example repeated pressurization of fuselage can cause fatigue failure of metal part in an airplane. The repeated application of wheel loadings can also cause fatigue in HMA. Fatigue failure is the sudden failure of a material when the accumulation of damage increases reaches a critical level. Generally speaking, all structures fail finally. Some have a longer life, while others have a shorter one. In a structure, fatigue cracking usually initiates at relatively high stress and strain areas. High stress/strain usually suggests a short fatigue life. The stress and corresponding strain amplitudes and cycles to failure for many materials follow an inverted relationship. There is an ideal threshold called endurance limit (or fatigue strength) below which the fatigue life tends to infinity. This essentially means fatigue will not or will not likely happen when the stress level stays below a

www.manaraa.com

certain level. Figure 3.20 illustrate the concept of endurance limit. For steel, this number can be around one half of its ultimate tensile strength.

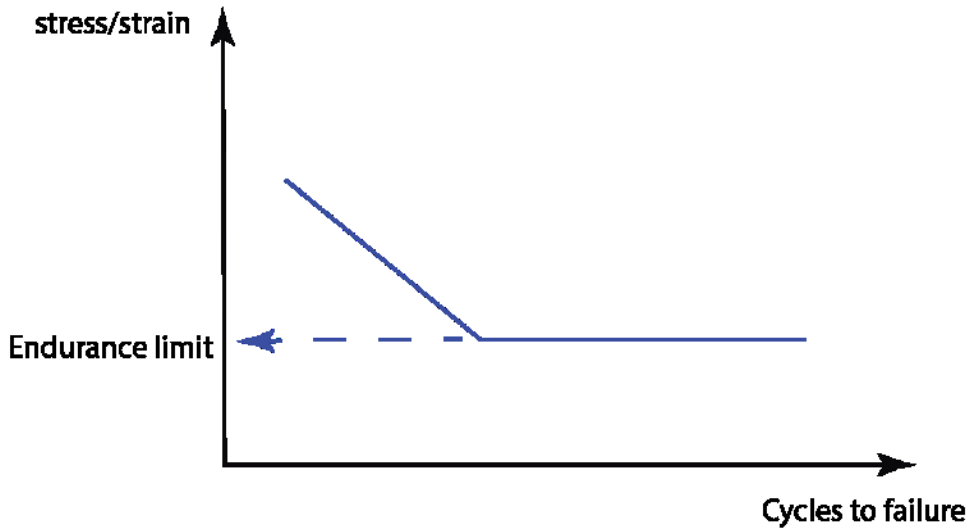

Figure 3.20 Concept of endurance limit

Pavement materials exhibit fatigue from repeated application of vehicle loads. A full capacity of truck trafficking in a year can amount to 300 million axle repetitions for roads. A more likely traffic stream for real situation would also produce around 120 million cycles of loading (Prowell, et al. 2010).

There has been significant research to demonstrate the fatigue behavior of HMA. It is found that asphalt content amount, stiffness, and HMA air-void ratio all have an effect on fatigue life (Rao Tangella, et al. 1990).

Two types of fatigue testing are generally available in the lab (Yoder and Witczak 1975): controlled amplitude stress testing and controlled amplitude strain testing. In the controlled amplitude stress testing, after repeated loading, the test specimen will

www.manaraa.com

demonstrate a decreased stiffness and an increased strain. In the controlled amplitude strain testing, the test specimen will also demonstrate a decreased stiffness and a reduced stress amplitude level due to the accumulated damage in the material. Usually, the former is more applicable to thick HMA pavements because the structural layers carry most of loading. The latter is more applicable to thin HMA pavements because strain in this case is usually governed by the underlying layers and doesn't change greatly. Figure 3.21 illustrates two types of fatigue testing (El-Basyouny and Witczak 2005).

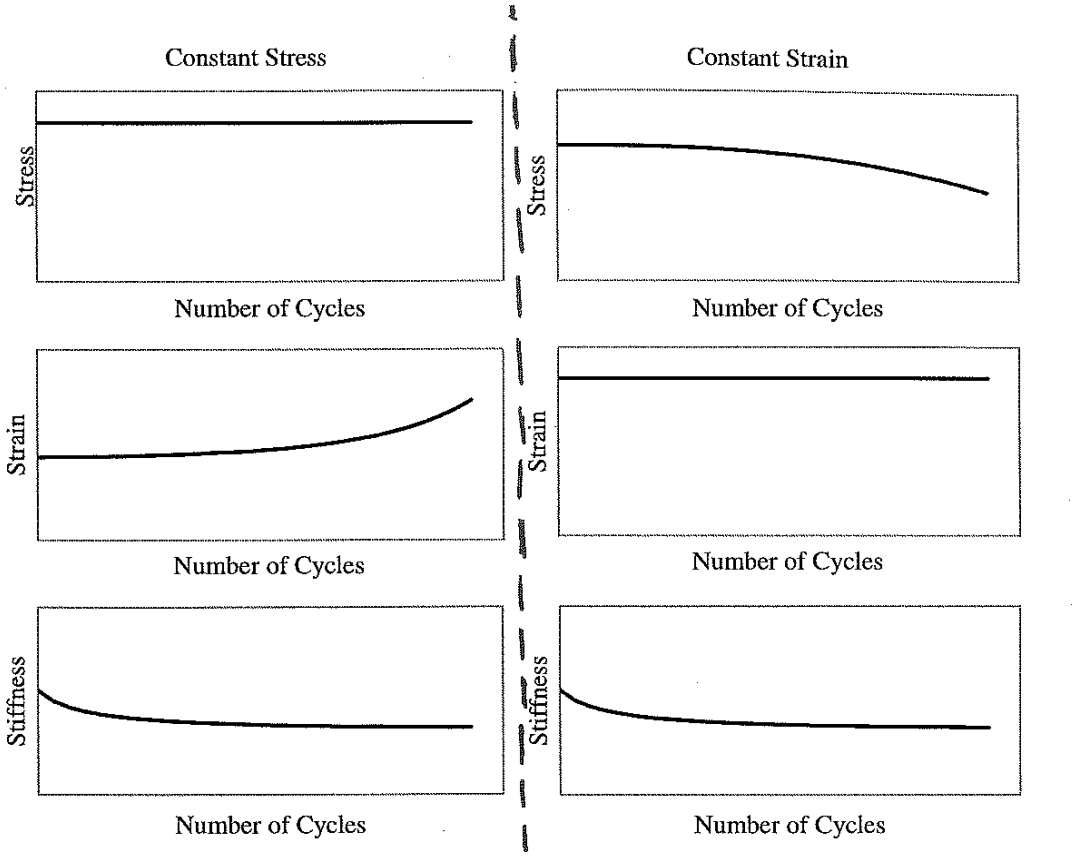

Figure 3.21 Controlled amplitude stress and strain fatigue tests (El-Basyouny and Witczak 2005)

www.manaraa.com

Fatigue models of HMA could be developed to predict the fatigue life. Most commonly, the HMA fatigue life is predicted by strain levels and material stiffness (young's modulus).

$$N_f = k_1 \left(\frac{1}{\varepsilon}\right)^{k2} \left(\frac{1}{E}\right)^{k3} \tag{3.14}$$

Here k_1 k_2 k_3 are all empirical (lab) regression coefficients.

Minor's law is used to predict the damage level.

$$D = \sum_{i=1}^{T} \frac{n_i}{N_{fi}} \tag{3.15}$$

Here D is damage level, n_i is the actual number of traffic loading repetitions, and N_{fi} is the predicted allowable number of traffic loading repetitions.

This type of model is introduced into the MEPDG (El-Basyouny and Witczak 2005). As mentioned before, efforts to identify the fatigue endurance limit of HMA has been performed in the lab and field. The Asphalt Institute (Peterson, et al. 2004) performed beam fatigue tests. They used controlled amplitude strain tests and "fatigue failure" is defined when the measured stiffness of the beam decreases to 50% of the original stiffness. The strain level affecting the fatigue life is seen in the Figure 3.22 and Figure 3.23. Carpenter, Ghuzlan and Shen (2003) also performed beam fatigue tests in the laboratory to identify the threshold value Additionally, Wills and Timm (2009) conducted an analysis of NCAT test sections to identify a field-based fatigue endurance limit.

www.manaraa.com

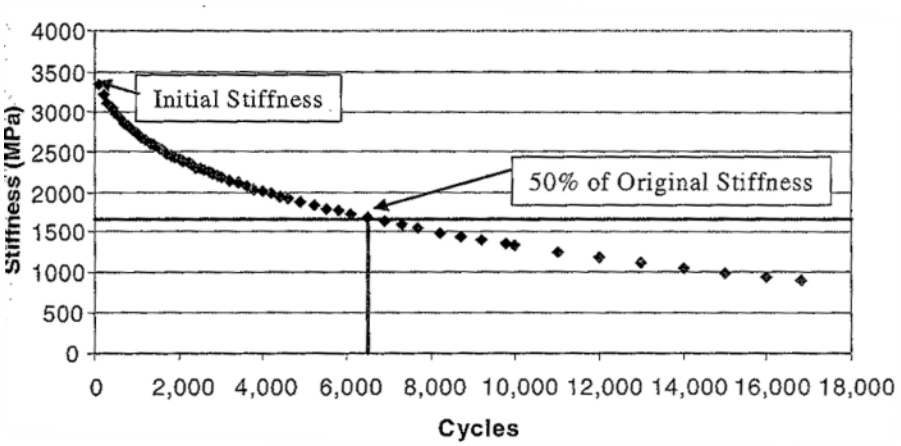

Figure 3.22 HMA fatigue test results, 800 microstrain

(Peterson, et al. 2004)

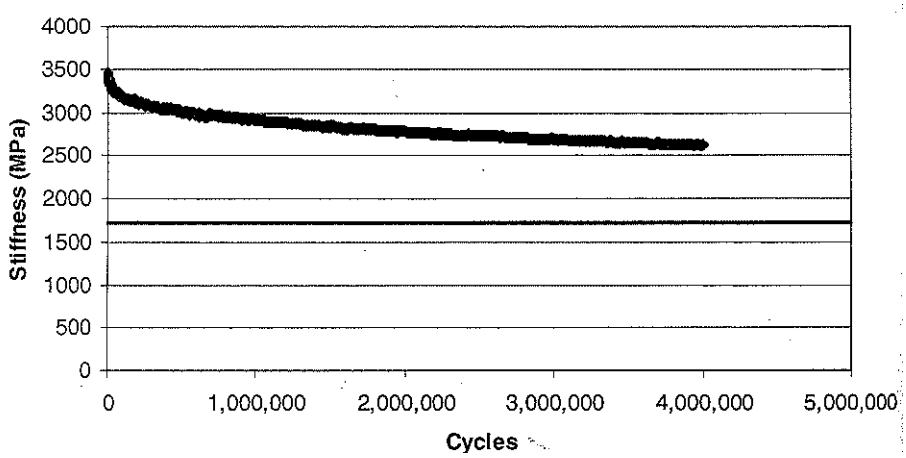

Figure 3.23 HMA fatigue test results, 70 microstrain

(Peterson, et al. 2004)

3.2.5 Temperature and Moisture Effects in HMA

HMA's physical properties are highly affected by temperature. During production, transport, and construction, it has to be maintained at a temperature around 150°C (300°F) because it has low viscosity at these temperatures which facilitates these operations.

www.manaraa.com

Once a flexible pavement is constructed, high in service pavement temperatures significantly decrease its modulus. As shown in Figure 3.24, the modulus at 30 C (86 F) is 90% lower than the one at 0 C (32 F).

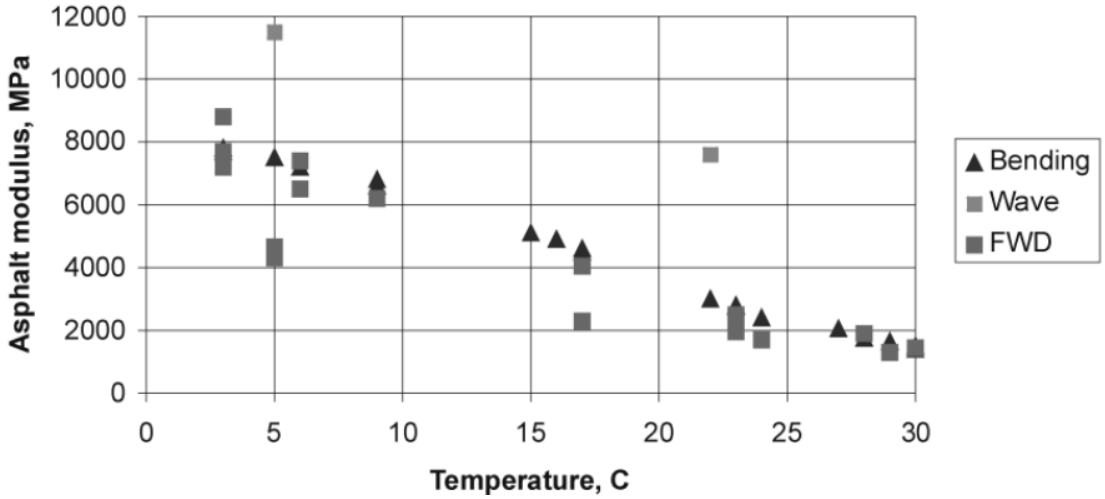

Figure 3.24 HMA moduli as a function of temperature
(Ullidtz 2002)

In a wet environment, water can accumulate in HMA. Also, in the winter time, water vapor can migrate with heat flow from warmer deep ground zones toward the cooler surface and increase moisture in pavement layers. Increased moisture not only affects the HMA modulus but also can break the bonds between the aggregate and binder. This process is known as stripping. The mechanisms of stripping include

1. Water migrates to the asphalt-aggregate interface. Heat and energy from repetitive traffic loading leads to emulsification of the asphalt cement which is then free to migrate.
2. Interfacial tension at the air-water-asphalt interface causes asphalt film coating aggregate to rupture

www.manaraa.com

3.2.6 Aging in HMA

Aging of HMA is related to age hardening of asphalt cement, which is generally caused by either combining of small hydrocarbon molecules in which oxygen is part of the enabling bonding or by volatilization (the phase change of light hydrocarbon molecules from liquid to gas). The result of aging is that HMA hardens. This age-hardening can be short or long term. Short term aging occurs during mixing, laydown, and compaction processes for HMA. Volatilization occurs during these processes. Long term aging occurs with time during the HMA pavement's service life (Galal, White and Hand 2000).

The age-hardening increases the HMA stiffness. In turn, the increased stiffness can reduce pavement rutting. However, the increased stiffness can reduce the fatigue life of HMA.

www.manaraa.com

CHAPTER IV

NCAT TEST TRACK STRUCTURAL STUDY

4.1 Overview

The NCAT Pavement Test Track contains multiple phases. It was originally built in 2000 in Opelika, Alabama as a full-scale, two-lane, closed-loop accelerated loading facility as shown in Figure 4.1. It was funded by a number of government agencies and industry sponsors. It includes forty six 200-foot-long pavement sections. The approximate rate of traffic application is 5 million equivalent single axle loads (ESALs) per year (Taylor and Timm 2009). A snapshot of truck trafficking is shown in Figure 4.2.

Figure 4.1 View of the NCAT test track

(Taylor and Timm 2009)

www.manaraa.com

Figure 4.2 Truck on the test track

(Willis, et al. 2009)

The first phase started in 2000 and ended in 2002. With some reconstruction of the pavement sections from phase 1, the second phase testing started in 2003 and ended in 2005. After the second phase was completed, 22 sections were milled or removed down to the subgrade for construction of the third phase. Trafficking on Phase 3 began in November 2006 and ran until December 2008.

Phase 3 features two large-scale studies: the mixture performance study and the structural study. In Phase 3, five sections were left in-place from second phase (N3 through N7) while six sections were reconstructed. The Sections N1 and N9 out of these six sections are of special interest to this thesis.

In the test sections of Phase 3, different types of unbound materials are utilized as base and subgrade for the structural study. For example, the materials used include lime rock from Florida, granite aggregate from Vulcan Inc, limestone from Missouri, and test

www.manaraa.com

track soil from Alabama and seale soil from Oklahoma. Objectives in the structural study include (Timm 2009):

- Verify the mechanistic models for pavement analysis
- Validate transfer functions for mechanistic-empirical design
- Recommend method for mechanistic characterization of material properties
- Determine field-based fatigue response thresholds for perpetual pavements

4.2 Sections N1 and N9

The compositions of layers of sections N1 and N9 can be seen in Figure 4.3 (Taylor and Timm 2009).

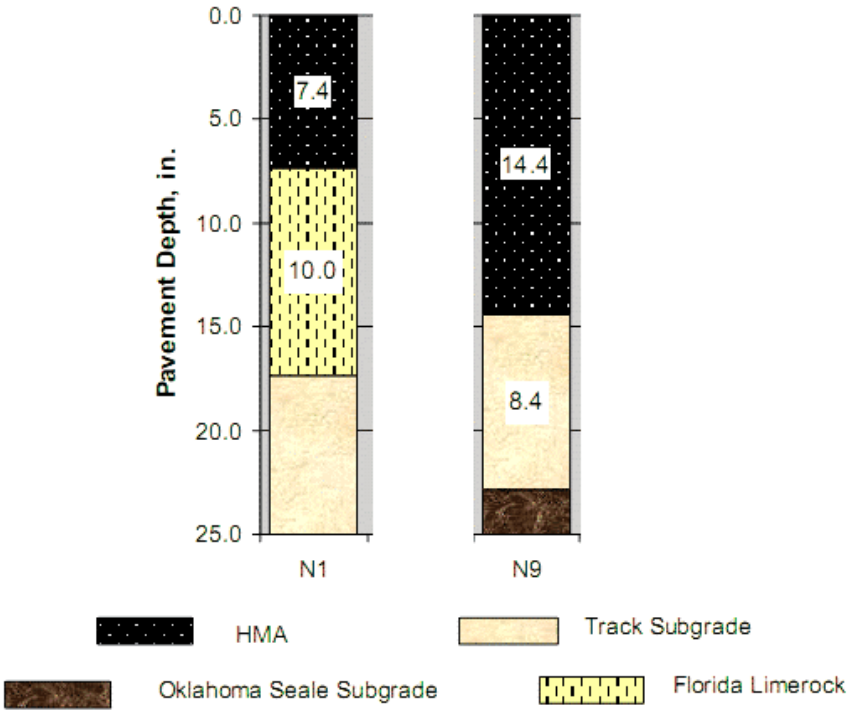

Figure 4.3 The layer thickness and materials of section N1 and N9 (Taylor and Timm 2009)

www.manaraa.com

The test section N1 was sponsored by the Florida Department of Transportation (FDOT). It consists of 7.4 inches of HMA as the surface layer and 10 inches of limerock base as the base layer.

The test section N9 was sponsored by the Oklahoma Department of Transportation (ODOT). This is the thickest sections in the study and was built to study the perpetual pavement concept. N9 consists of 14.4 inches of HMA which includes a rich bottom layer. The rich bottom layers are essentially the same mixture with higher asphalt content and lower air voids (2%).

The HMA binder grade, mix gradation, asphalt content, air void content and density for test sections N1 and N9 are summarized in Table 4.1 and Table 4.2. The unbound base and subgrade material gradations, densities and moisture content are summarized in Table 4.3 and Table 4.4.

Table 4.1 The HMA layer components and properties for test sections N1 and N9

Layers	Binder Grade & Gradation Type	Asphalt Content %	Air Voids %	Depth (in.)
N1-1	67-22 Dense	4.9	2.7	2.2
N1-2	67-22 Dense	4.9	4.2	1.9
N1-3	67-22 Dense	4.6	5.9	3.3
N9-1	76-28 SMA	7.0	4.9	2
N9-2	76-28 Dense	5.1	3.0	3.5
N9-3	64-22 Dense	5.0	3.4	3.1
N9-4	64-22 Dense	4.6	3.8	2.6
N9-5	64-22 Dense	7.1	1.7 rich bot	1.9

(Timm, 2009)

www.manaraa.com

Table 4.2 The HMA layer density for test sections N1 and N9

Density	
N1	N9
145.6 pcf	144 pcf
OR 2332 kg/m^3	OR 2306 kg/m^3

(Taylor and Timm, 2009)

Table 4.3 The Unbound layer material gradations for N1 and N9

Percent Passing Sieve		
Sieve Size	Limerock Base (N1)	Track Soil (N1, N9)
1 ½'' (38 mm)	100	100
1'' (25.4 mm)	100	83
3/4'' (19 mm)	100	81
1/2'' (12.5 mm)	88	78
3/8'' (9.5 mm)	81	75
#4 (4.76 mm)	61	71
#8 (2.38 mm)	44	68
#16 (1.19 mm)	32	66
#30 (0.595 mm)	26	64
#50 (0.297 mm)	23	61
#100 (0.149 mm)	21	56
#200 (0.074 mm)	18.8	48

(Taylor and Timm, 2009)

www.manaraa.com

Table 4.4 The Unbound layer material in-situ densities and moisture content for test sections N1 and N9

Wet Density	
Limerock Base (N1)	Track Soil (N1, N9)
127 pcf	132 pcf
OR 2034 kg/m^3	OR 2114 kg/m^3
Moisture Content	
Limerock Base (N1)	Track Soil (N1, N9)
11.9%	11%

(Taylor and Timm, 2009)

4.3 Instrumentation

Each section had 12 strain gauges at the bottom of the asphalt layers, two earth pressure cells and four thermistors at different depth of pavement layers. Twelve CTL Strain gauges (Figure 4.4) were installed in a 3 by 4 array in the outside wheel paths. They measure both the longitudinal and transversal stains at the bottom of the HMA layer (Figure 4.4 to Figure 4.6). The three gauges arranged in a row are to capture the effect of wheel-wander effects.

www.manaraa.com

Figure 4.4 Strain Gauge

(Taylor and Timm 2009)

www.manaraa.com

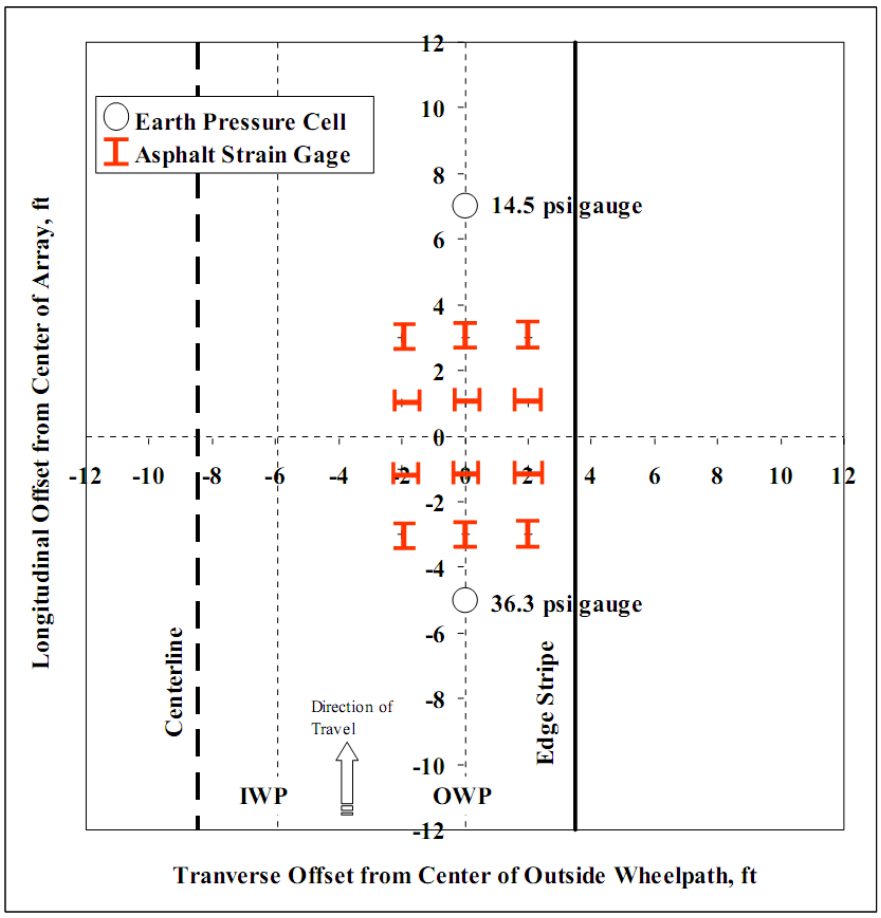

Figure 4.5 Strain Gauge Arrangement—2D View

(Willis and Timm 2009)

www.manaraa.com

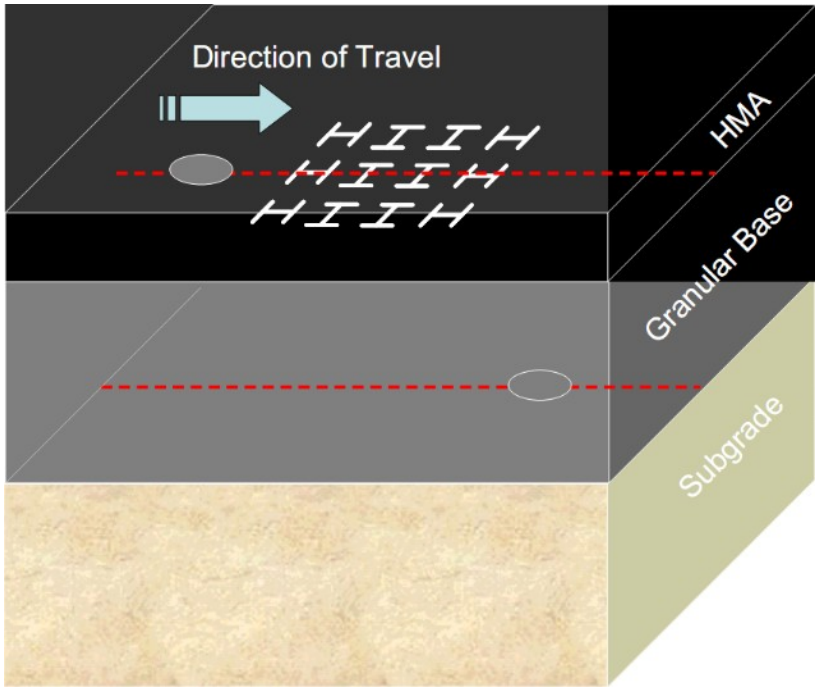

Figure 4.6 Strain Gauge Arrangement—3D view

(Taylor and Timm 2009)

Two Geokon pressure plates were used to measure vertical pressure at the top of base and subgrade layer. The locations are shown in Figure 4.5 and the gauge is shown in Figure 4.7. Thermistors were used to measure temperature and are shown in Figure 4.8. Three were installed for the HMA layer, with one at the surface, one at mid-depth and one at the bottom. One more was installed 3 inches below the HMA layer (Taylor and Timm 2009).

Section N9 was partially funded by the FHWA to install extra strain gauges and thermistors to study the pavement response and temperature with depth. The instrumentation of N9 is shown in Figure 4.9.

www.manaraa.com

Figure 4.7 Earth pressure cell

(Taylor and Timm 2009)

Figure 4.8 Thermistors

(Taylor and Timm 2009)

www.manaraa.com

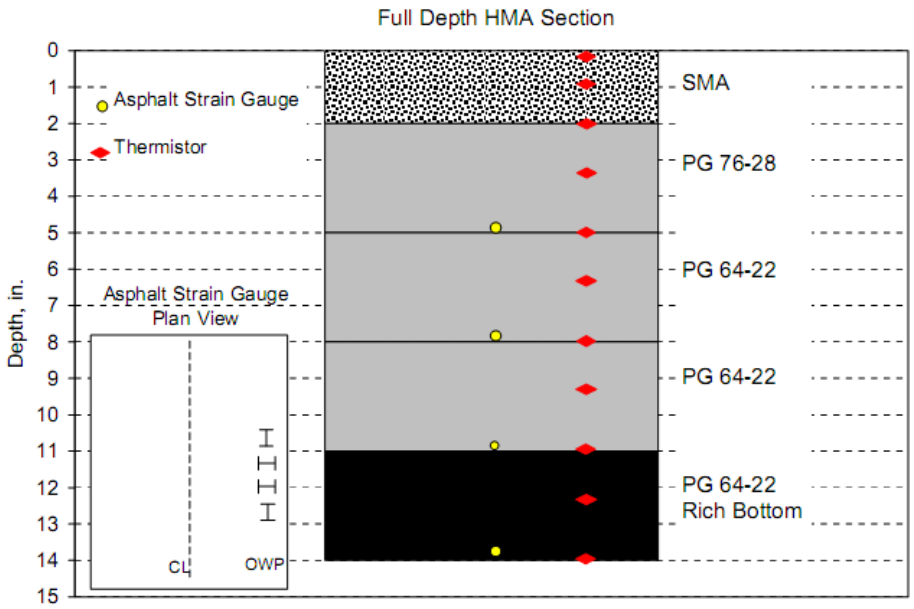

Figure 4.9 Section N9's Supplemental Instrumentation

(Timm 2009)

4.4 Test Track Truck Configuration

Four triple flat-bed trailer trucks and one triple box trailer were used to apply traffic in the 2006 test sections. These tractors were also used at WesTrack, which is a multimillion dollar accelerated pavement test (APT) facility located on Nevada Automotive Test Center (NATC) near Reno, Nevada (Westrack 1999). The difference is that the tractors at WestTrack were driverless and at NCAT the tractors were driver operated. Typically traffic was applied from 5:00 am until 10:40 pm Tuesday through Saturday. The trucks are shown in Figure 4.10. Each truck has eight axles in total, which include one steering axle, two tandem axles, and five single axles. The average axle weights are shown in Table 4.5. Average traffic speed was 45 miles per hour (20 m/s). The axle spacing of the truck is shown in Figure 4.11.

www.manaraa.com

Figure 4.10 The triple flat-bed trailer and box trailer.

(Willis and Timm 2009)

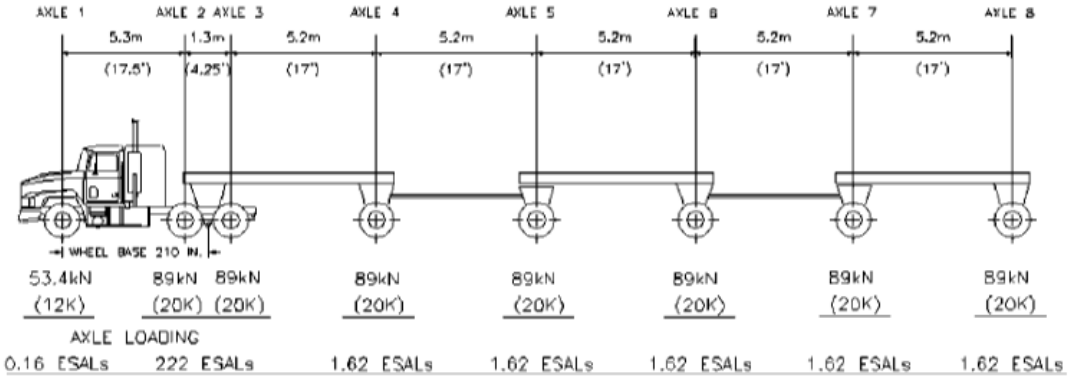

Figure 4.11 The axle spacing of the truck

(Westrack 1999)

Table 4.5 Average axle weight

Axles	Steer	Tandem1	Tandem2	Single1	Single2	Single3	Single4	Single5
weight (klbs)	10.6	20.3	20.3	20.8	20.8	21.3	20.6	20.6

(Willis and Timm 2009)

4.5 Strain Data

Strain data for a complete tractor-trailer unit in two seasons of the year are shown in Figure 4.12 and Figure 4.13.

www.manaraa.com

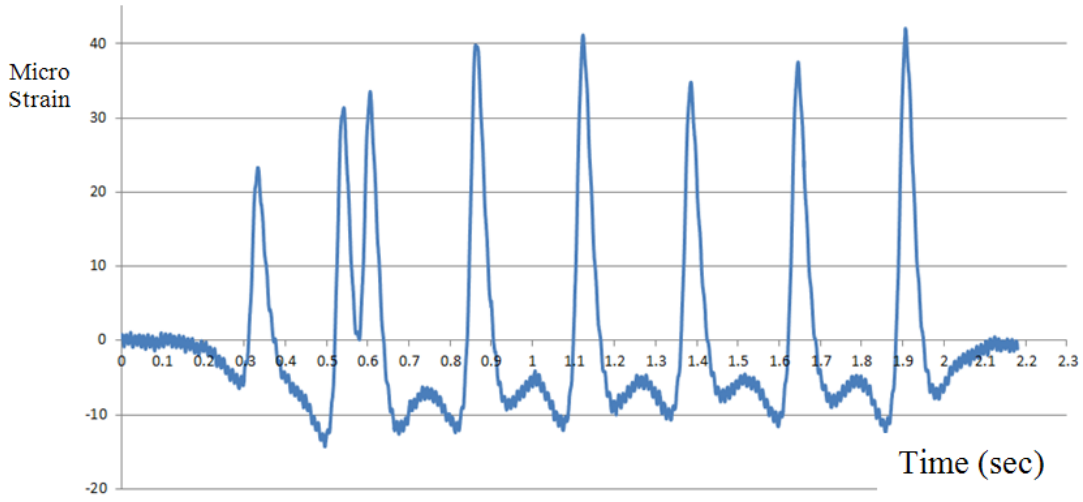

Figure 4.12 Strain data for N9 during 2006 winter afternoon

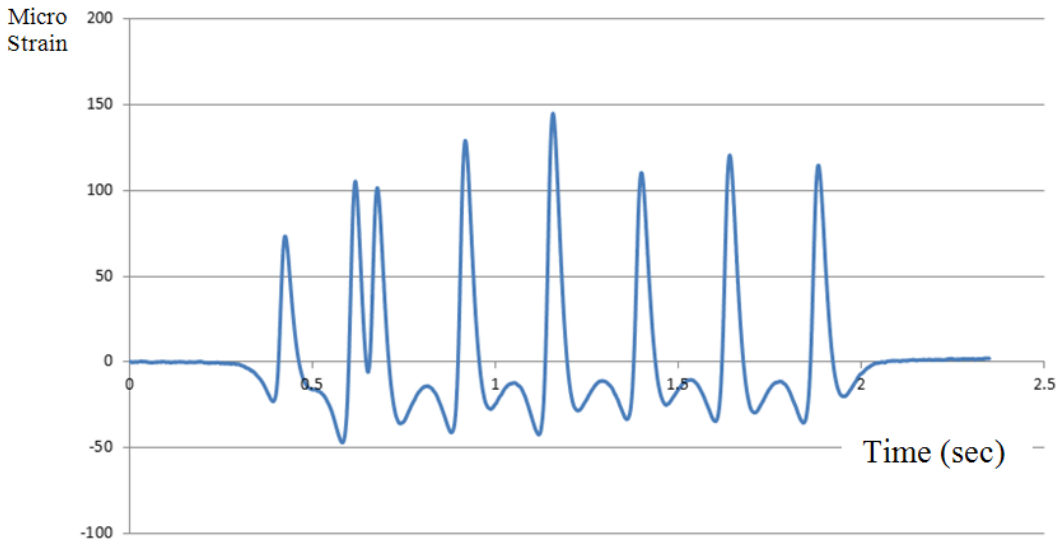

Figure 4.13 Strain data for N9 during 2007 summer morning

www.manaraa.com

CHAPTER V

FINITE ELEMENT MODELING FOR PAVEMENTS

The pavement models are built using Abaqus (Abqus 2009). In this section, the basic components of the modeling process are introduced.

5.1 ABAQUS

Abaqus is a powerful commercial FEA software that can be used to solve complex engineering problems in many different disciplines. In Abaqus, a model can be built using a graphical interface (GUI), which will yield a ".cae" and a ".inp" file. Or it can be built by making an input file using a command line interface (CLI). The graphical interface contains 11 modules, for example, Part, Property, Assembly, Step, Interaction, Load, Mesh, etc. (See Figure 5.1).

Modifying the model can be done in GUI or simply by editing the input file. The input file contains keyword lines, data lines and comment lines. Keyword lines usually have parameters. Each parameter has a value and is divided by a comma. For example, a complete file usually includes PARTS, MATERIALS, INTERACTIONS, BOUNDARY CONDITIONS, STEP, LOADS (based on step), etc (Abaqus, 2009).

Every command in Abaqus can also be created using Python scripting (Abaqus 2011). Scripts can be effectively used to perform repetitive tasks and save time. Also, scripts can be used to simulate multiple changes of a model more easily. The scripts can

www.manaraa.com

be written to create a part, property, assembly, step, interaction, load, mesh, etc. It can also be used to perform post processing and visualization of the modeling results. Figure 5.2 illustrates how the different ways of scripting interface commands interacts with Abaqus/CAE kernel.

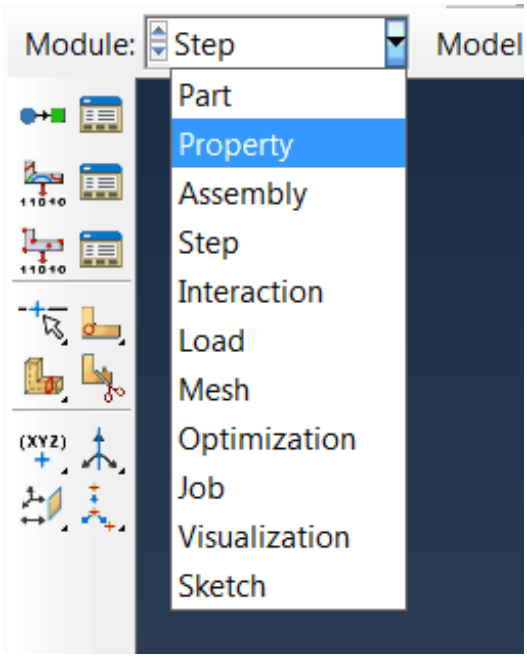

Figure 5.1 Modules in Abaqus

www.manaraa.com

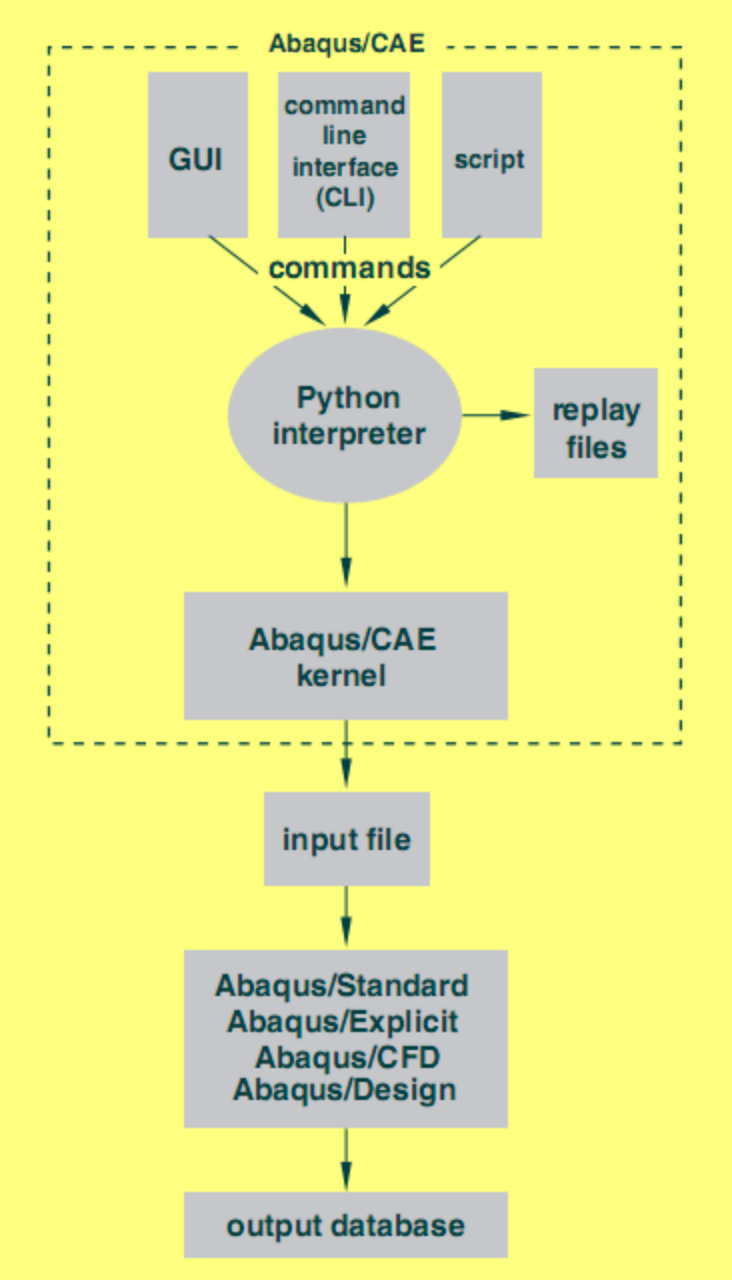

Figure 5.2 Abaqus Scripting Interface commands and Abaqus/CAE (Abaqus, 2009)

5.2 Part Geometry

For the conventional pavement sections of N1, three parts were modeled, i.e. HMA layer, Florida limerock layer, and soil subgrade layer. For the thicker pavements of

www.manaraa.com

section N9, two parts were modeled here, i.e. HMA layer and the soil subgrade layer. The model geometries are shown in Figure 5.3, Figure 5.4 and Figure 5.5.

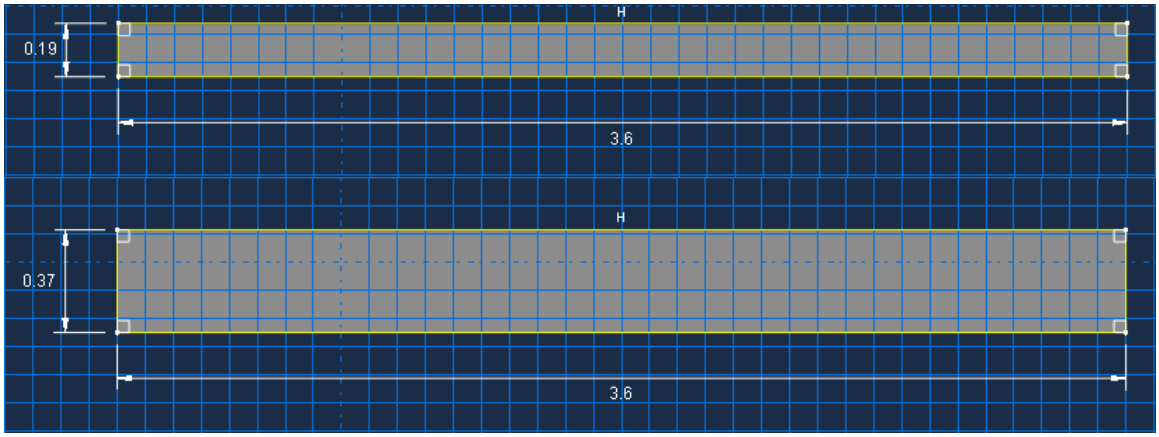

Figure 5.3 The HMA layer dimension for N1 and N9 sections.

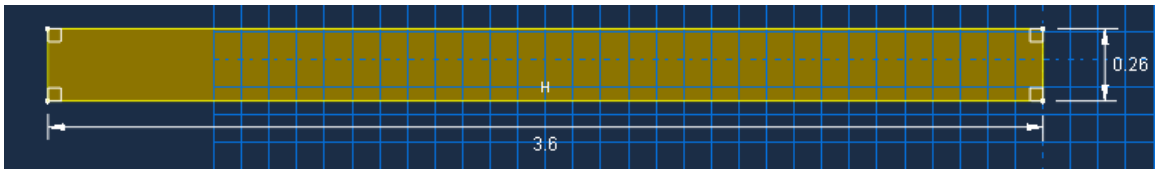

Figure 5.4 The base layer dimension for N1 section.

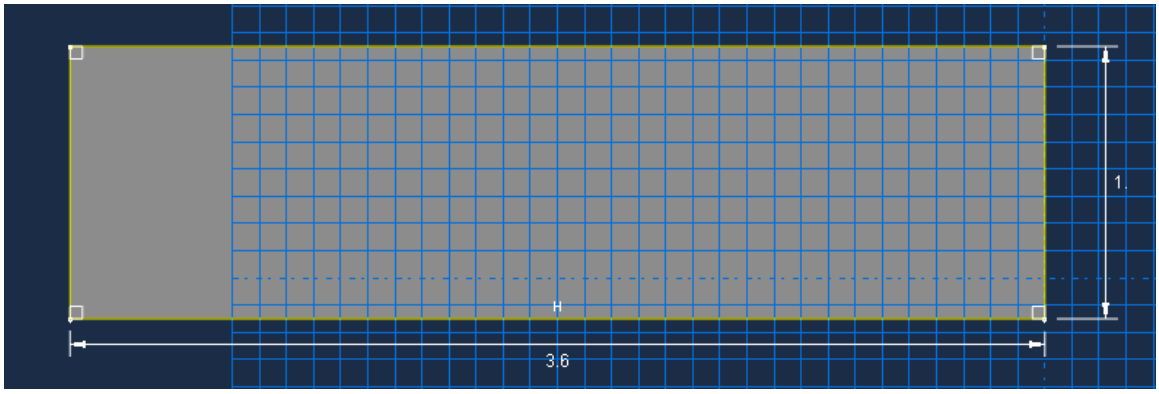

Figure 5.5 The subsoil layer dimension for N1 and N9 sections.

www.manaraa.com

As shown in Figure 4.5 in the previous chapter, the top part is partitioned to capture four wheel paths trafficked by the testing truck. The tires on the truck are 295/75 R22.5. Here "295" indicates the tire width is 295 mm. 75 shows that the distance from the bead to the top of the tread is 221 mm (295 x0.75). "R 22.5" indicates the wheel size rather than the tire size. R and half-inch sizing of wheel means it's for tubeless, radial truck tires, number after R shows diameter of wheel is 571 mm (22.5 inches). The tire pressure was 100 psi (equivalent to 700000 Pascal). Since the axle weight of the truck is around 20, 000 lbs, per tire is 5000 lbs. The approximate tire contact area is estimated as 50 square inches (divide wheel load by tire pressure). In this research, because steering axle has smaller values and does not produce worst results, only the single axle was simulated. Based on the data from NCAT, the tire print is estimated as 280 mm (or 11 inches) in the transverse direction and 100 mm (or 4.1 inches) in the longitudinal direction. These dimensions will guide the part geometry construction shown in Figure 5.7 and Figure 5.8. Each partition corresponds to a single tire contact area.

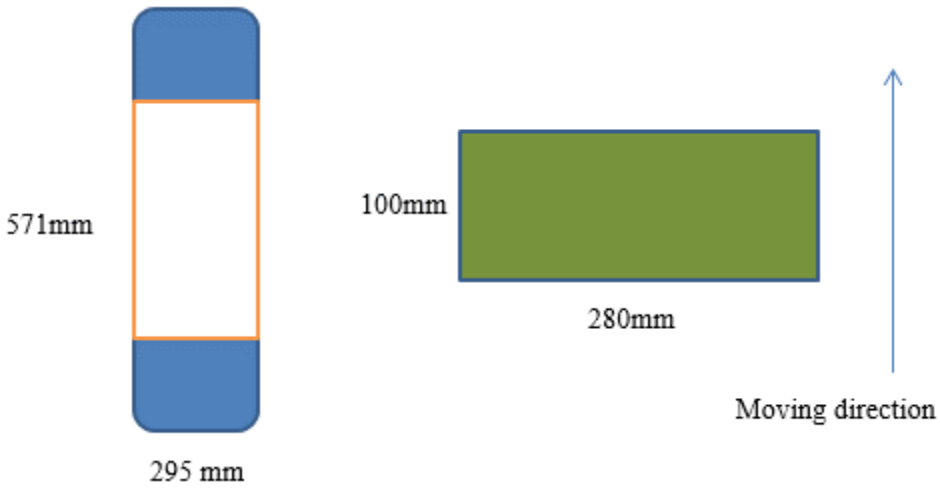

Figure 5.6 Tire (elevation from rolling direction) and tire print (plane) dimensions

www.manaraa.com

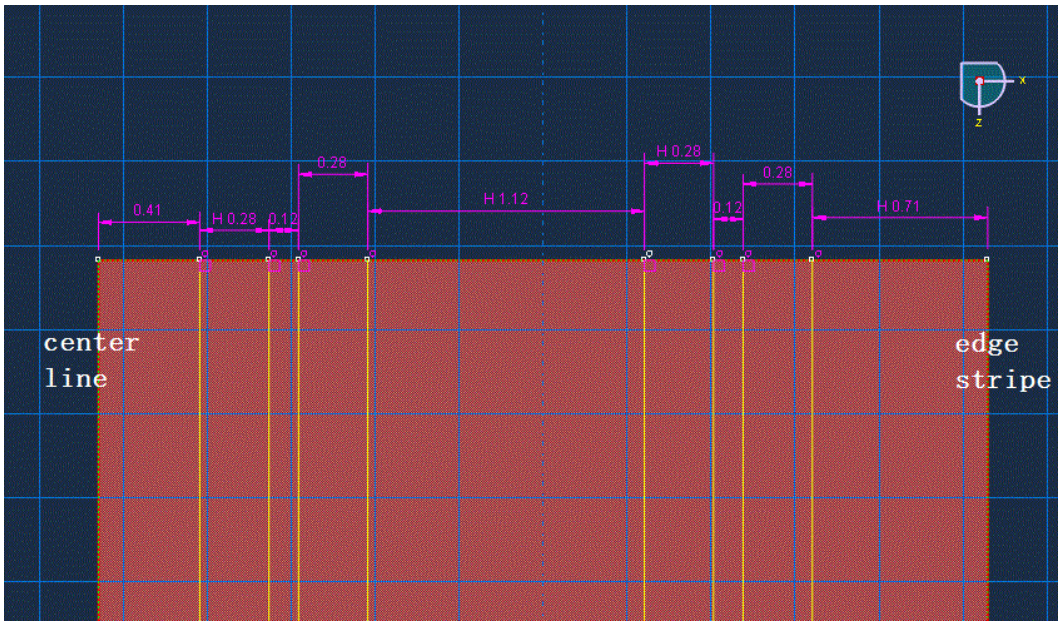

Figure 5.7 Four wheels paths with center line and edge stripe

(Unit: m)

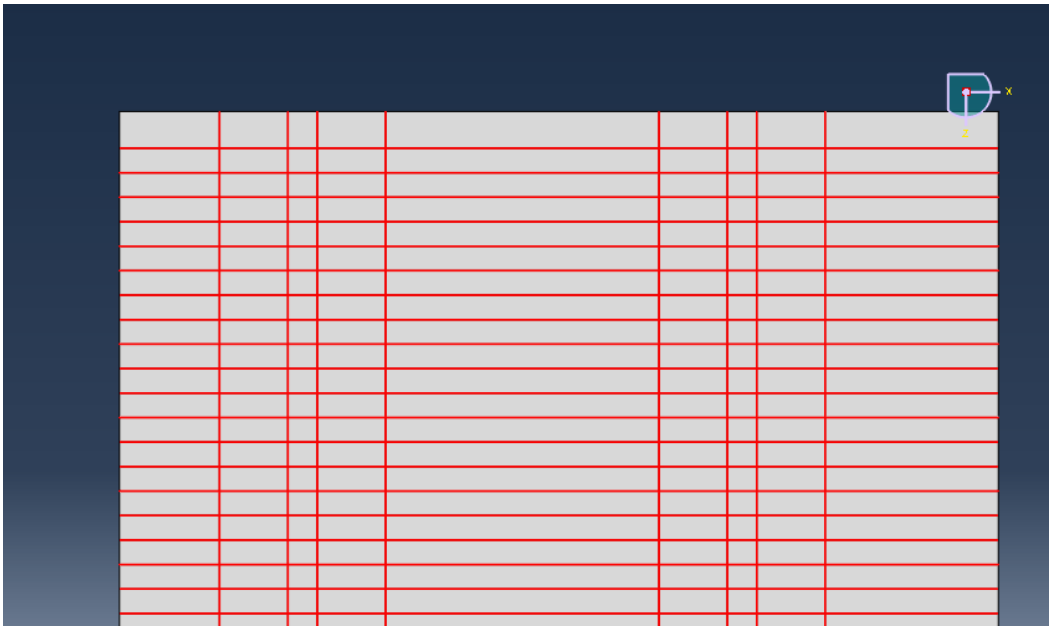

Figure 5.8 The partition of HMA layers based on the actual wheel paths

www.manaraa.com

5.3 Materials

The materials modeled include HMA, aggregate, and soil. All the materials used in the model are assumed to be homogeneous and isotropic. Density, Young's modulus, Poisson's ratio, and viscoelastic and plasticity parameters were used to characterize HMA, aggregate, and soil. Solid homogeneous sections were used to model the continuum layers. In Abaqus, sections contain material's property and part contains geometry. For three different layers, three sections were applied to the corresponding parts after their types and materials were defined in Abaqus.

There are several test methods to determine pavement layers' elastic parameters Triaxial tests are the most common tests for soils. For asphalt layers, bending tests in a lab can be used to find the material modulus. Also, deflection tests such as the Falling Weight Deflectometer (FWD) are popular in situ tests used to back-calculate the pavement layer moduli.

As discussed before, the asphalt's property is affected by gradation, binder content, and temperature. A series of FE runs were made to evaluate properties from NCAT Test Track reports and several other sources (Kassem, Grasley and Masad 2013, Maher and Thomas 2008, Das 2008), the best estimate of the material property is listed in the Table 5.1, Table 5.2 and Table 5.3.

www.manaraa.com

Table 5.1 Asphalt properties

	International System	US System
Density	2300 kg/m^3	144 pcf
Young's modulus	2x10^9 Pa	300000 psi
Poisson's ratio	0.3	0.3
Creep model		
A	5x10^{-5}	5x10^{-5}
n	0.8	0.8
m	-0.7	-0.7
cohesion	2E5 Pa	30 psi
Friction angle	50 degree	50 degree

Table 5.2 Soil properties

	International System	US System
Density	2000 kg/m^3	125 pcf
Young's modulus	2x10^7 Pa	3000 psi
Poisson's ratio	0.4	0.4
cohesion	5000 Pa	0.75 psi
Friction angle	30 degree	30 degree

For section N1 only

Table 5.3 Aggregate Properties

	International System	US System
Density	2300 kg/m^3	144 pcf
Young's modulus	2x10^8 Pa	30000 psi
Poisson's ratio	0.35	0.35
cohesion	E5 Pa	15 psi
Friction angle	40 degree	40 degree

5.4 FE Steps and Analysis

In setting up the FE Analysis, there are three steps that were used to frame the analysis: INITIAL, GRAVITY, and WHEEL. In the first step INITIAL, boundary

www.manaraa.com

conditions were set up. In GRAVITY, the whole pavement structure is subjected to universal gravitation. In this step, two interactions were also created. For conventional pavements, i.e. three are interfaces between HMA layer and base layer and between the base layer and soil layer. Only one interface exists for perpetual pavement. See Figure 5.9 and Figure 5.10. At the interfaces, friction is allowed and the tangential behavior is assumed to happen in the interfaces with friction coefficient is assumed to equal to 0.5. In WHEEL step, the wheel loadings are defined loadings. It is worth noting that in Abqus the boundary conditions were propagated to the second and third step, while gravity loading and interactions were propagated to the third step. The step time varies in different models and steps. The first two steps use the default values and the third step uses the actual time. When analyzing, it usually starts with a small fraction of the total time and continues until the ending of the events.

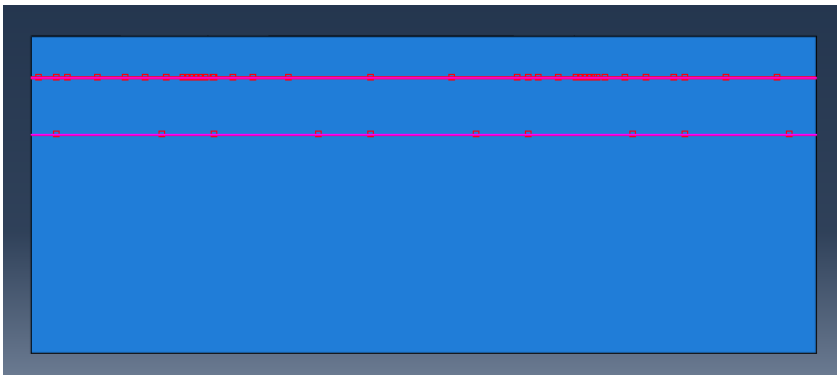

Figure 5.9 Interaction for conventional pavement

www.manaraa.com

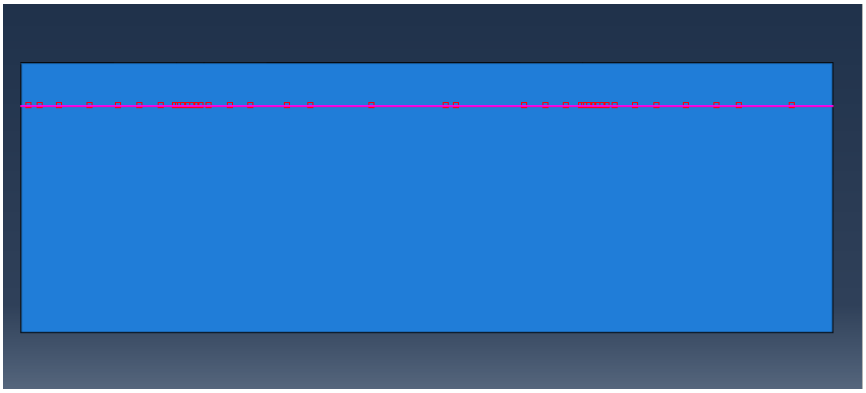

Figure 5.10 Interaction for perpetual pavement

Each step in an Abaqus analysis is divided to increments. In this research, both automatic time incrementation and fixed time incrementation are used. In Abaqus, Newton's method is used to solve nonlinear equilibrium equations. It's an iterative algorithm used to find the root of an equation or system of equations. In each increment, iterations are needed to obtain equilibrium. This incrementation and iteration process help to solve complex nonlinear problems. In either linear or nonlinear analyses, the solution of large-scale systems of linear equations (LE) is a challenging task. Direct or iterative solvers can be used in Abaqus to solve the systems. The direct LE solver (out-of-core algorithm) uses the Gauss elimination method as the analysis basis and can yield exact solutions for the equations. This method is the most suitable for beams, trusses and shells, which can produce sparse stiffness matrices. In Abaqus, the iterative method (in-core-algorithm) uses a domain-decomposition based analysis technique and may have convergence problems. This method could take less time for large blocky structures but could consume significant memory (Abaqus 2009). In this research, since the direct

www.manaraa.com

method produced good performance after some trial runs, all the analysis uses the direct sparse solver as the analysis method.

5.5 Elements

There are many types of elements to choose in Abaqus. For example, 1-D elements like truss and beam elements, 2-D elements like membrane and shell elements, 3-D solid continuum elements as shown in Figure 5.11 (Abaqus 2009). Due to the geometry and complexity of loading of real pavements, three dimensional solid continuum elements defined in the global X, Y, Z space are chosen in this research. Specifically, a linear brick element with 8-nodes is used in the mesh covered in the next section. See Figure 5.12. In Abaqus, displacements are calculated at the nodes of the element and interpolated between nodes. Stresses and strains are evaluated at the integration points and then interpolated and averaged in nodes. All the elements of the model are based on a Lagrangian formulation.

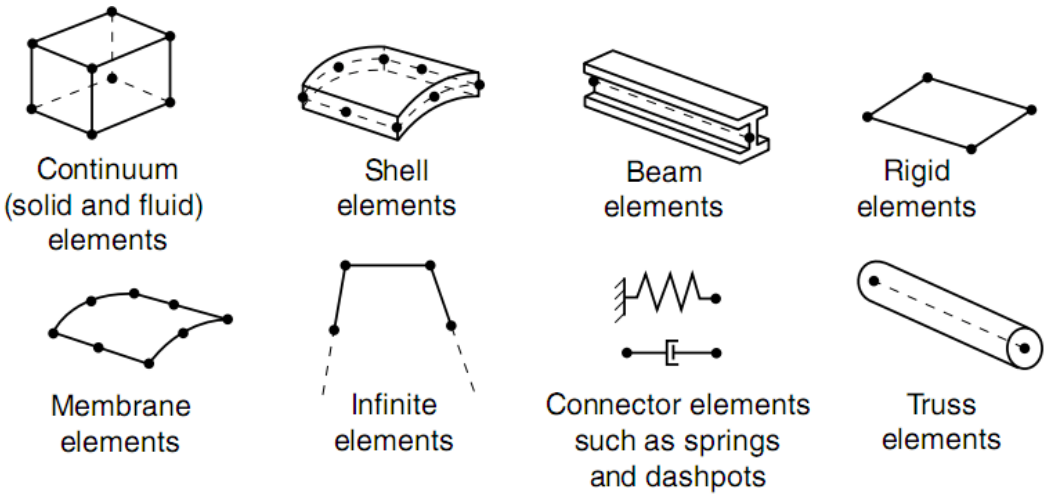

Figure 5.11 Element types in abaqus

(Abaqus 2009)

www.manaraa.com

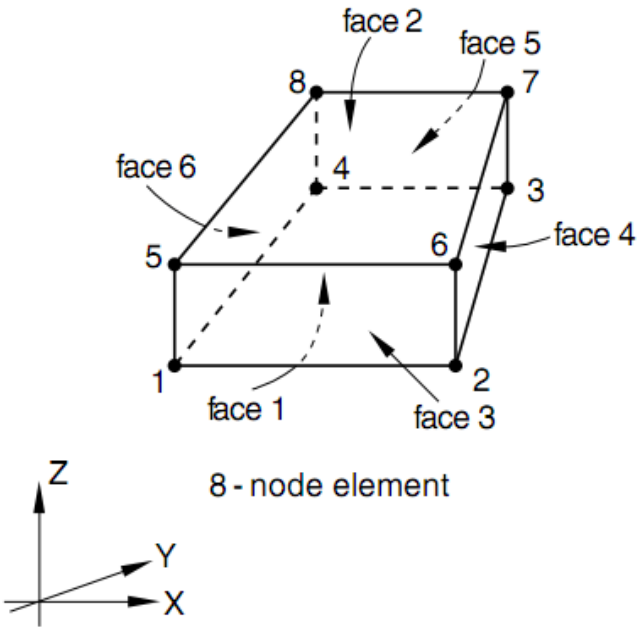

Figure 5.12 A linear brick element with 8 nodes

(Abaqus 2009)

5.6 Meshes

The steps in building a mesh include partitioning and seeding. Partitioning can assist the seeding process. For the HMA layers, the meshes are based on the partitions and the local seeds along the depth of the HMA layers. Due to the complexity of loading at the surface of the pavements, single bias seeding is adopted to ensure denser elements at the top of the pavements. There are six elements along the depth with the bias ratio equal to 2. See Figure 5.13.

For other layers, evenly distributed seeding was adopted. This will result in equal edge lengths of elements. Along the vertical directions, the base layer for N1 and the subgrade for N1 and N9 are seeded evenly with three and six elements respectively. In the transverse horizontal direction, there are six elements. In the longitudinal horizontal

www.manaraa.com

direction, there are ten elements. The seeding and meshes are shown in Figure 5.14 to Figure 5.16. Please refer to section 5.2 for the dimensions of these meshes.

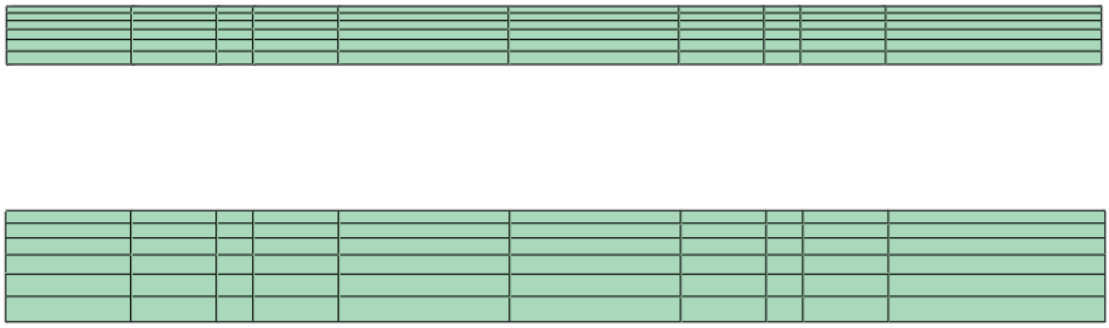

Figure 5.13 The mesh size of the asphalt sections.

Top N1. Bot N9.

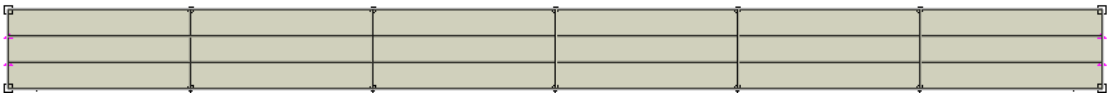

Figure 5.14 Seeding for the base layer of N1

www.manaraa.com

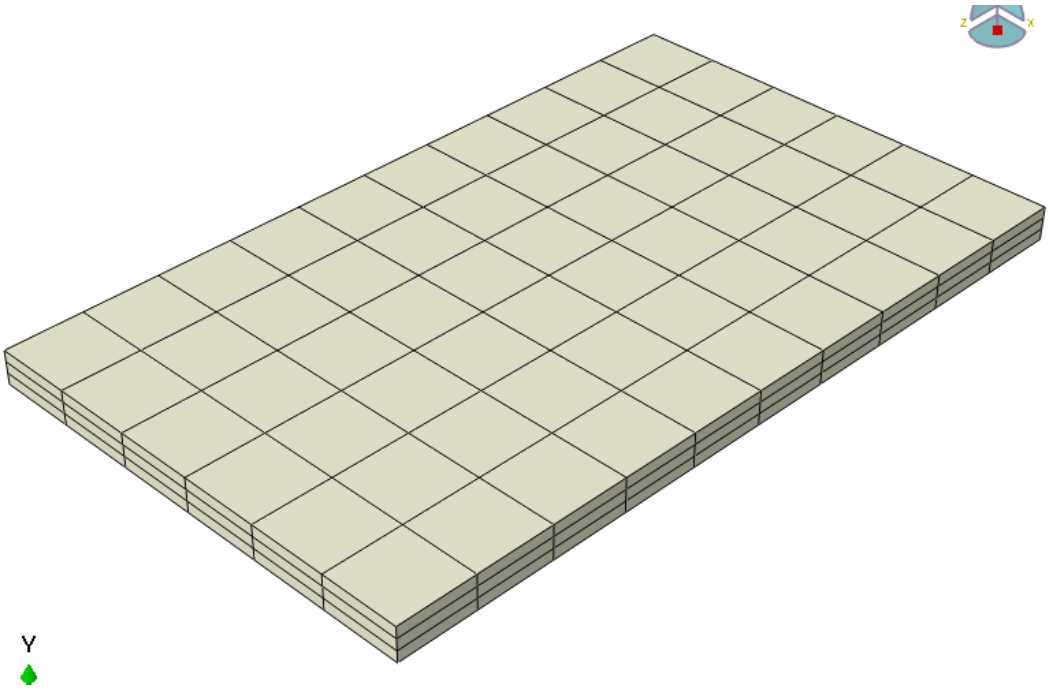

Figure 5.15 Meshes for the base layer of N1

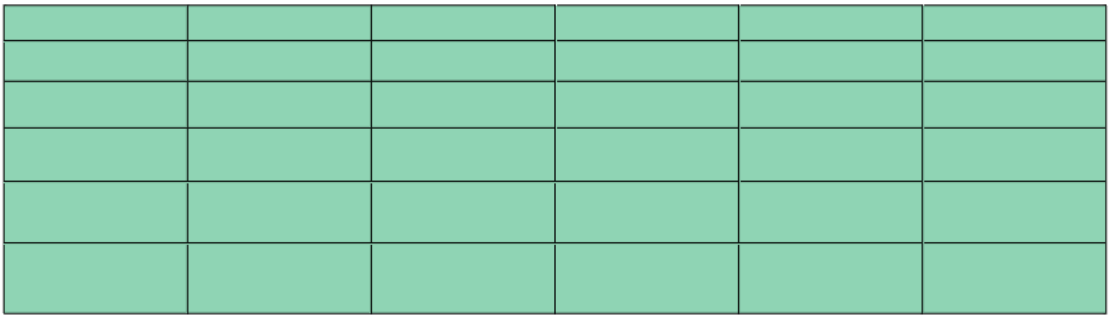

Figure 5.16 The mesh size of the soil foundations

5.7 Load and Boundary Conditions

In the analysis, gravity is applied as a body force at the whole model. The value is simply the pavements and the foundations' weight, which is calculated by Abaqus provided the gravity acceleration is provided. The duration is the default step time in

www.manaraa.com

Abaqus. The gravity loading amplitude verse time curve is seen in Figure 5.17. Wheel loading is applied as surface pressure on one element in the track and the amplitude value is 70000 Pa (single axle loading in the test sections). To simulate the moving effect of the wheel, a trapezoid-shaped amplitude curve was used (Figure 5.18). According to the speed of the truck (20 m/s) and the element length (100 mm), the time that the wheel applied on one element is estimated as 0.005 second.

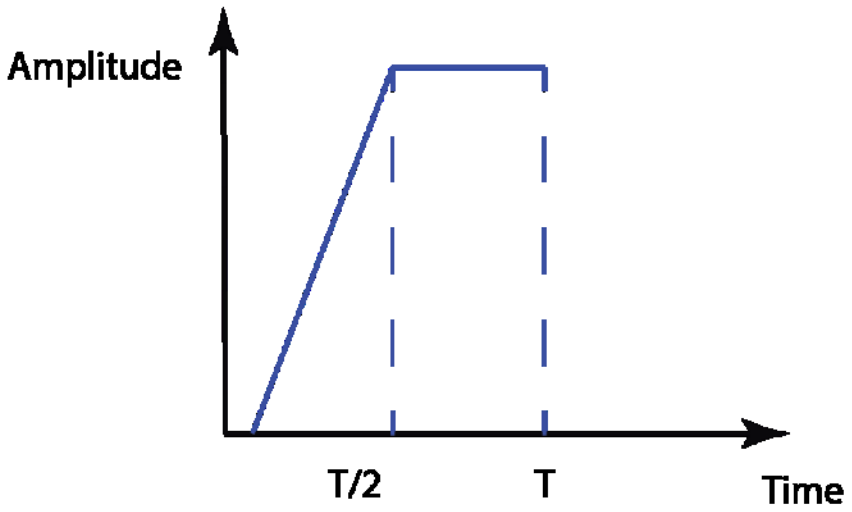

Figure 5.17 Loading amplitude for gravity

www.manaraa.com

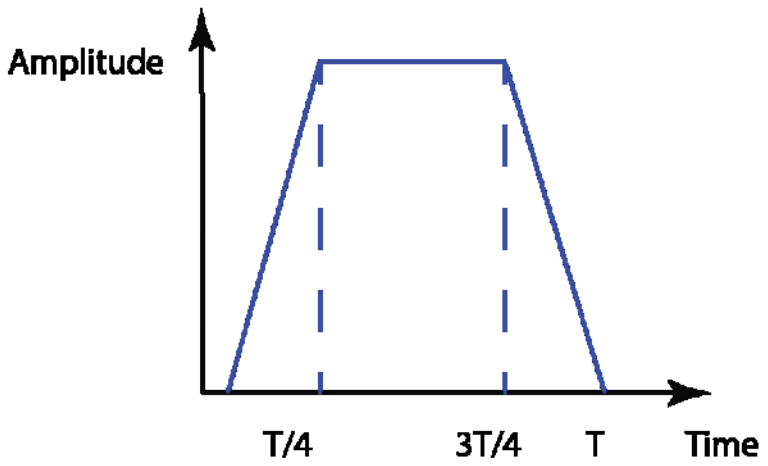

Figure 5.18 Loading amplitude for wheel load

For all the models, the bottom surface is constrained in the Y direction (Figure 5.19 shows the X, Y, Z direction for the models). The front and back surfaces are constrained in the Z direction because of the pavement is infinitely continuous in this direction. The left surface is constrained in the X direction because only one lane (i.e. the right lane) of two symmetric lanes is modeled in this research. The right surface contacts the pavement shoulder, which is made of a different material (soils). The boundary conditions for this surface are simplified as fully constrained (no linear displacements) in the X direction (See Figure 5.19). This is done because of the computation power consideration. To prove this simplification is valid, the next section provides the research analysis behind the decision.

www.manaraa.com

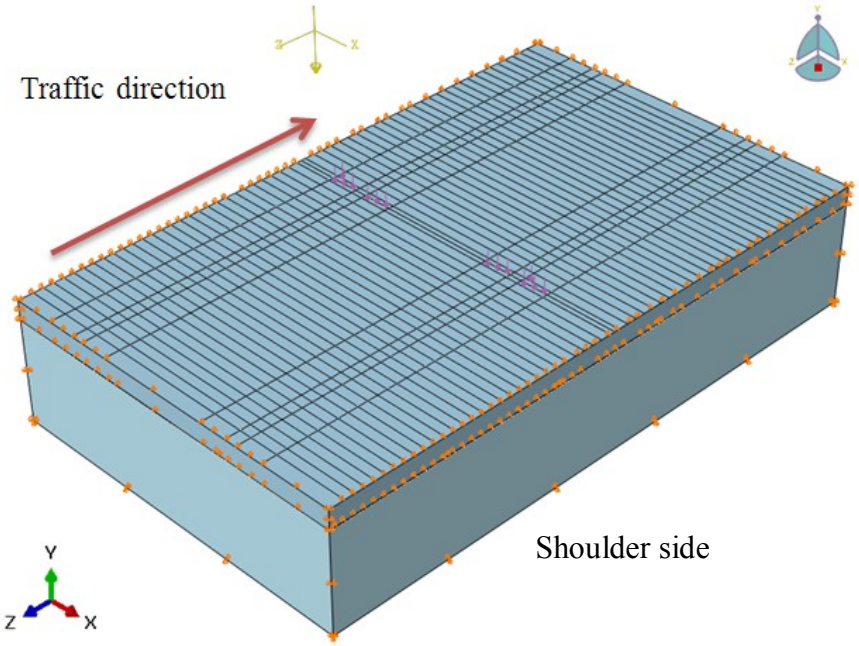

Figure 5.19 An example of the boundary conditions and loadings

5.8 The BCs for the Pavement Shoulder Side

As is shown in Figure 4.2, the NCAT test section includes two lanes. The trucks are trafficking on the outer (right) lane with the lane division line on the left and pavement shoulder on the right. To accurately consider boundary conditions of this surface that contacts pavement shoulder, either a full scale pavement shoulder needs to be modeled or it can be simplified as linear spring constraints with certain modulus values.

A hypothesis is made that the stiffness of pavement shoulder would not make a significant difference in the analysis result. To prove this, the pavement model is redone without giving any constraints on the shoulder side but only full constraints on the centerline side. Figure 5.20 shows the new model with constraints only on the centerline side (the red surface).

www.manaraa.com

Figure 5.21 to Figure 5.25 summarize the results between the two cases: a) The original case with BC on the shoulder side. b) The new testing case without BC on the shoulder side. The results for a) are placed on the left in Figure 5.21 to Figure 5.25, while the results for b) are placed on the right in Figure 5.21 to Figure 5.25.

This section examines the longitudinal strain of the N9 section. As for the detailed information about longitudinal strain, please refer to section 6.2 in the next Chapter for a good explanation. After running several analyses, no significant difference was found in longitudinal strains at either transverse or longitudinal sections for both surface and bottom of pavements. The largest discrepancy in longitudinal strains between case a) and b) is found at bottom of pavements under right wheel track, which is only around 4% (See Figure 5.23). The differences in longitudinal strains for all the other locations, namely the surface of pavements, the bottom of pavements under left wheel track, are even less, which is less than 1%. Therefore, this section proves that the BC on the right shoulder does not influence the analysis greatly. In the next Chapter, the right shoulder sides of all the models are fully constrained in the X directions (horizontal directions).

www.manaraa.com

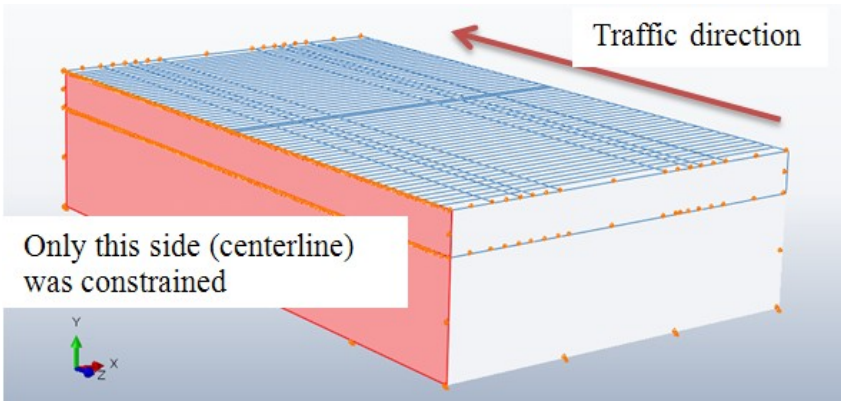

Figure 5.20 Pavement with constrains only on the left side (centerline side).

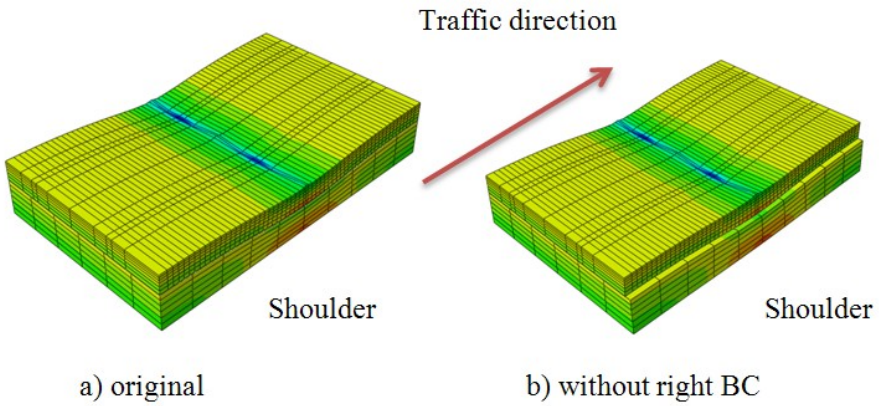

Figure 5.21 The longitudinal strain for two cases

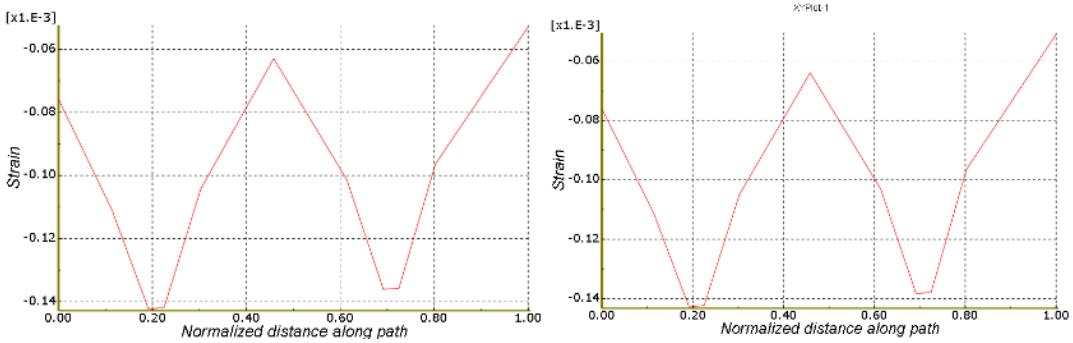

Figure 5.22 Longitudinal strains at surface of pavement for N9 (transverse section)

www.manaraa.com

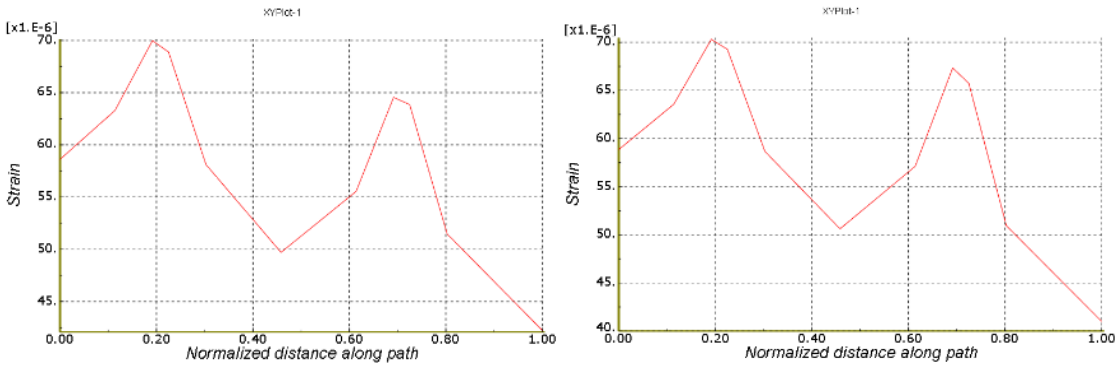

Figure 5.23 Longitudinal strains at bottom of pavement for N9 (transverse section)

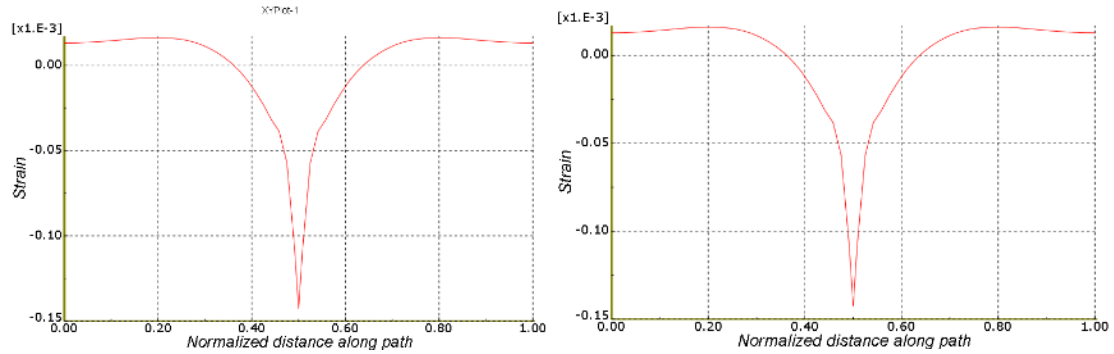

Figure 5.24 Longitudinal strains at surface of pavement for N9 (longitudinal section)

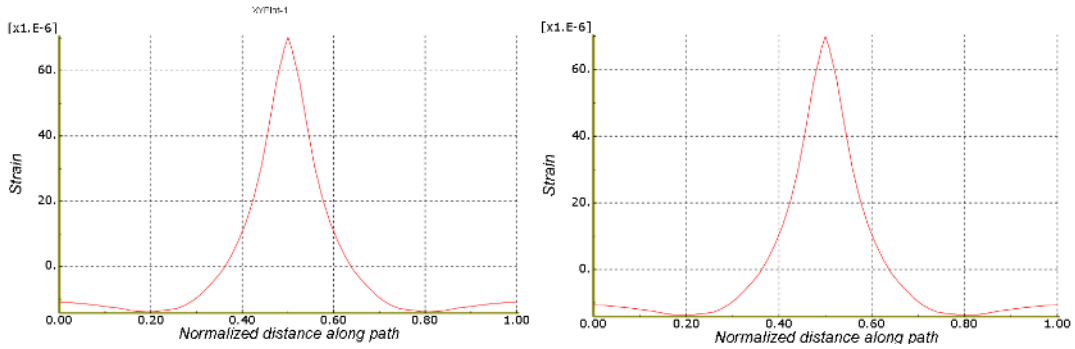

Figure 5.25 Longitudinal strains at bottom of pavement for N9 (longitudinal section)

www.manaraa.com

CHAPTER VI

THE FINDINGS FROM FEA

This chapter presents results of FEA on models of NCAT Phase 3 test sections N1 and N9. Subsequently, different types of theoretical strains are examined near and under loading wheels. The similarity and difference between two types of pavements are presented. Also, FEA is conducted to reflect the effects of factors such as layer and pavement thickness, dynamic loading, temperature, moisture, etc.

6.1 Validation of FE Models for Two Types of Pavements

The sets of strain data for a certain length of time for the two test sections, N1 and N9, were obtained for Phase III of the NCAT Test Track (Operated from the end of 2006 through the end of 2008). Plots of these strain data are shown in Figure 6.1 and 0. To make use of the data provided by NCAT and bound the analysis, the 2006 winter data were used as the basis for analysis. The specific time range is from November 2006 to February 2007, which is the typical winter time for Alabama and US Deep South regions.

Truck loading includes one steering axle, two tandem axles, and five single axles (Figure 4.11). Because the steering axle has a smaller axle weight than tandem and single axle, also the empirical data shows the single axle produces the largest strain values (See Figure 4.12, Figure 6.1). This section will focus on the results from the single axle. For the N1 section (the thinner one), the longitudinal strain values at the bottom of the HMA

www.manaraa.com

layer are concentrated in the range from 150 to 200 microstrain (Figure 6.1). For the N9 section (the thicker one), the strain values are concentrated in the range from 75 to 100 microstrain (0).

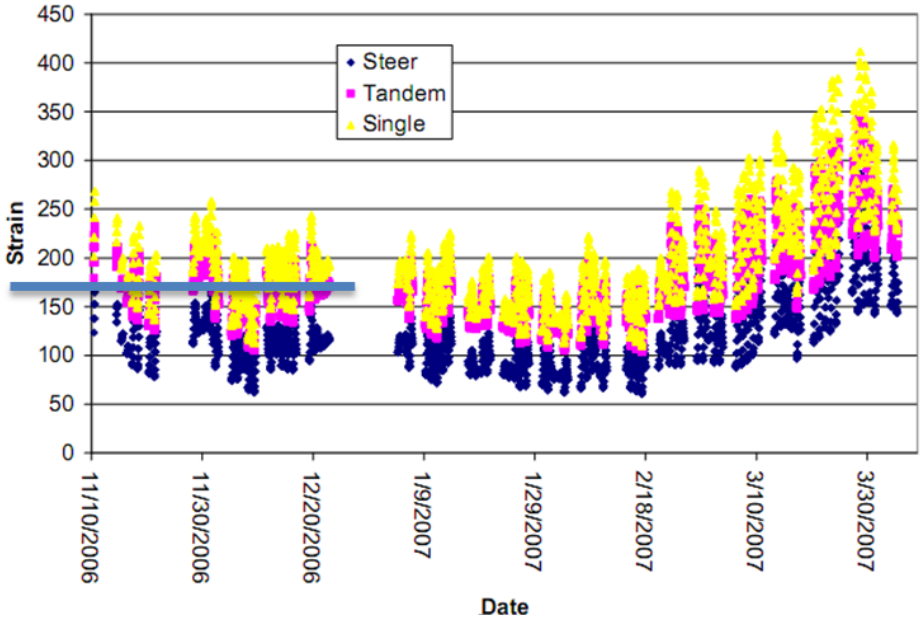

Figure 6.1 Longitudinal strain data by date for section N1 (Willis and Timm 2009)

www.manaraa.com

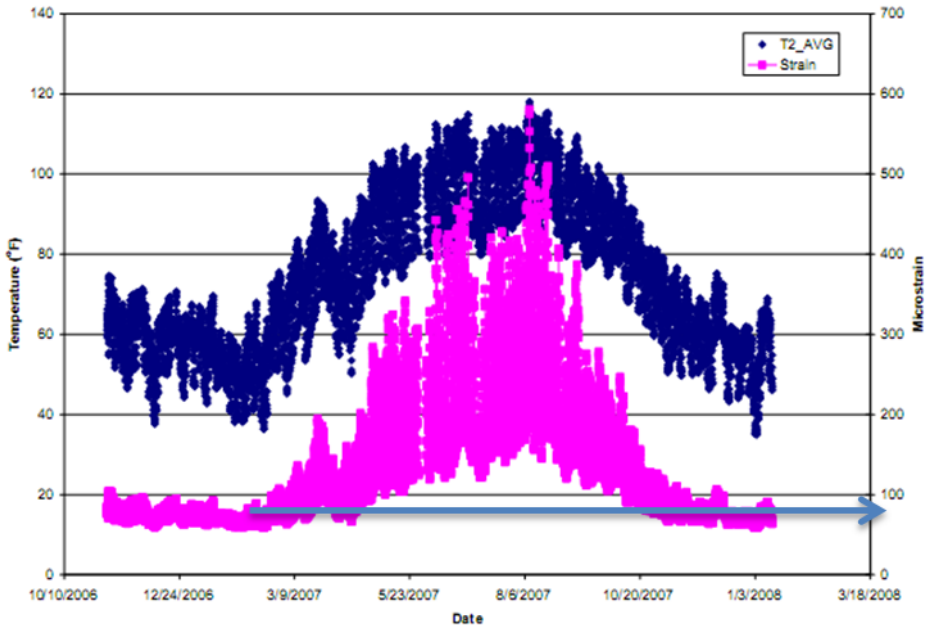

Figure 6.2 Longitudinal strain and mid-depth temperatures for section N9. (Willis, Timm and West, et al. 2009)

As described in Chapter 5, two FE models were created for section N1 and N9. The response under gravity and one application of the axle loading for the truck was simulated in the models. FE results for N1 and N9 are obtained from the second loading step of FE analysis. Unique nodal values at the bottom of asphalt layers below the right most tire (the one close to the edge in Figure 5.7) contact area were selected. They are summarized in Figure 6.3. Note that only longitudinal strain data were provided in the NCAT report for Phase 3. Therefore, to make use of the data available, only longitudinal strain from the FE results were used to validate the experimental data of NCAT.

www.manaraa.com

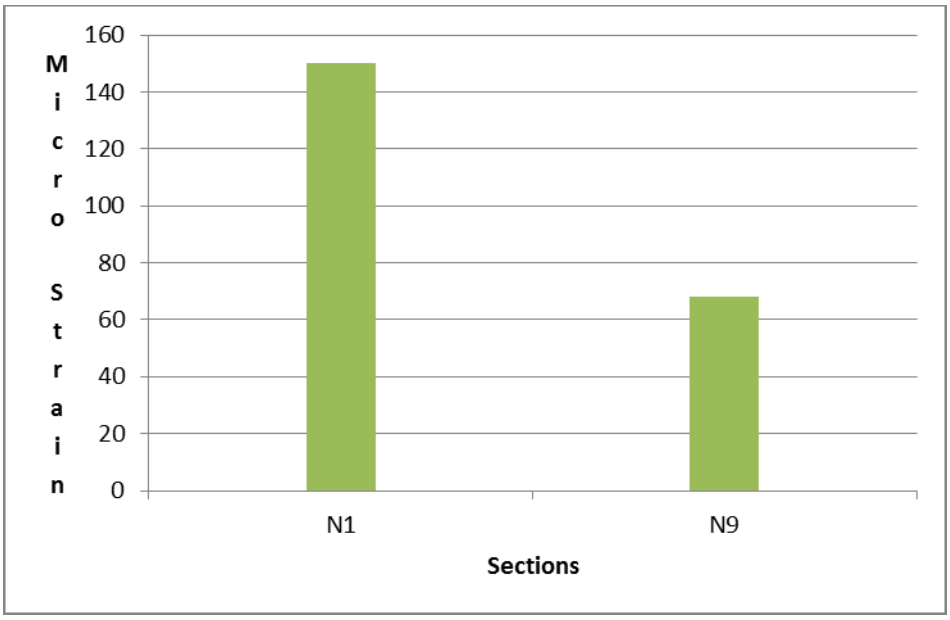

Figure 6.3 Strain data for FE Models of section N1 and N9

(Time 0.005s)

A comparison of FE analysis with NCAT test results is shown in Figure 6.4. It is seen that the FE simulation results and the empirical results from NCAT have a fairly good agreement. Thus, the FE models for both the conventional pavements and perpetual pavements are validated for this study.

www.manaraa.com

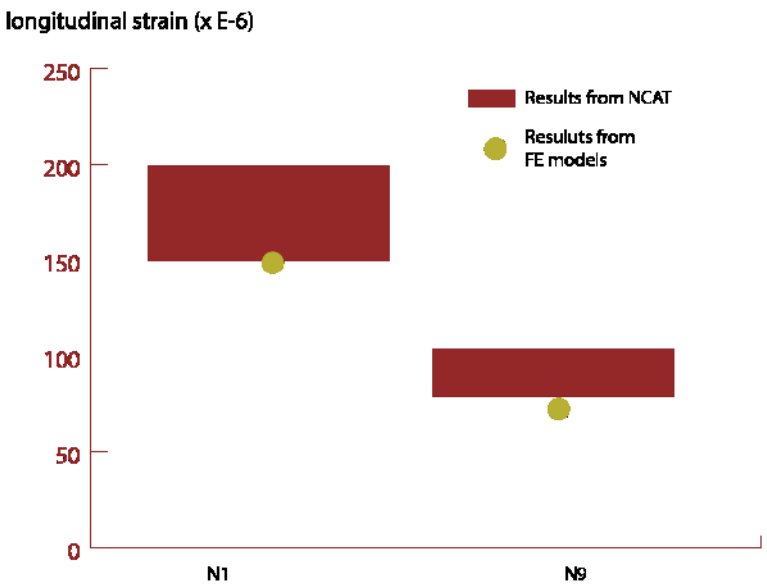

Figure 6.4 Comparison of strain results from NCAT and FE models

6.2 A Further Examination of the Theoretical Strain Distribution for N9 Section

Two main categories of strains were examined, i.e., normal and shear strains. Also, the normal strain contains three types, i.e., the normal strain along the traffic direction (longitudinal), the strain perpendicular to the traffic direction (transverse), and the vertical strain. Strain in NCAT test section was only measured at the bottom of the HMA layer in the assumption that this horizontal tensile strain is critical to determining the pavement performance. In the current study, different strain types near and under a tire is studied to better understand the type, orientation, magnitude and location of the critical strain. In this section, the N9 section is the focus. Horizontal strains are examined first, vertical strain second and shear strain last.

www.manaraa.com

6.2.1 Horizontal Strains: Longitudinal and Transverse Strains

Figure 6.5 and Figure 6.6 show the longitudinal and transverse strain at the bottom of the HMA layer of the N9 section. The values show that the magnitude of longitudinal strains is over three times the magnitude of the transverse strains. In the traditional and current mechanistic design, one criterion was specified as "maximum horizontal tensile strain at the bottom of HMA layers" without specification of orientation (See section 2.2.3). This research proposes that longitudinal normal strains should be specified in the failure criterion. The similar trend could also be found at the surface of the pavements. In the following sections, longitudinal strains are selected to be examined in detail.

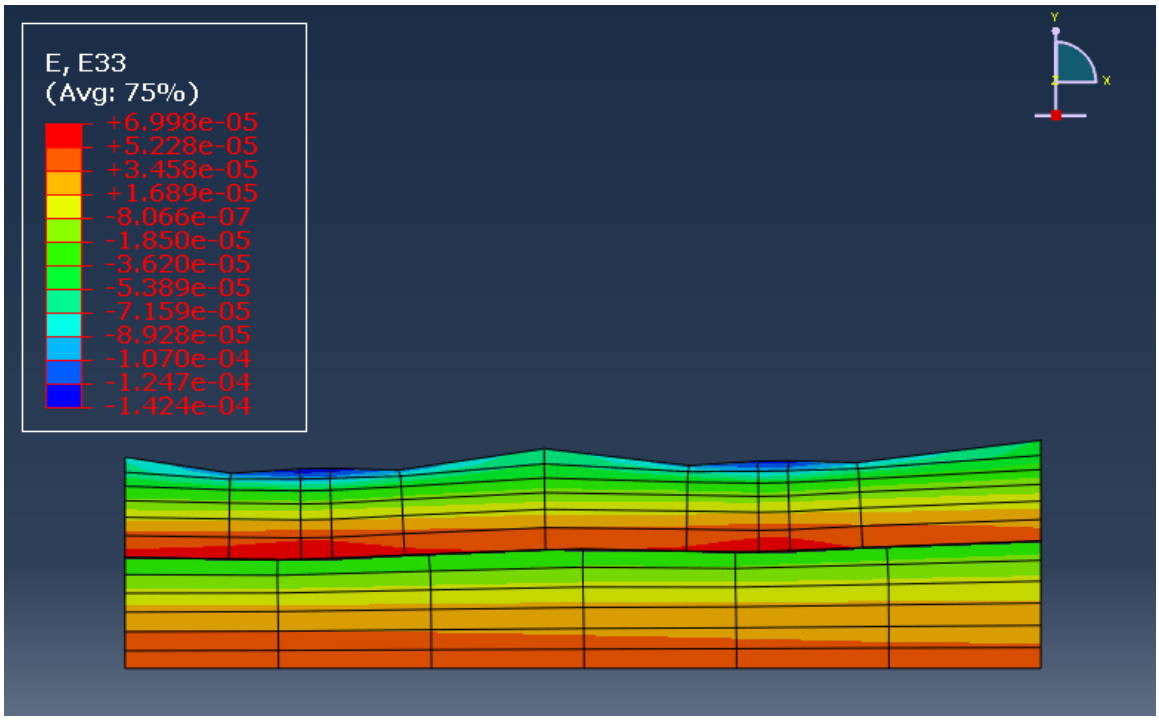

Figure 6.5 Longitudinal strains for section N9

www.manaraa.com

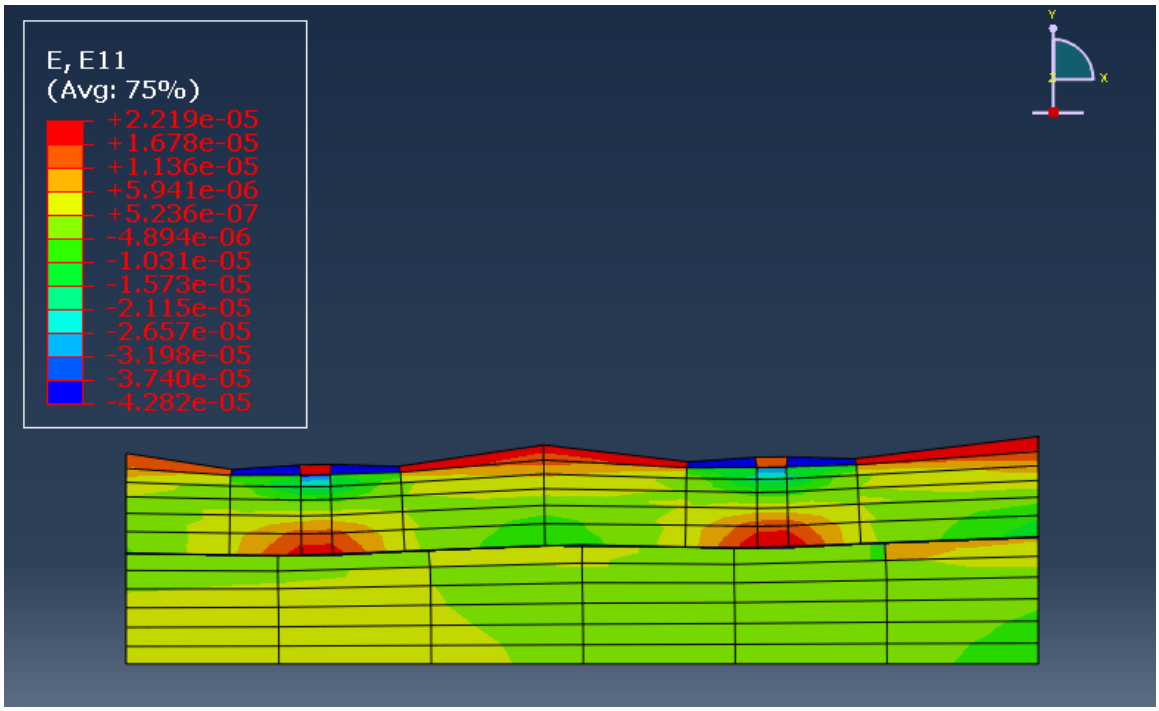

Figure 6.6 Transverse strains for section N9

6.2.2 Strains at Outer or Inner Wheel Paths

In the NCAT Test Track, the distance between the outer wheel path and the edge stripe (around 1m) is greater than the distance between the inner wheel path and the centerline (around 0.7m). See Figure 4.5, strain gauge arrangement and Figure 5.7. This section explores whether the strain could vary greatly for these two spatial locations at bottom of the HMA layer. Using the longitudinal strains of section N9 for example, the FE results show that the difference in longitudinal strain at the bottom of HMA layer between inner and outer wheel path is around 9% (Figure 6.11). Although this is not a significant variation, it could provide guidance to the instrumentation of field instrumentation. The strain gauges placed in the inner wheel path could produce higher strain than the one placed in the outer wheel path (as in the NCAT results).

www.manaraa.com

6.2.3 Longitudinal Strain Distribution with Depth in the HMA Layer

We can conclude from the above figures and Figure 6.7 that the magnitude of longitudinal strains (compressive) at the surface (where the tires are in contact with the surface) are about two times as large as the magnitude of longitudinal strains (tensile) at the bottom of the HMA layers. This result could be considered in the design because surface fatigue cracking could be more likely than bottom-induced fatigue cracking. The same trend is also observed for transverse strain along the depth of HMA layer. Figure 6.8 demonstrates the orientation and magnitudes (the length of the arrows stand for magnitudes) of the horizontal strains at surface and bottom of HMA layer.

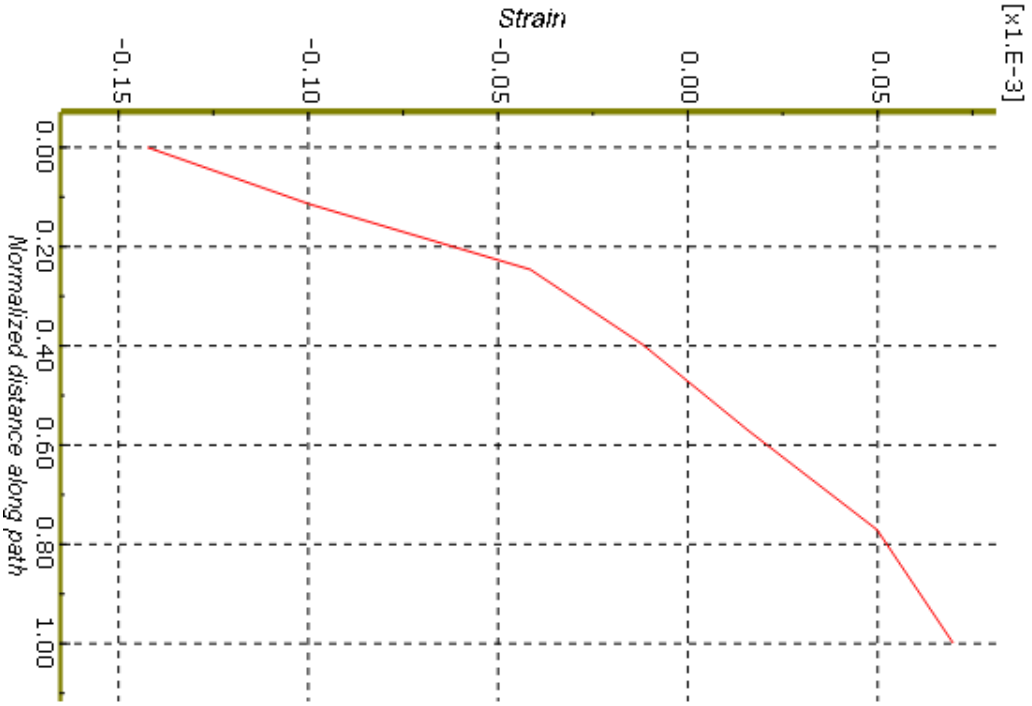

Figure 6.7 Longitudinal strain distribution along the depth of HMA layer

www.manaraa.com

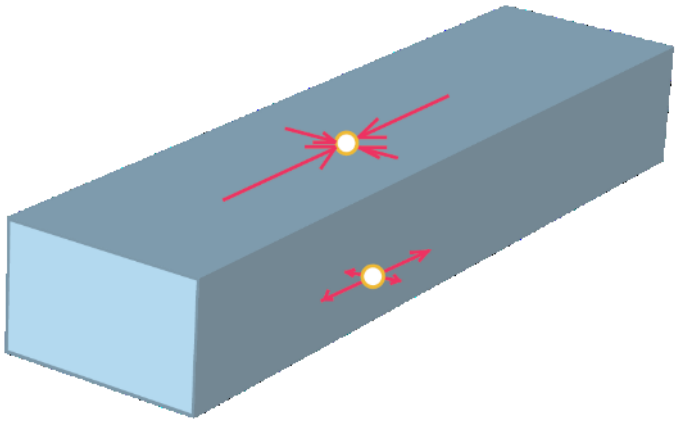

Figure 6.8 Horizontal strains at surface and bottom of pavement HMA layer

6.2.4 Longitudinal Strain Distribution in the Transverse Section (Wheel's Left and Right)

The strain distribution in the transverse direction can show the effect of wheels and the response between the wheel paths. In this section, both the stain at the surface and bottom are investigated. See Figure 6.9. Figure 6.10 and Figure 6.11 show that maximum horizontal compressive strain are at the top of layers, while the maximum horizontal tensile strain happen at the bottom of HMA layers. Two peaks indicate where the wheel loads are applied. Also, the inner wheel (left in the figure) paths demonstrate relative larger values. This characteristic is discussed in section Figure 6.8.

www.manaraa.com

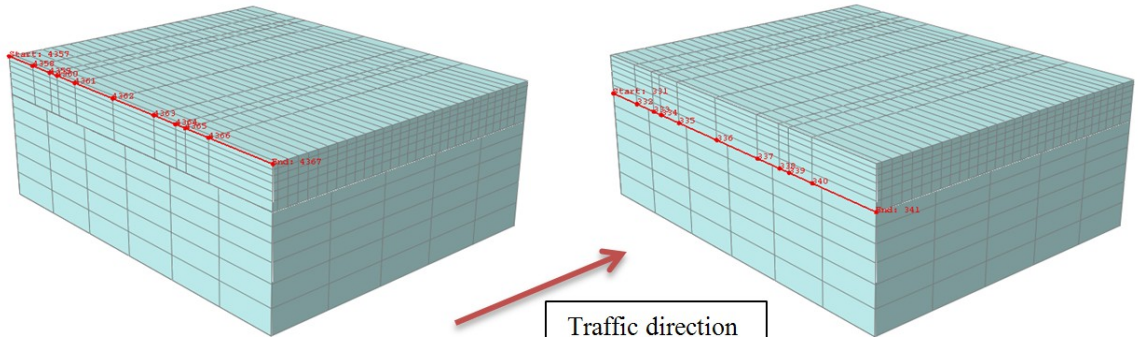

Figure 6.9 Illustration of the position of the strain at surface and bottom

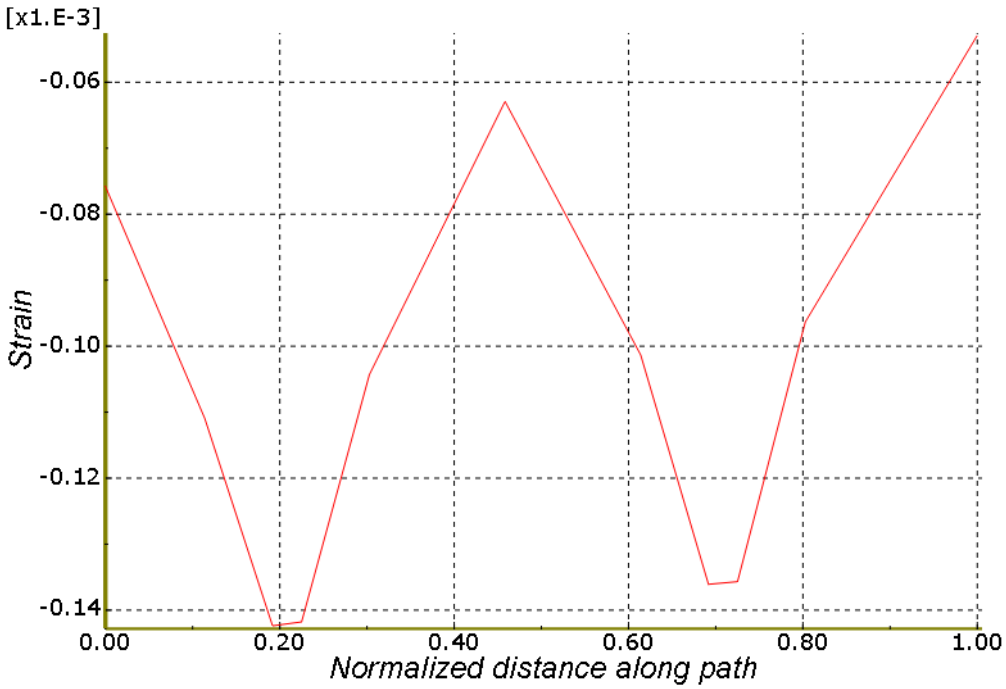

Figure 6.10 Longitudinal strains at surface of pavement for N9 (transverse section)

www.manaraa.com

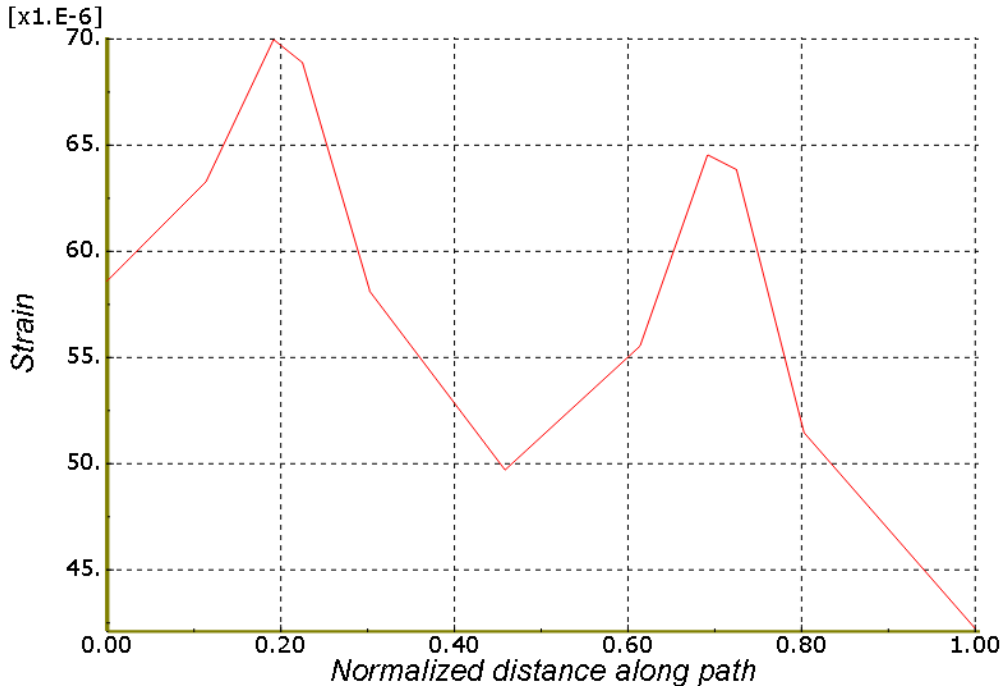

Figure 6.11 Longitudinal strains at bottom of pavement for N9 (transverse section)

6.2.5 Longitudinal Strain Distribution in the Longitudinal Section (Wheel's Front and Back)

The strain distribution in the longitudinal direction can show the effect of wheels along the path. In this section, both the strain at the surface and bottom are investigated. See Figure 6.12. Figure 6.13 and Figure 6.14 show that at the back and front of the wheel, the strain change from tension to compression to tension at the top of HMA layer, with the trend being opposite at the bottom of HMA layer. Also note that the surface has significant larger values than the bottom. This characteristic is already shown in section 6.2.2.

www.manaraa.com

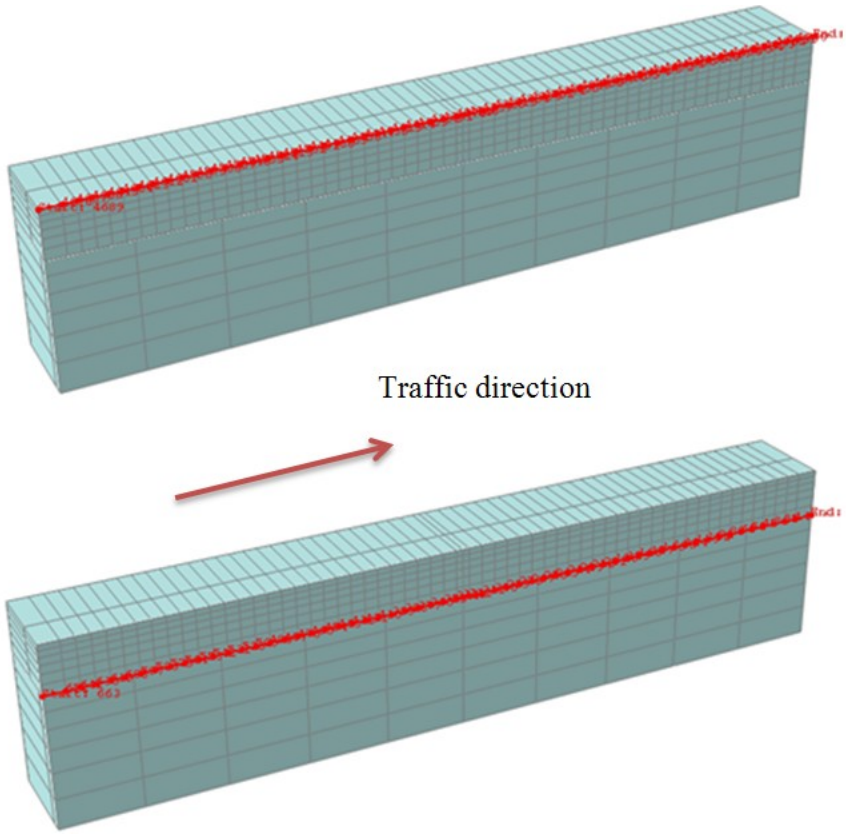

Figure 6.12 Illustration of the position of the strain at surface and bottom

www.manaraa.com

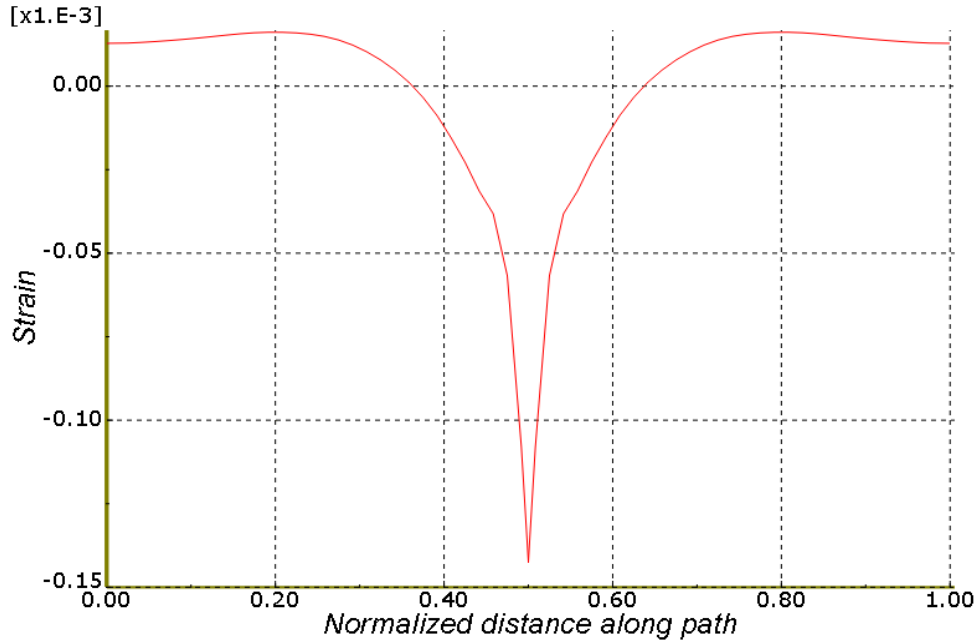

Figure 6.13 Longitudinal strains at surface of pavement for N9 (longitudinal section)

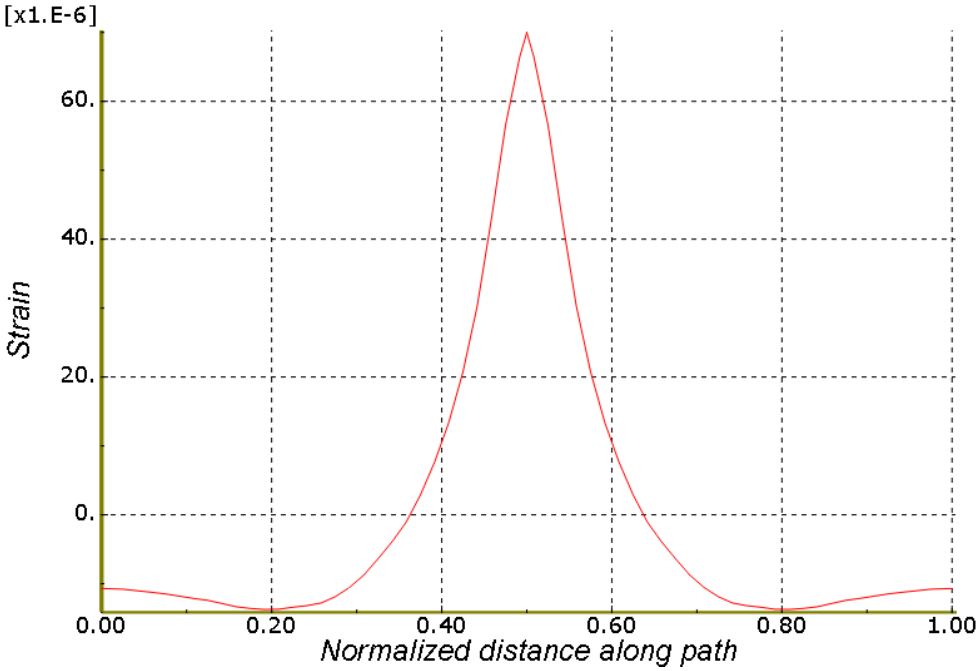

Figure 6.14 Longitudinal strains at bottom of pavement for N9 (longitudinal section)

www.manaraa.com

6.2.6 Vertical Stress and Strain

The vertical stresses and strains predicted in FEA are all compressive. The distribution of vertical stresses is shown in Figure 6.15 to Figure 6.18. The distribution of vertical strains is shown in Figure 6.19 to Figure 6.18. A comparison of N9 and N1 vertical stresses and strains is made in the next section.

In general, the vertical compressive stresses and strains decrease with depth in the HMA layer. At the top of the soil subgrade the strain abruptly increases (Figure 6.21) because soil modulus is much lower than HMA modulus. Also, the vertical strain at the HMA surface under vehicle loadings is large (around 150 microstrain, see Figure 6.21). Both vertical stress (Figure 6.17 and Figure 6.18) and strain (Figure 6.20 and Figure 6.21) are shown for the whole history of loading. FEA allows self-weight (gravity loading) unlike the common layered elastic analysis. In this research, the vertical strain at the top of the subgrade was determined for the HMA self-weight and then for the added wheel load. For the N9, the strain from the HMA self-weight represents over 50% of the total strain (250 compared to 500 microstrain).

www.manaraa.com

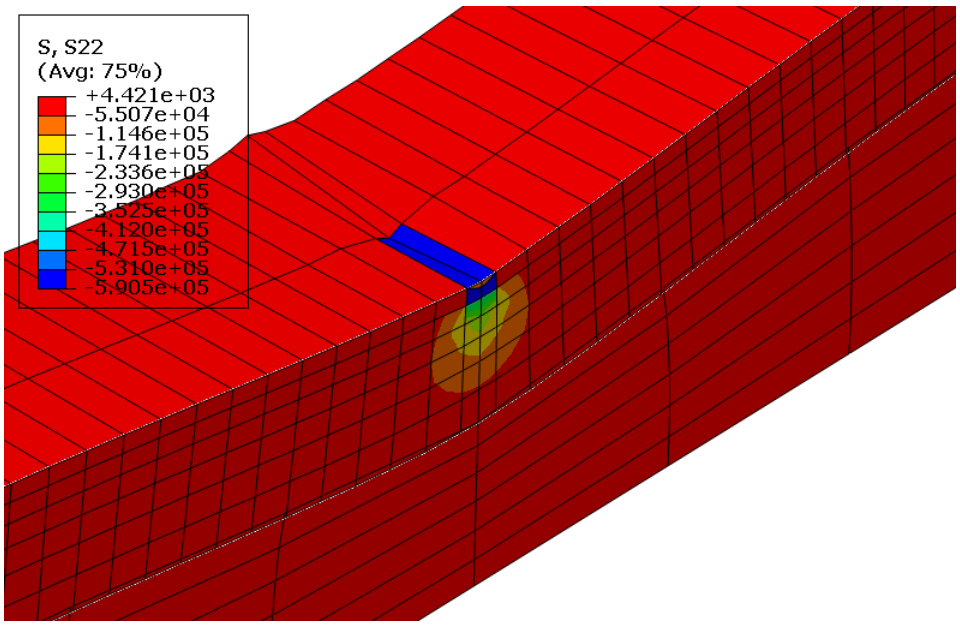

Figure 6.15 Vertical stress in longitudinal view

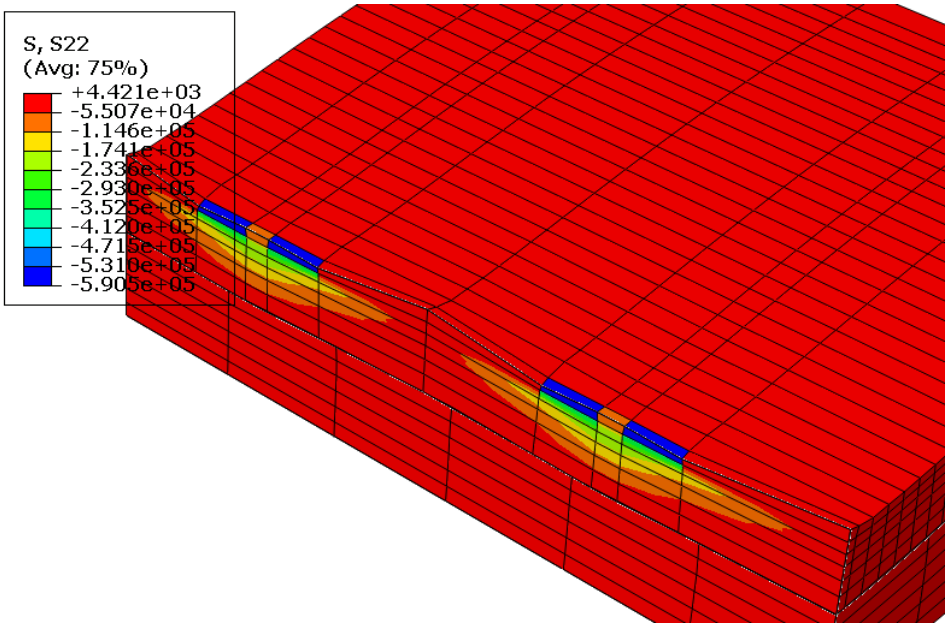

Figure 6.16 Vertical stress in transverse view

www.manaraa.com

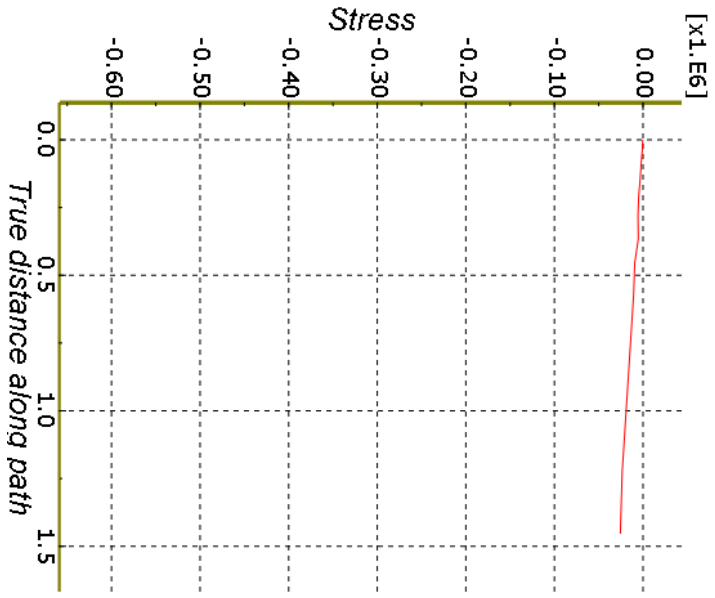

Figure 6.17 Vertical stress with depth of pavement and foundation for N9.

(Under gravitation only)

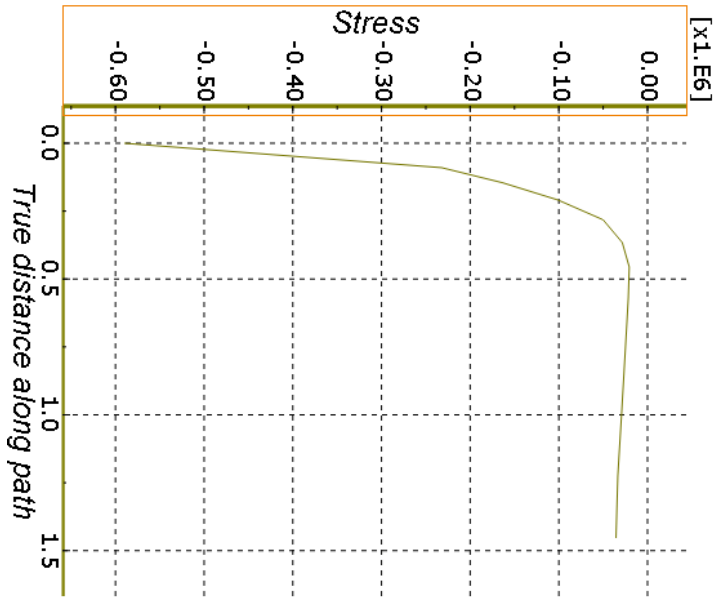

Figure 6.18 Vertical stress with depth of pavement and foundation for N9.

(Under gravitation and wheel loading)

www.manaraa.com

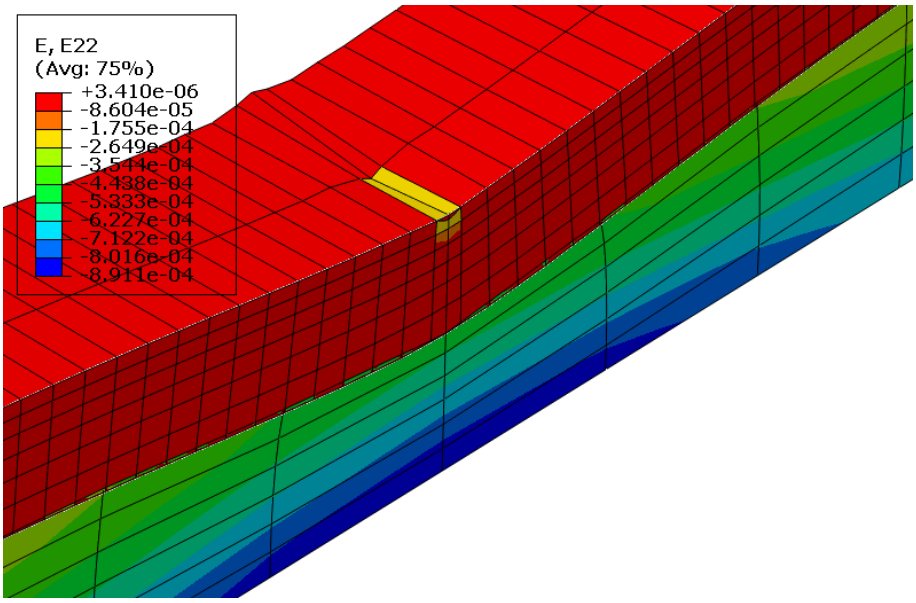

Figure 6.19 Vertical strain for N9

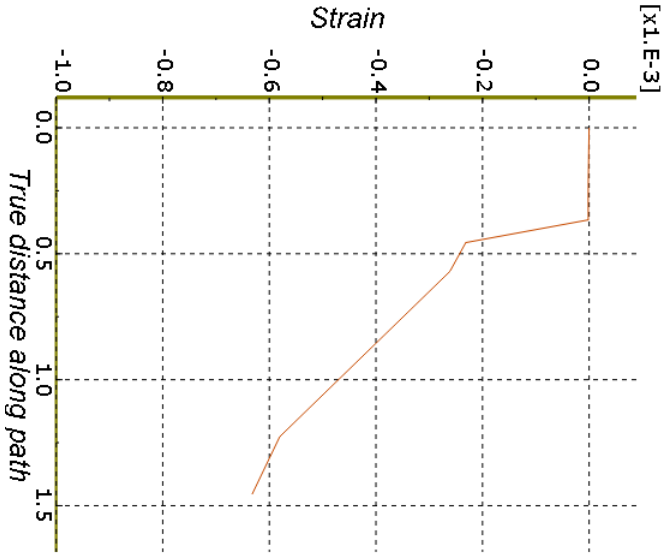

Figure 6.20 Vertical strain with depth of pavement and foundation for N9.

(Under gravitation only)

www.manaraa.com

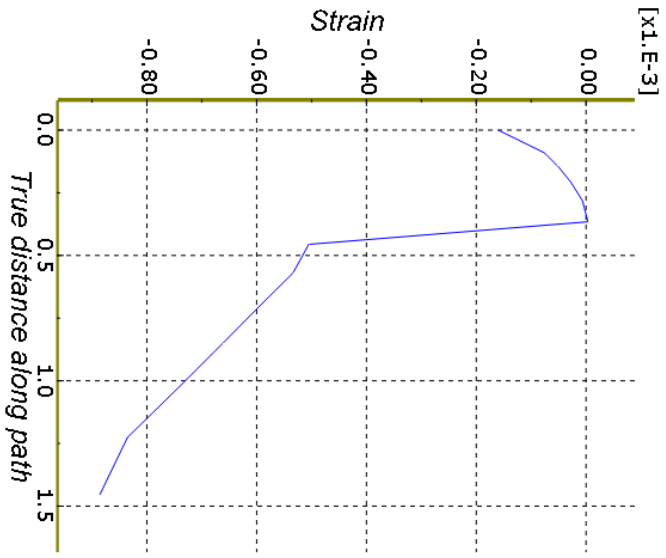

Figure 6.21 Vertical strain with depth of pavement and foundation for N9. (Under gravitation and wheel loading)

6.2.7 Shear Strain Distribution under Wheel

It is known that shear failure is common for soil and other geologic materials. In this section, the shear strain distribution under each wheel is studied. Two types of shear strains are investigated. The first one is associated with shear distortion in the longitudinal sections (abbreviated as longi-shear herein). This type of shear strains are usually connected to the shear components on the transverse plane. The second type is associated with shear distortion in the transverse sections (abbreviated as trans-shear herein). This type of shear strains are usually connected to the shear components on the longitudinal plane. In the figures below, red and blue color indicates the shear strain has different signs at left and right of pavement along the traffic direction. Red means positive (clockwise), while blue means negative (counterclockwise).

For the longi-shear strain (Figure 6.22 and Figure 6.23), the maximum shear strains are concentrated close to the tire load. However, for the trans-shear strain (Figure

www.manaraa.com

6.24 and Figure 6.25), the max shear strains are the centerline and the edge of the pavements.

The maximum shear strain is near the surface of pavements for longi-shear. This could be an explanation of top-down cracking for perpetual pavements. It is also noted that the peak values of longitudinal shear strains form an inverted Y shape (Figure 6.26). This conforms to the shape of top-down cracking observed in some thick pavements. The magnitude of the longi-shear one (51 microstrain) is about 30% larger than the trans-shear one.

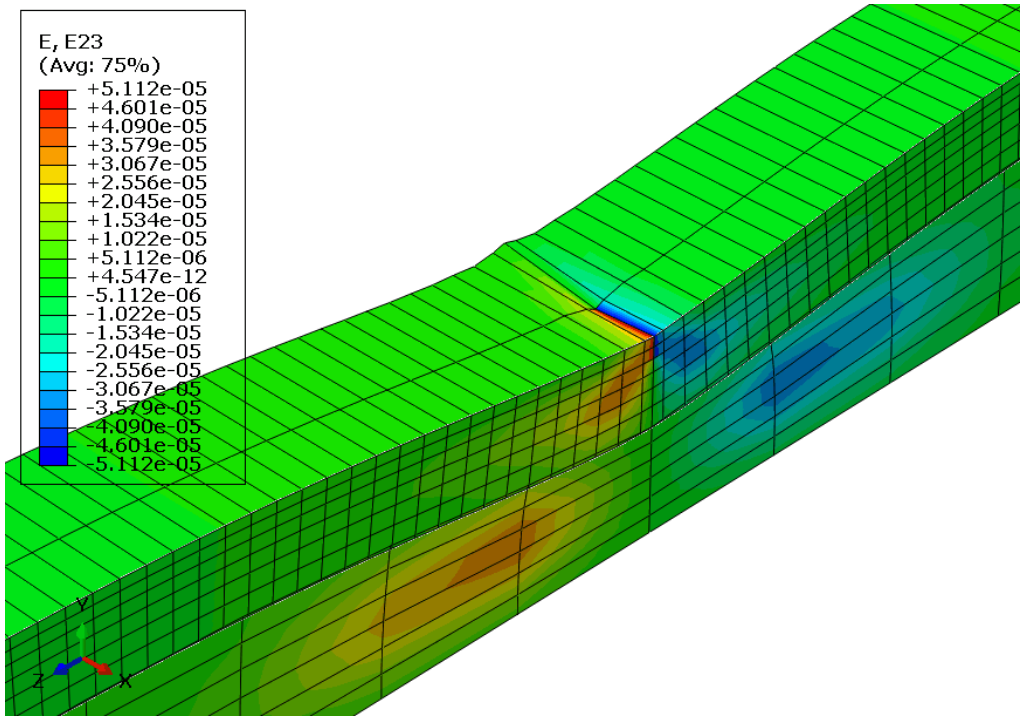

Figure 6.22 Longi-shear strain distribution in 3D

www.manaraa.com

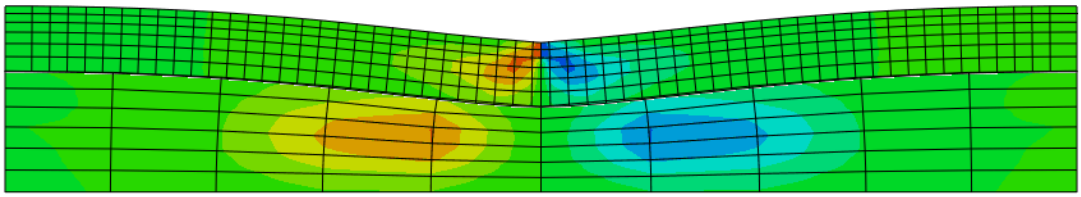

Figure 6.23 Longi-shear distribution

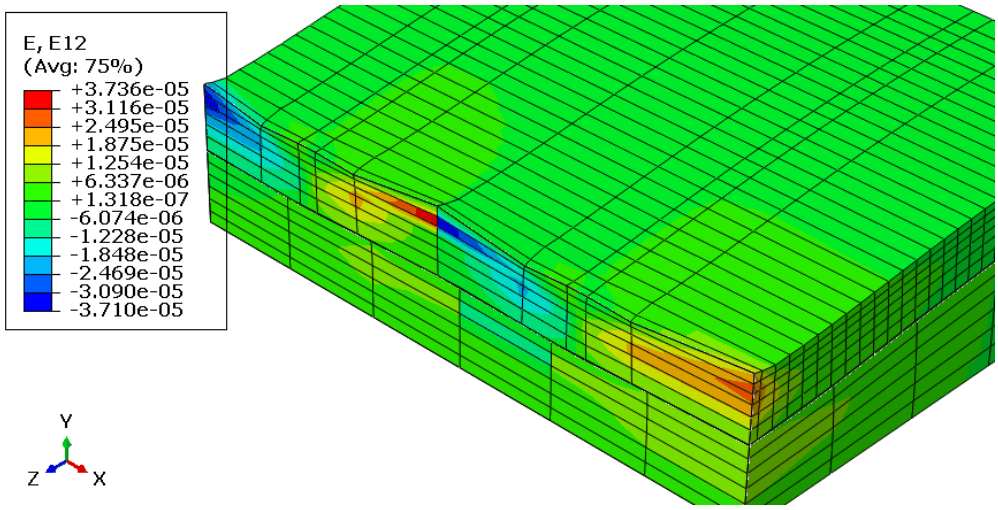

Figure 6.24 Trans-shear strain distribution in 3D

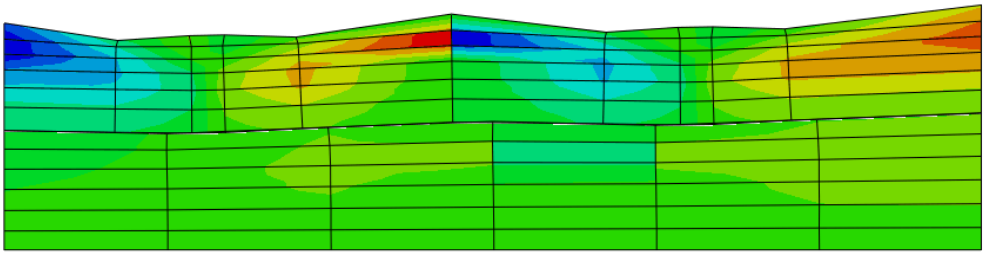

Figure 6.25 Trans-shear strain distribution

www.manaraa.com

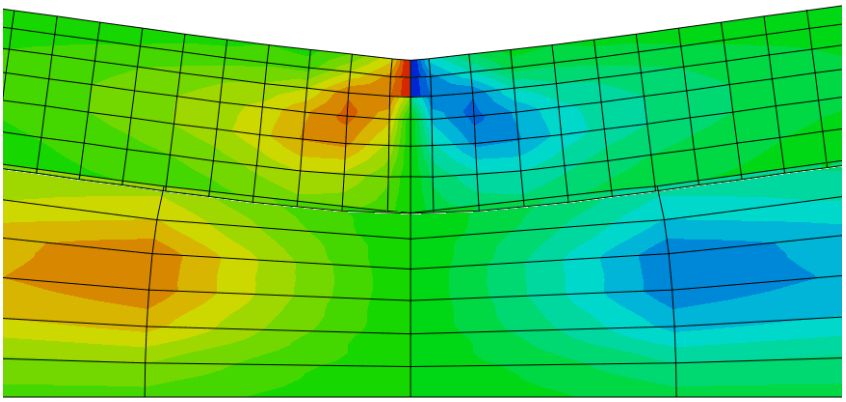

Figure 6.26 A close-up look of longi-shear strain distribution

6.3 N9 Section VS N1 Section

In the analysis of the N9 model above, the magnitude of longitudinal strains was found to be over **three** times of the magnitude of the transverse strains. Meanwhile, the magnitude of longitudinal compressive strains at the surface is about **two** times as large as the magnitude of longitudinal tensile strains at bottom of the HMA layers. The same trends for section N1 are shown in Figure 6.27 to Figure 6.35 although the multiplier is smaller.

www.manaraa.com

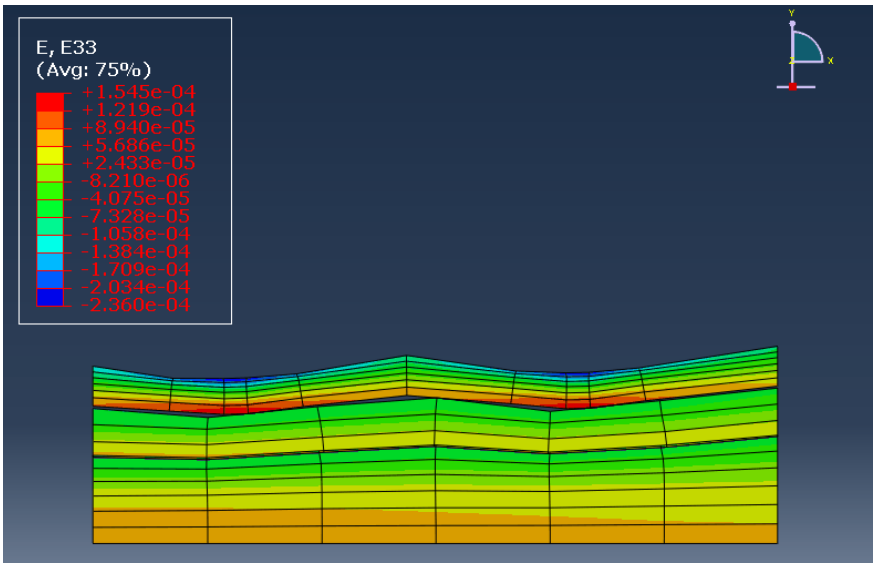

Figure 6.27 Longitudinal strains for section N1

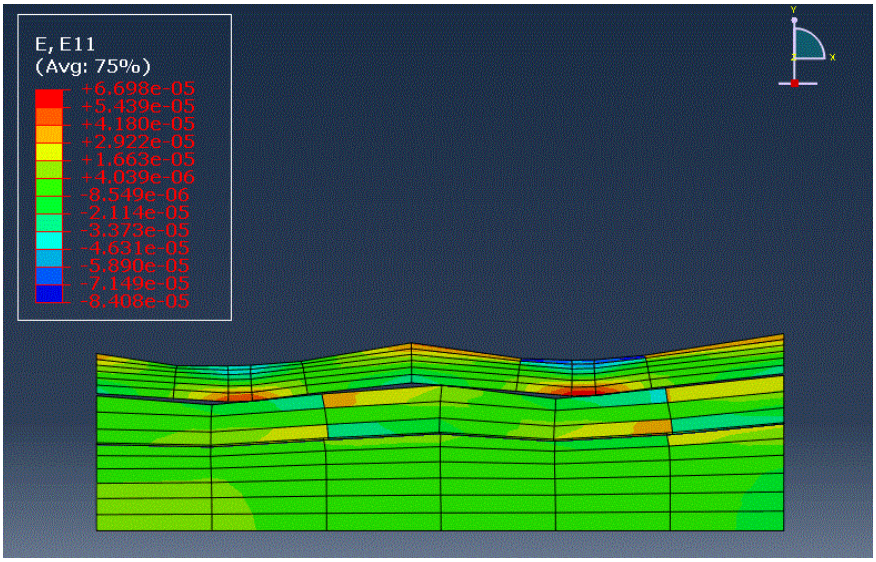

Figure 6.28 Transverse strains for section N1

www.manaraa.com

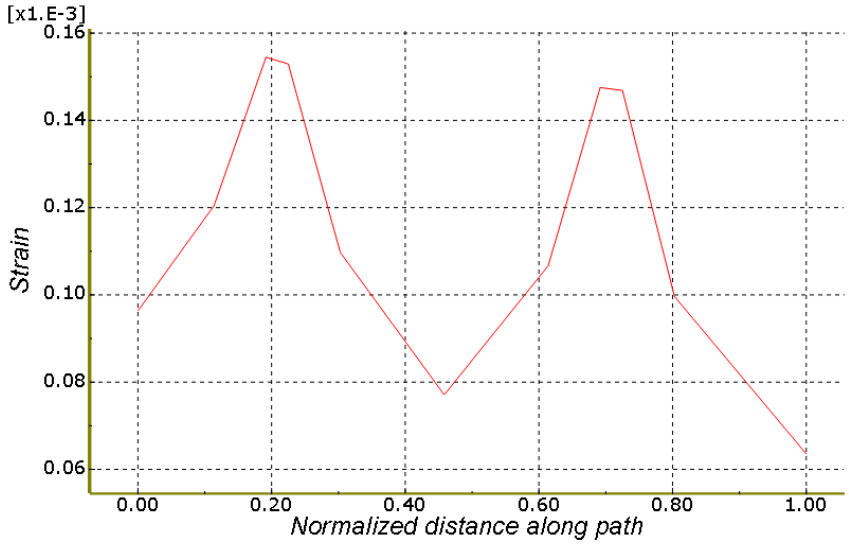

Figure 6.29 Longitudinal strains at surface of pavement for N1 (transverse section)

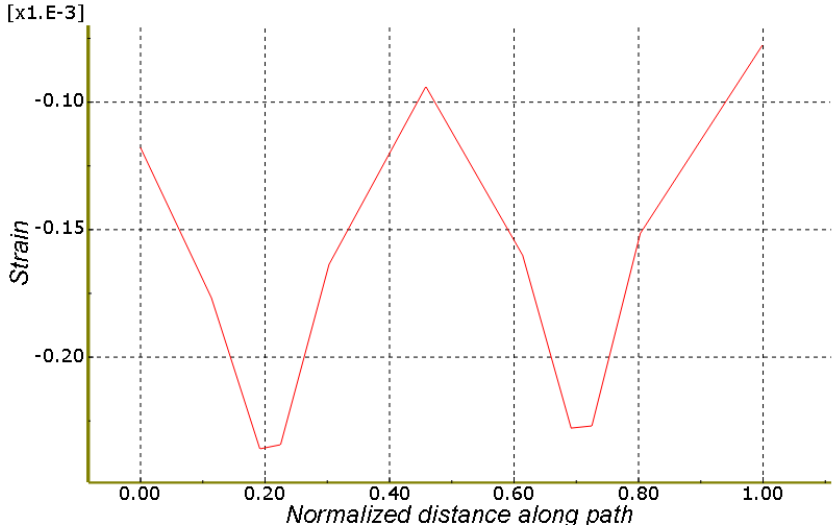

Figure 6.30 Longitudinal strains at bottom of pavement for N1 (transverse section)

www.manaraa.com

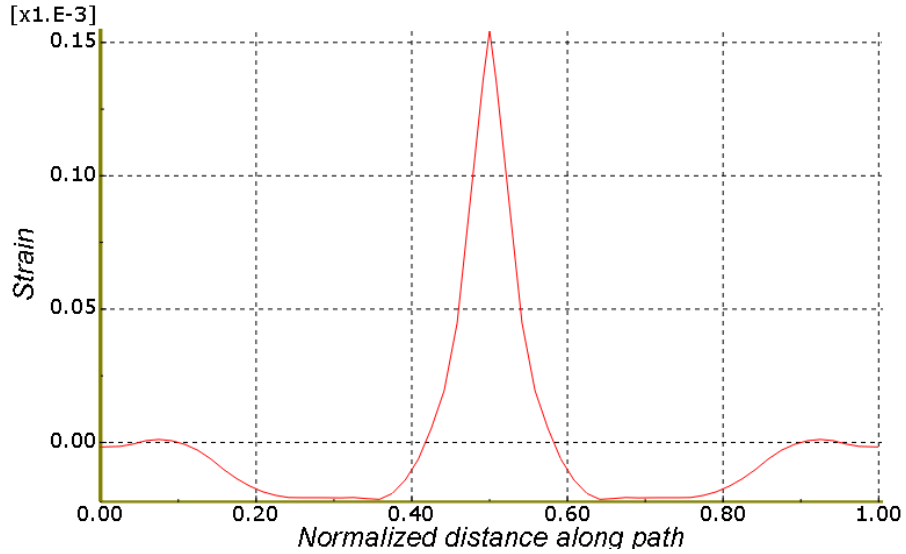

Figure 6.31 Longitudinal strains at surface of pavement for N1 (longitudinal section)

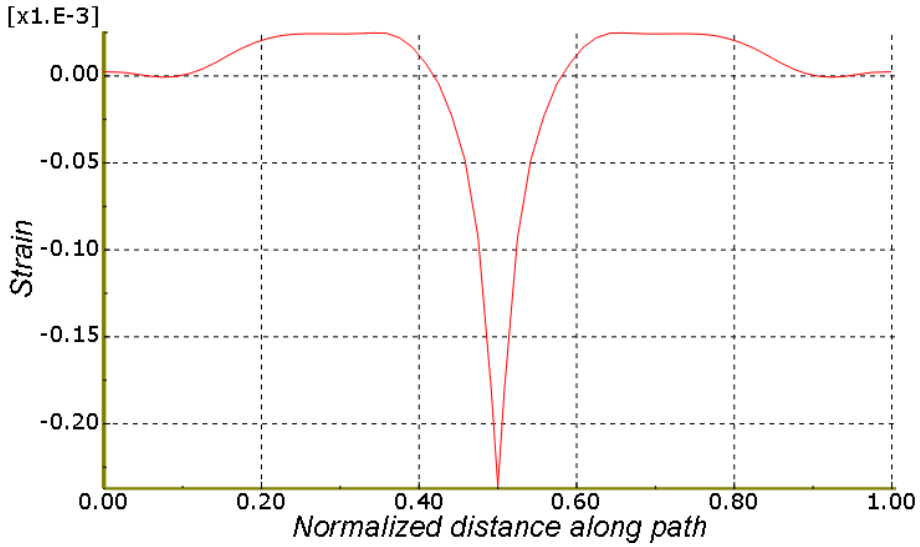

Figure 6.32 Longitudinal strains at surface of pavement for N1 (longitudinal section)

The vertical compressive strains and stresses for N1 are shown in Figure 6.33, Figure 6.34, and Figure 6.35. The vertical compressive strain for N1 at the top of

www.manaraa.com

subgrade is not much different from the one for N9. The thick pavement is not very effective in reducing strain and stress at top of subgrade.

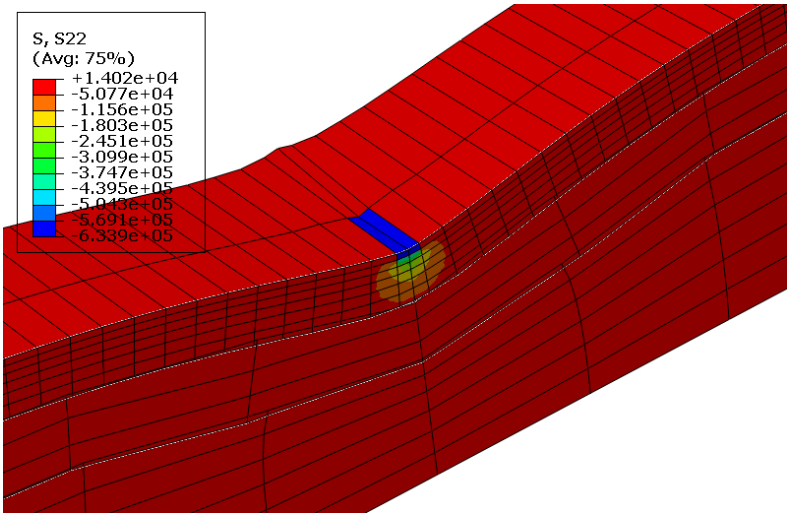

Figure 6.33 Vertical stress for N1 in longitudinal view

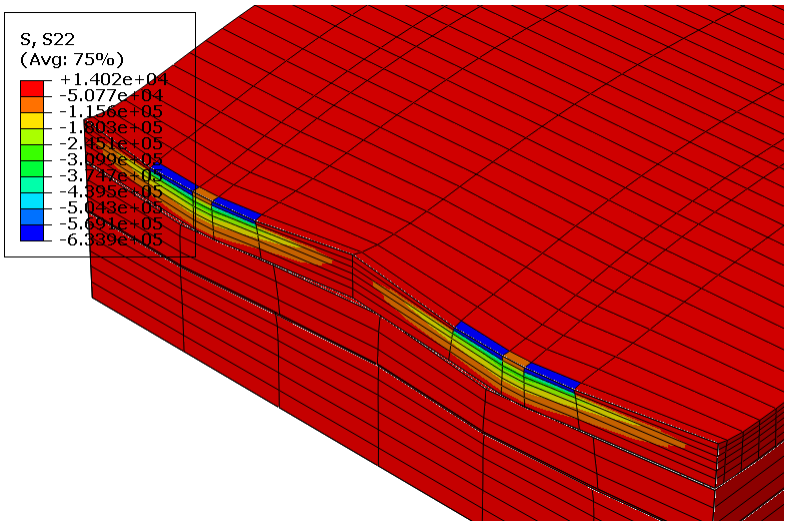

Figure 6.34 Vertical stress for N1 in transverse view

www.manaraa.com

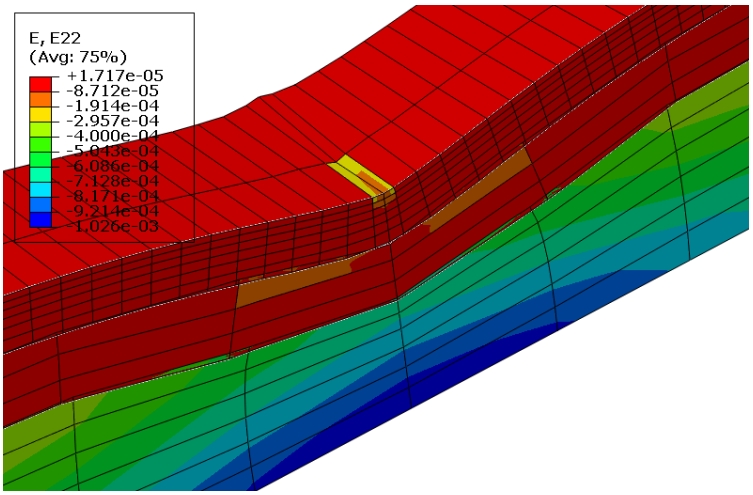

Figure 6.35 Vertical strain for N1

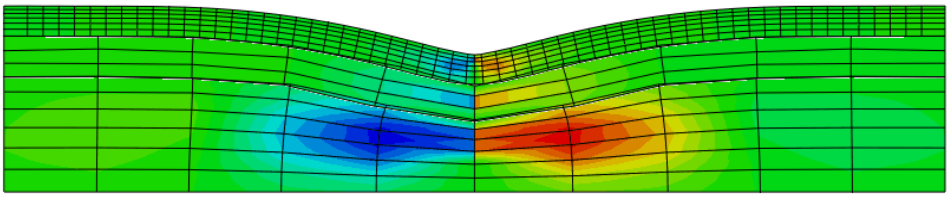

Figure 6.36 Longi-shear strain distribution for N1

www.manaraa.com

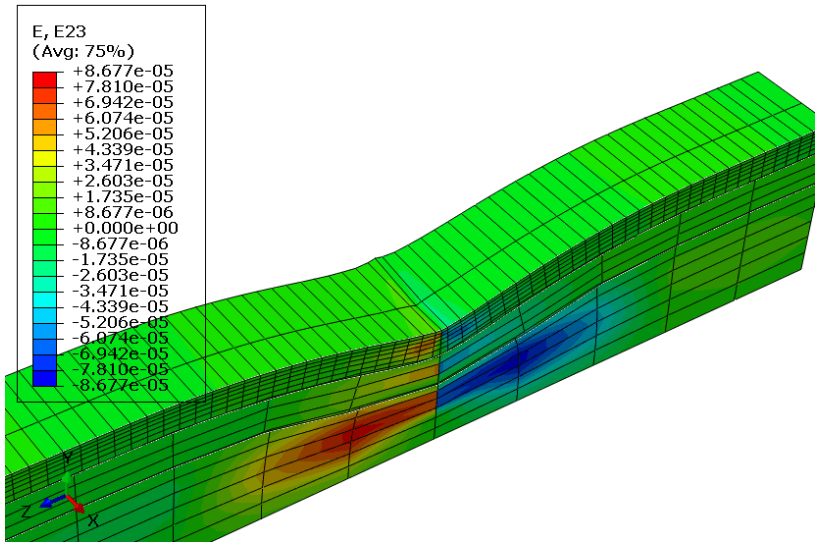

Figure 6.37 Longi-shear strain distribution in 3D for N1

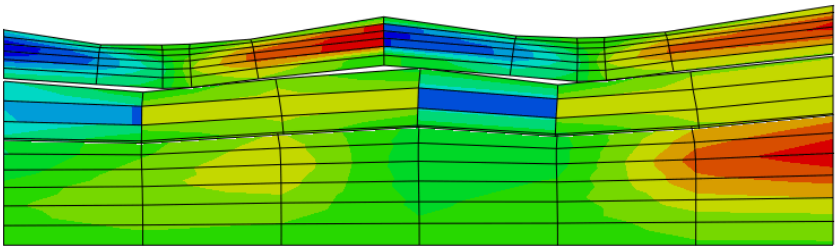

Figure 6.38 Trans-shear strain distribution for N1

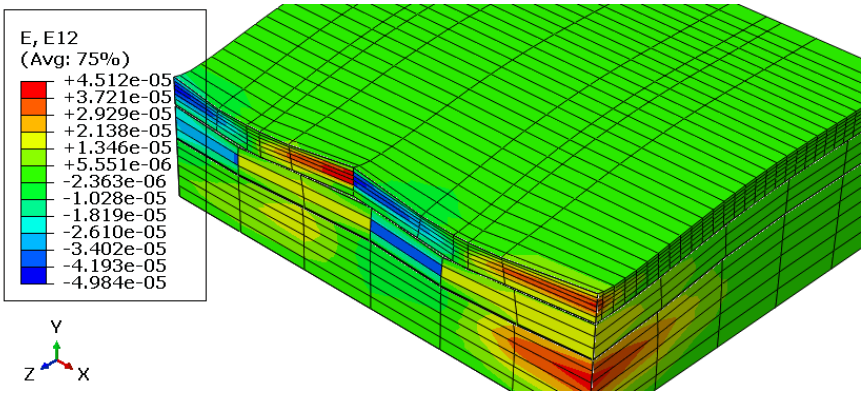

Figure 6.39 Trans-shear strain distribution in 3D for N1

www.manaraa.com

6.4 The Effect of Thickness

This section and the following sections will look into effects of layer thickness, wheel path, static and dynamic loading temperature, and moisture on pavement response. Since section 6.2.1 shows that the longitudinal strain is larger than the transverse strain, longitudinal strain will be used as the basis for examining these effects. To investigate the effect of layer thickness and better understand perpetual pavements, two additional pavement FE models with half and twice the thickness of N9 were developed using Abaqus. In these analyses, N9 is designated as T2. The model with a thinner HMA layer of 0.19m (7.4 inches) is T1 and the model with a thicker HMA layer of 0.75m (28.8 inches) is T3 as shown in Figure 6.40 and Figure 6.41. The results of longitudinal strain for T1 and T3 are shown in Figure 6.42 to Figure 6.47.

www.manaraa.com

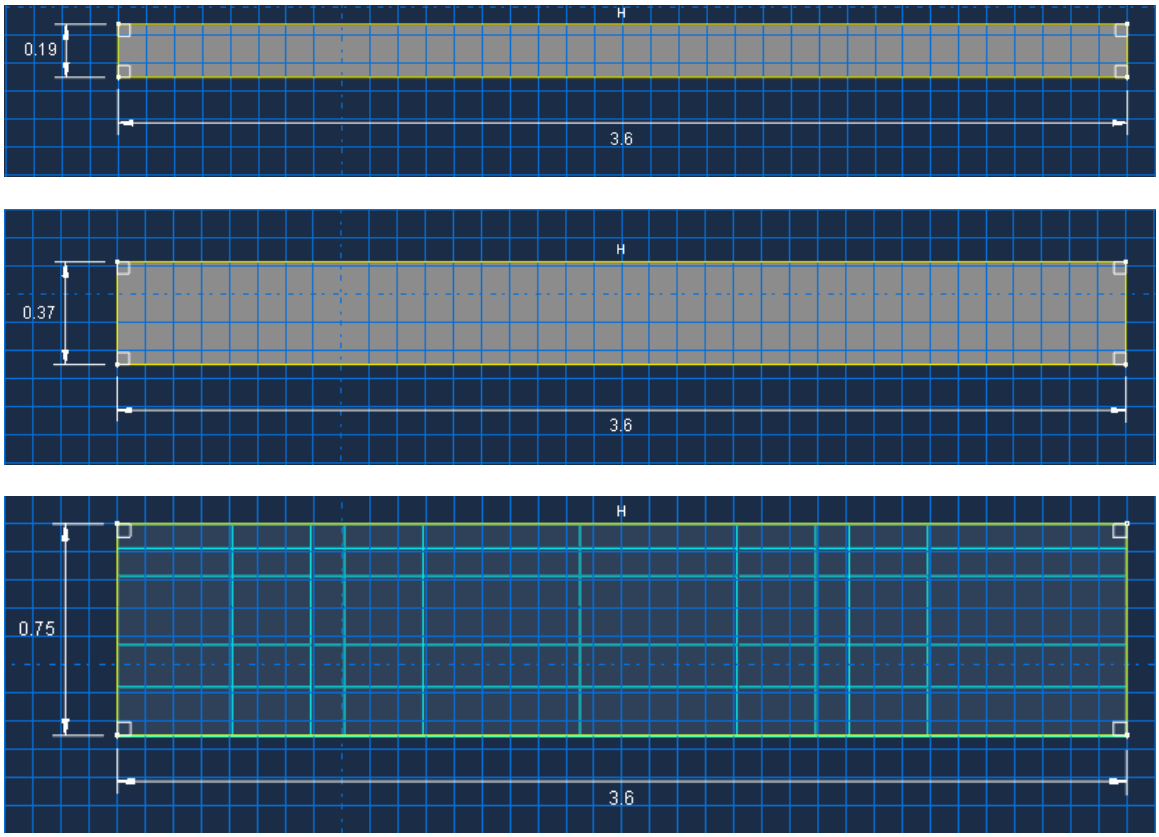

Figure 6.40 The size of the HMA layer for the pavement models T1, T2 and T3 (from top to bottom)

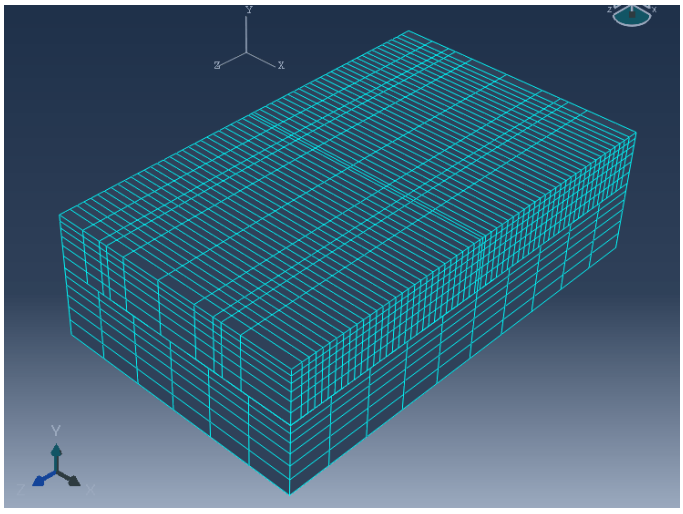

Figure 6.41 The mesh for the pavement model (T3 is shown as an example)

www.manaraa.com

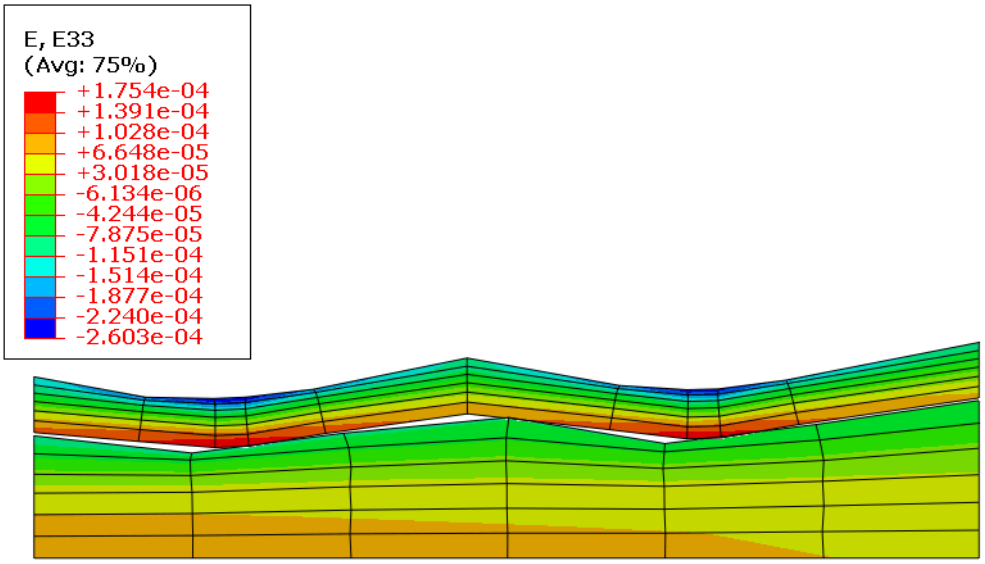

Figure 6.42 Longitudinal strains for section T1

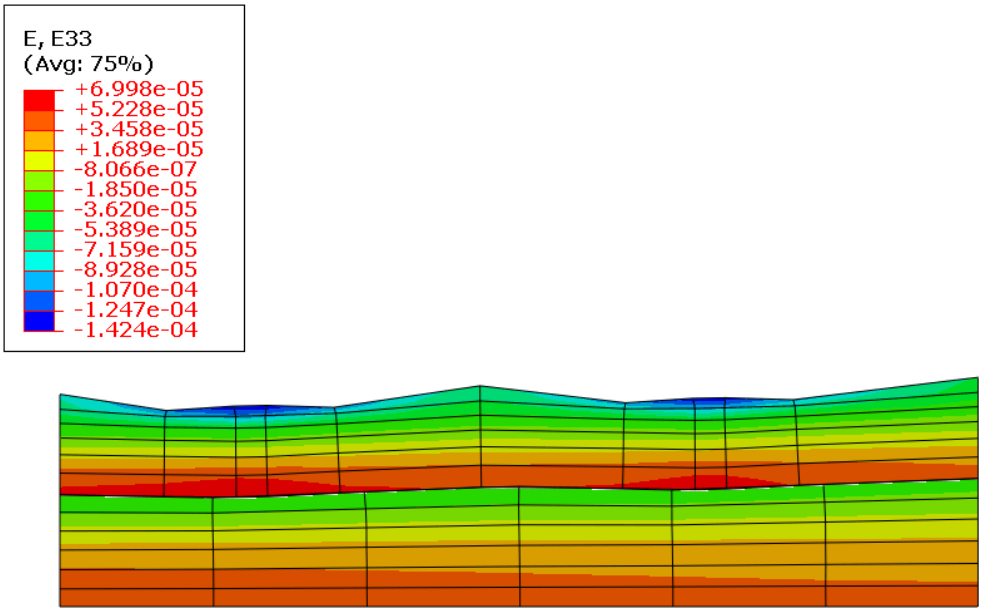

Figure 6.43 Longitudinal strains for section T2

www.manaraa.com

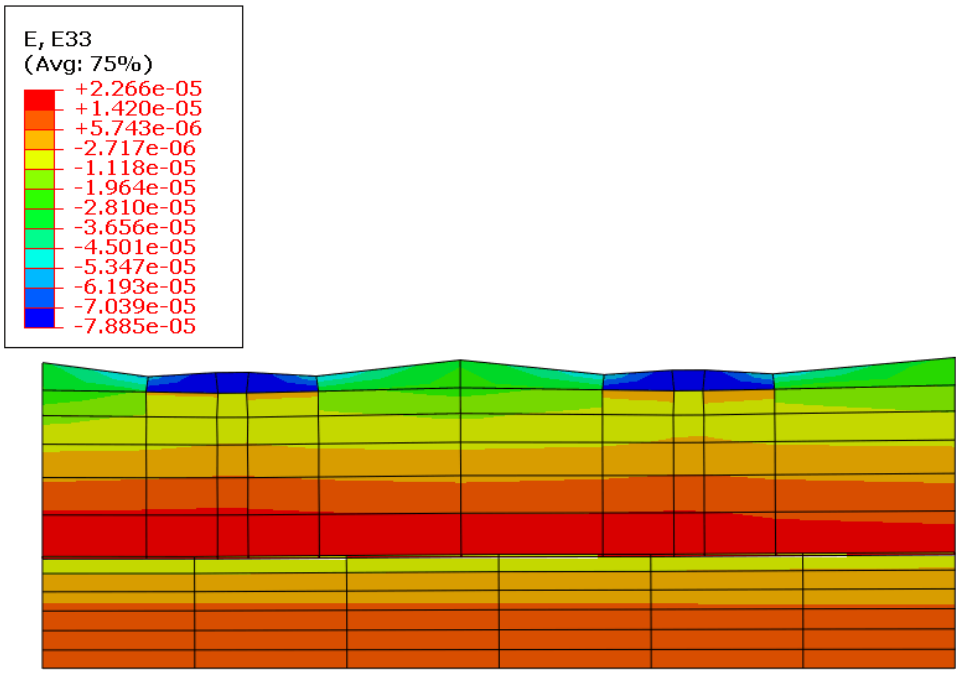

Figure 6.44 Longitudinal strains for section T3

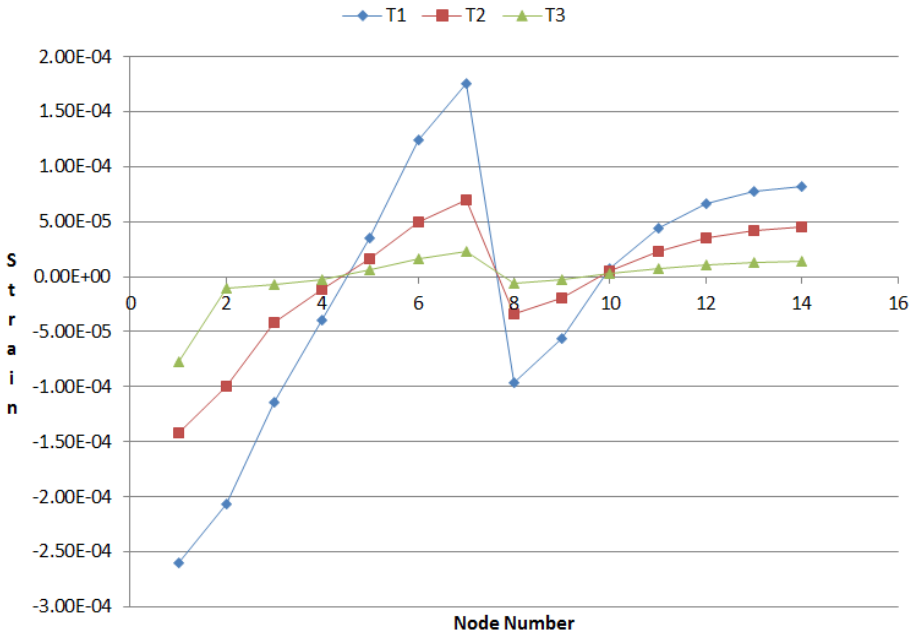

Figure 6.45 The longitudinal strain distribution with depth of pavement (HMA layer and foundations) for T1, T2 and T3

(Node number 0 indicates the surface, 14 indicates the bottom)

www.manaraa.com

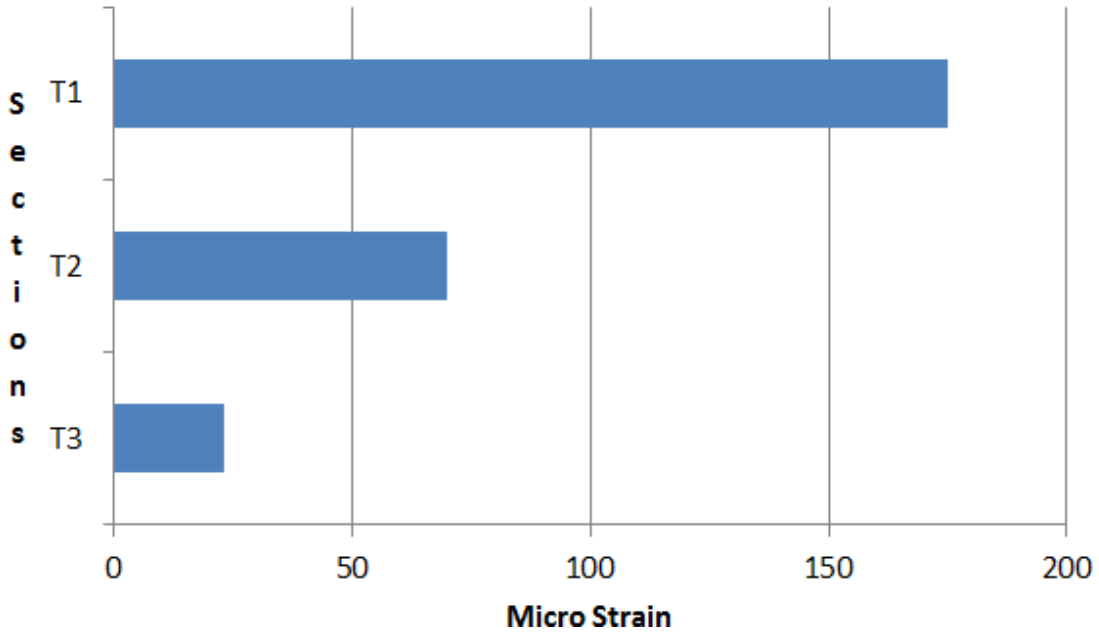

Figure 6.46 Longitudinal tensile strain at bottom of HMA layer for T1, T2 and T3

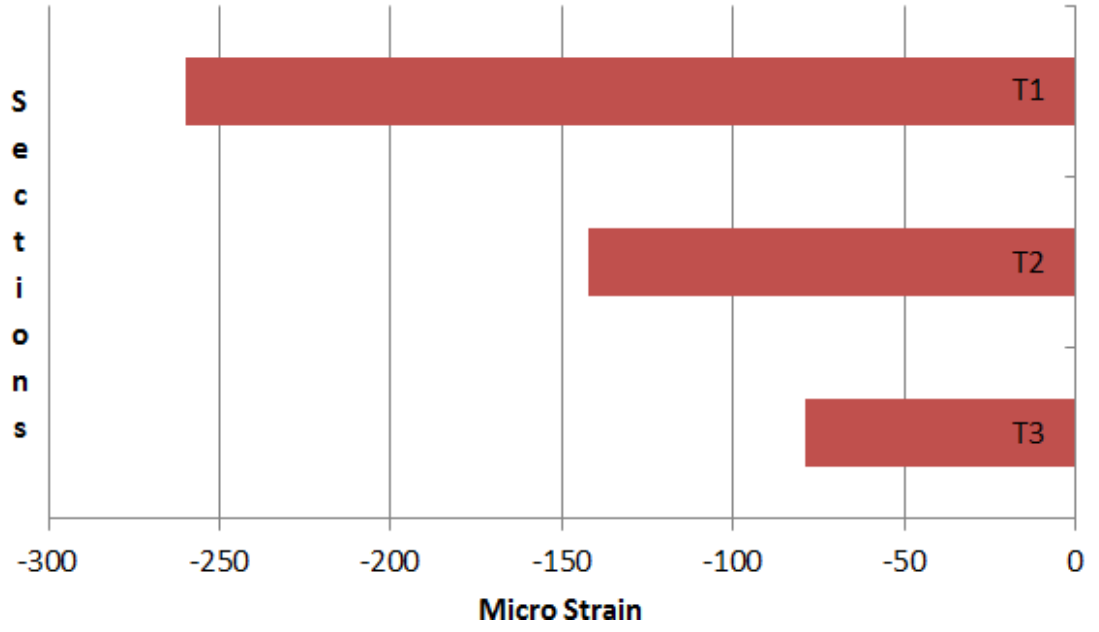

Figure 6.47 Longitudinal compressive strain at top of HMA layer for T1, T2 and T3

www.manaraa.com

At bottom, the longitudinal strain for sections T1 through T3 is 175, 70, 23 microstrain respectively. However, at top, the longitudinal strain for T1 through T3 is -260, -142, -79 microstrain respectively. (Figure 6.46 and Figure 6.47) Therefore, when the pavement thickness increases, the longitudinal strain at the bottom was greatly reduced but it was not reduced as significantly at top of the pavements. In Figure 6.48, it shows these characteristics. The lengths of the line segments represent the relative magnitude of strain values. While T3 is four times the thickness of T1, at bottom, the strain of T3 is almost 1/8 of the one of T1. Figure 6.49 shows a trend of reduction of strain with thickness (the top of pavements for thinnest section T1 is assigned a value of one, the other values are relative to this one.)

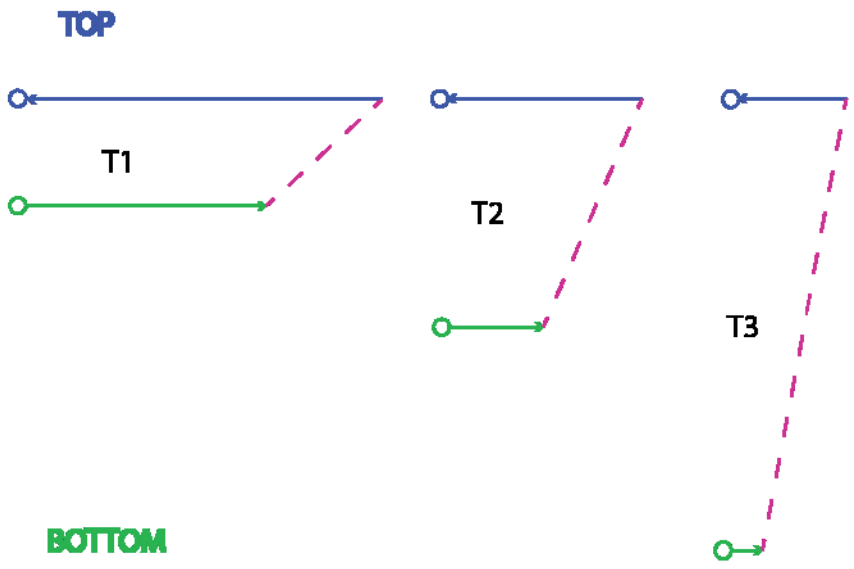

Figure 6.48 Pavement response (longitudinal strain) variation with thickness

www.manaraa.com

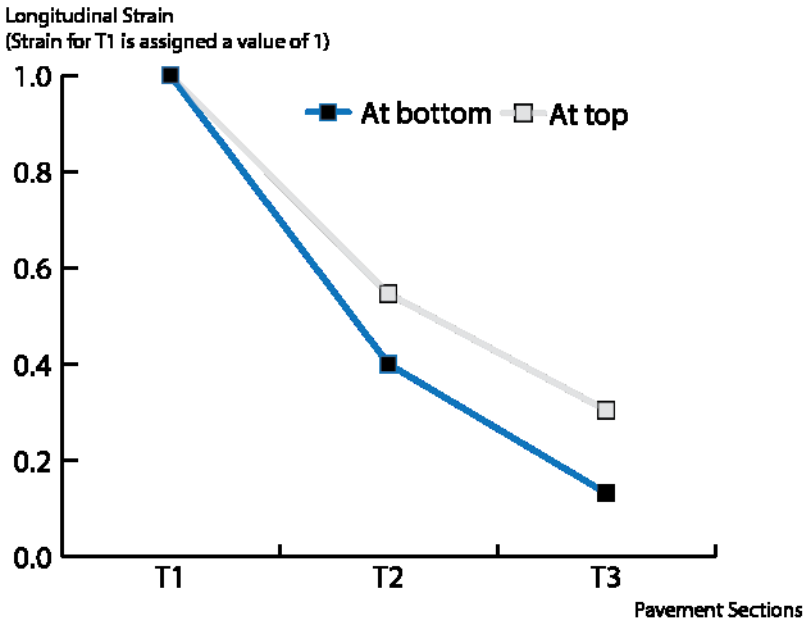

Figure 6.49 Relative strain reduction with thickness

At surface, the strain also decreases as the thickness increases, but to a lesser extent. Therefore, the absolute difference in longitudinal strain responses between the top and bottom of HMA layer is larger for thick pavements than for thin ones. For thick pavements, the top and bottom are all critical locations, but the top of pavements become more important as thickness increases. If we also consider the dynamic moving of wheels on pavements (Figure 6.50), the nature of repetitive application of compressive and tensile strain at surface could also result in severe fatigue cracking (top-down cracking). Previously, tensile strain at the bottom of pavements is the criteria. However, based on a dynamic point of view, it is proposed in this research that a maximum difference between compression and tension should be the governing criteria. It is worth noting that tension values are much smaller than compression values (<10% in this case, See Figure 6.13).

www.manaraa.com

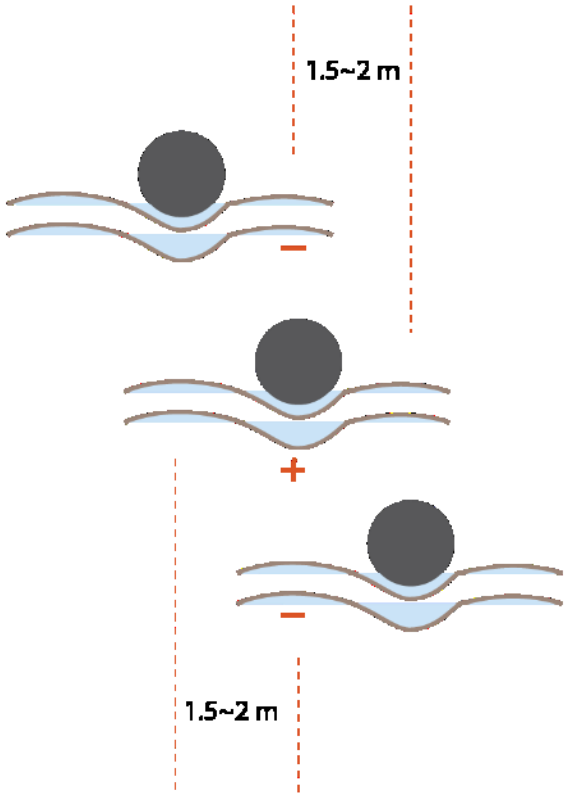

Figure 6.50 Illustration of the behavior of the pavement under dynamic loading

The vertical strain and stress for T1 is compared with thicker pavement T2 (N9). This can also provide insight into the effect of thickness on pavement responses. As discussed in section 6.2.6, the top of the pavements have relative large compressive strain values under the wheel. This also holds true for section T1. However, at the top of the subgrade, the gravitation-caused strain is about twenty-five percent of total gravitational and load induced train (150 compared to 600 microstrain). Since vertical strain at the top of the subgrade is considered to be related to pavement rutting, this comparison shed some lights on both strain and rutting. Gravitation-caused strain tends to play a more

www.manaraa.com

important role in thicker pavements. Also, the thicker pavement does NOT provide a better rutting resistance if the same material is used because strain is not reduced greatly.

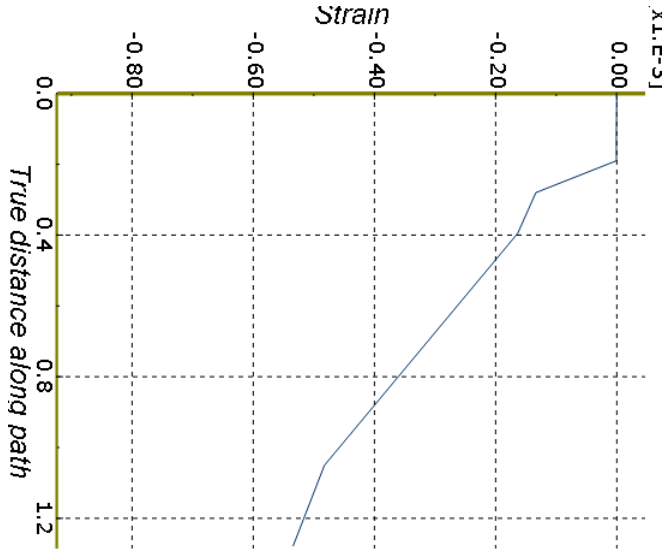

Figure 6.51 Vertical strain along the depth of pavement and foundation for T1. (Under gravitation only)

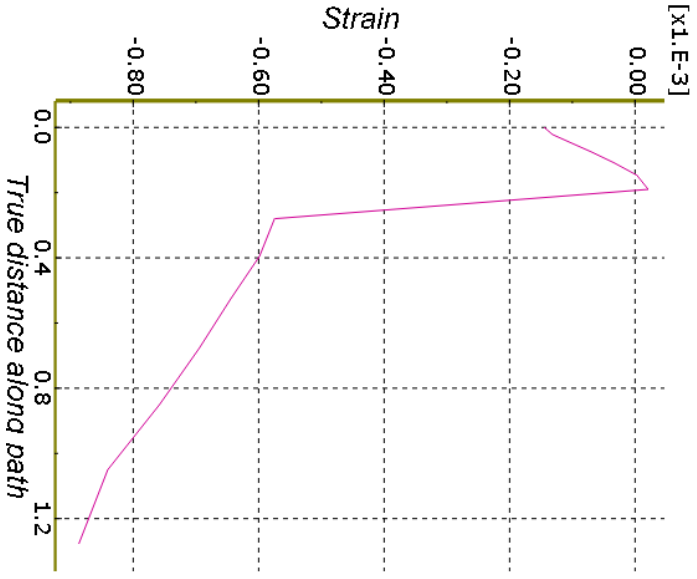

Figure 6.52 Vertical strain along the depth of pavement and foundation for T1. (Under gravitation and wheel loading)

www.manaraa.com

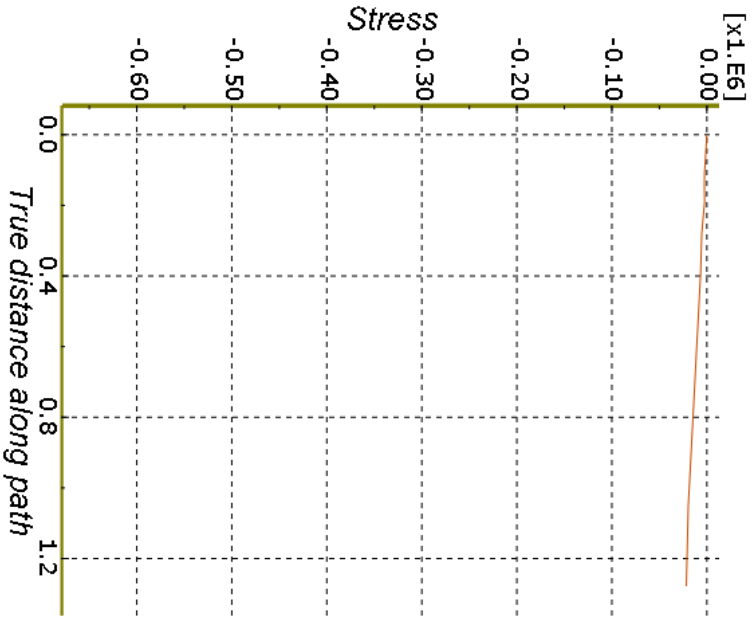

Figure 6.53 Vertical stress along the depth of pavement and foundation for T1. (Under gravitation only)

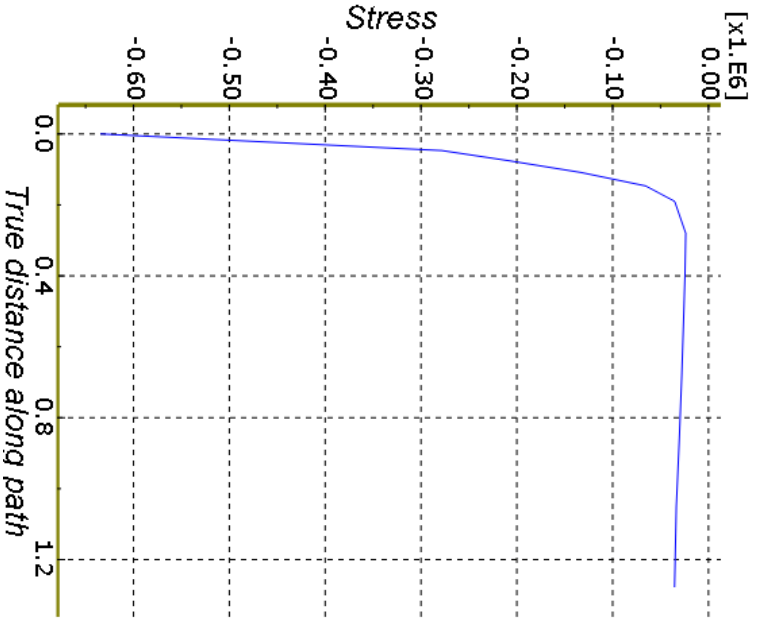

Figure 6.54 Vertical stress along the depth of pavement and foundation for T1. (Under gravitation and wheel loading)

www.manaraa.com

6.5 The Range of Influence by Wheel Loading

In this section, the longitudinal strain at the bottom of HMA layer in front of the loading is examined. In other words, we want to find out how the pavements are affected at different distances from the point of loading. It is found that the bottom of the HMA is subjected to tension underneath the load and to maximum compression at about 1 to 2 meters away from the load. However, the compression rapidly decreases after 2 meters (Figure 6.55). This implies that when simulating wheel loading, 3 meters is sufficient to capture the influence of wheel loading. This characteristic is in agreement with NCAT Test Track time history data (afternoon, winter of 2006) as shown in Figure 6.58.

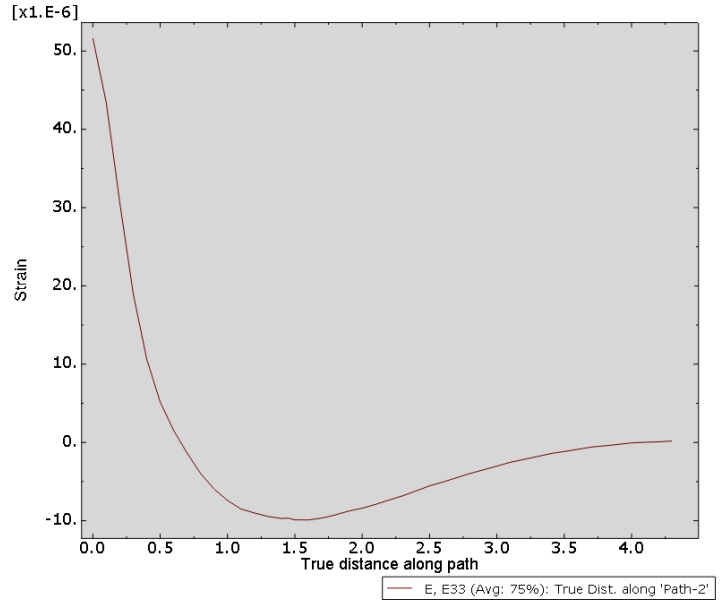

Figure 6.55 Extent of wheel load influence

www.manaraa.com

6.6 The Effect of Dynamic Loading

The sampling frequency of the strain gage at the NCAT test was 2000 Hz, which means the strain data is sampled every 0.0005 second. The strain data is used to evaluate possible moving load models. To be considered are the mesh dimensions, truck speed, wheel print dimensions, and longitudinal distance between axle loads (single axle trailer loads). A single, continuous loading step was considered first. With this approach, each mesh surface could be loaded sequentially for a time equal to 0.005 second with a certain phase shift. However, due to the vehicle speed, the loading time of a single element surface is quite short and the elements have no load the remainder of the time step. For this problem, if the total time is taken to be the time it takes the between the two single axles (5.3m) of a trailer, this means the load is applied for 0.005 second and is unloaded 0.255 second (51 times of loading time). If a small load increment is used to capture the transient loading effect, the model in Abaqus could run quite a long time.

Alternatively, the moving, dynamic loading is simulated with a set of discretized sequential loadings as shown in Figure 6.56.

www.manaraa.com

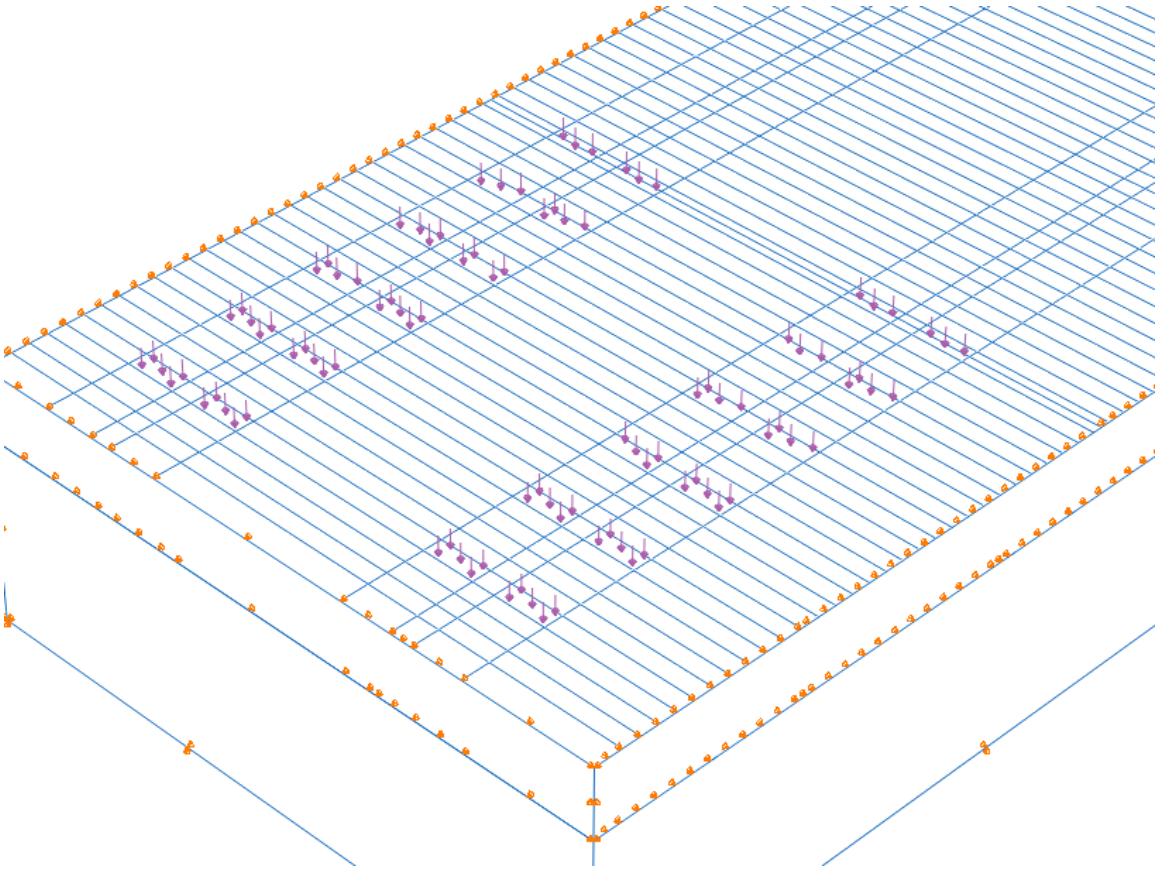

Figure 6.56 Sequential loadings of pavements

In this approach, several characteristic points are loaded. The time between these loadings is 0.025 second or an axle travel distance of 0.5m. The pavement response after these sequential loadings is shown in Figure 6.57. Compared with the experimental result from one winter afternoon (Figure 6.58), the FEM can capture the strain with a sufficient accuracy.

www.manaraa.com

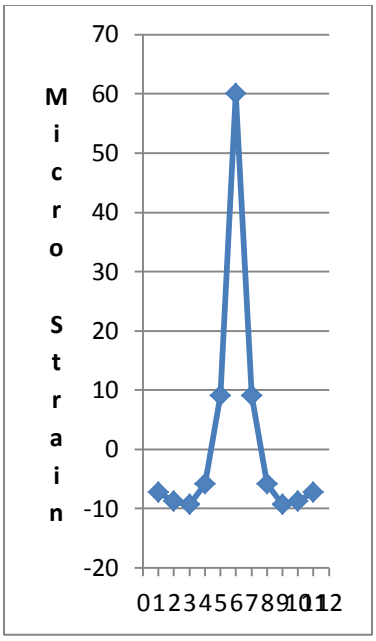

Figure 6.57 The result from theoretical analysis

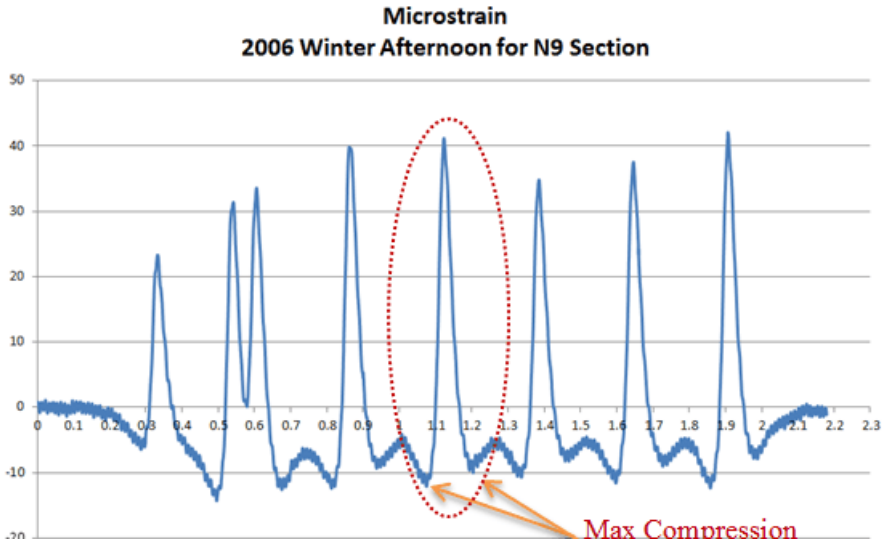

Figure 6.58 The NCAT Result

www.manaraa.com

6.7 The Effect of Temperature and Moisture

As discussed in 3.2.5, temperature and moisture could have a great effect on pavement material properties, hence affecting its response to loads. The modulus of HMA at a summer operating temperature of 140 F can be 90% of the one at 60-70 F. To account for this analysis, the modulus of HMA layer is reduced to 1/10 of the original value. To account for the effect of moisture change on the subgrade, the modulus of the soil subgrade is also reduced to 1/10 of the original value.

The results are shown in Figure 6.59 to Figure 6.64. The most obvious effect of temperature and moisture is that an increase of temperature or increase of moisture can cause an increase in the strain difference at the left and right wheel path of nearly 20% (In Figure 6.59 and Figure 6.62, the right edges of the figures correspond to the shoulder sides of real pavements). There are also significant increases in strain at both the top and bottom of pavements. However, there is no significant change predicted in the vertical stress distribution. This conforms to the theory that the stress distribution below a point load on soil surface is not affected by the material (See layered elastic theory and also Boussinesq's formula). Also, for a high moisture condition, at bottom of the pavement and in the vicinity of the wheel loading, the maximum compressive strain is further away from the loaded areas (the rapid decrease of maximum compressive strain is not seen in this case) (Figure 6.63). This implies that the wheeling load affects a larger area of the pavement at the high moisture condition. This effect is similar to the radius of relative stiffness of concrete pavements (Yoder and Witczak 1975). The FEA results also show

www.manaraa.com

that significant plastic strain was developed at the bottom of HMA layer and the top of the subgrade as shown in Figure 6.65.

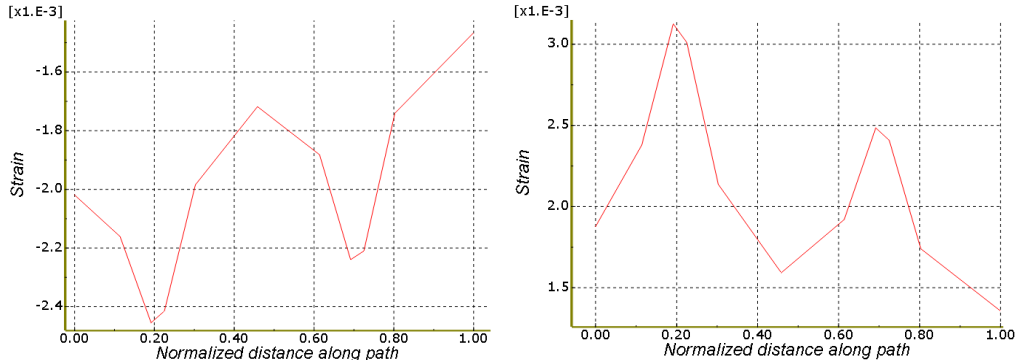

a) At top b) At bottom

Figure 6.59 The strain in transverse section of N9 during hot temperature

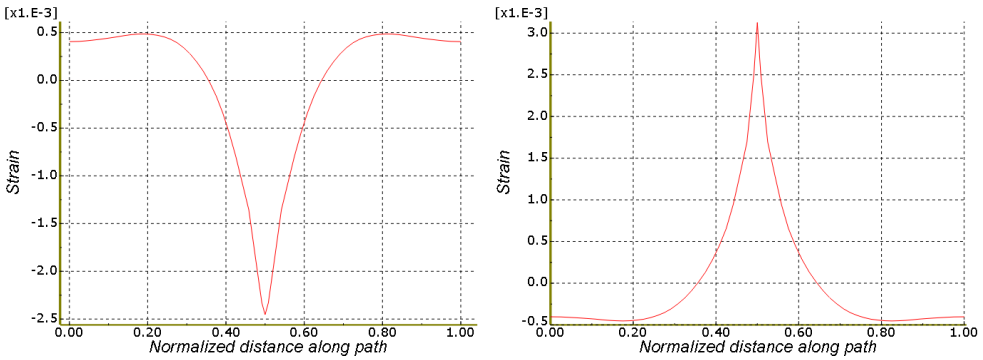

a) At top b) At bottom

Figure 6.60 The strain in longitudinal section of N9 during hot temperature

www.manaraa.com

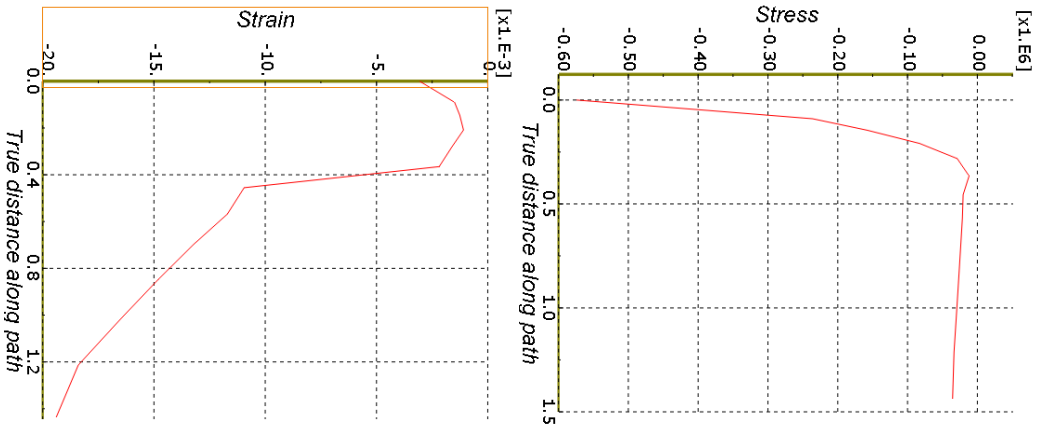

a) Vertical strain b) Vertical stress

Figure 6.61 Vertical strain and stress along depth of pavement of N9 during hot temperature

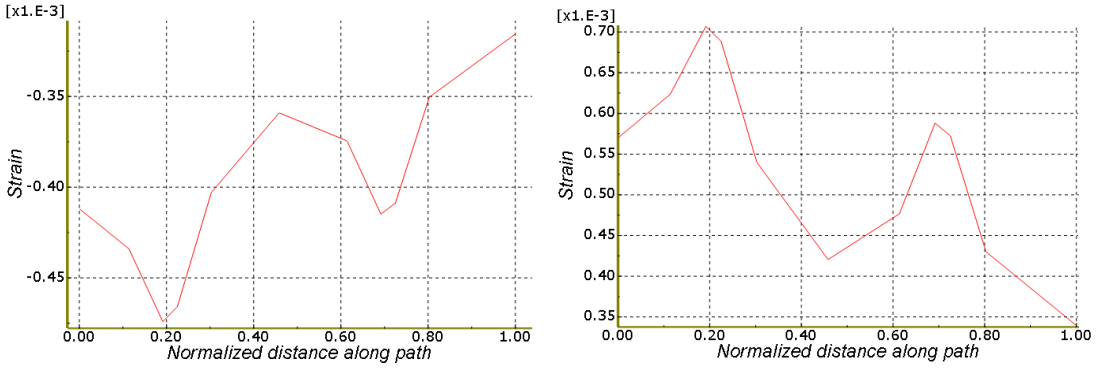

a) At top b) At bottom

Figure 6.62 The strain in transverse section of N9 during high moisture level

www.manaraa.com

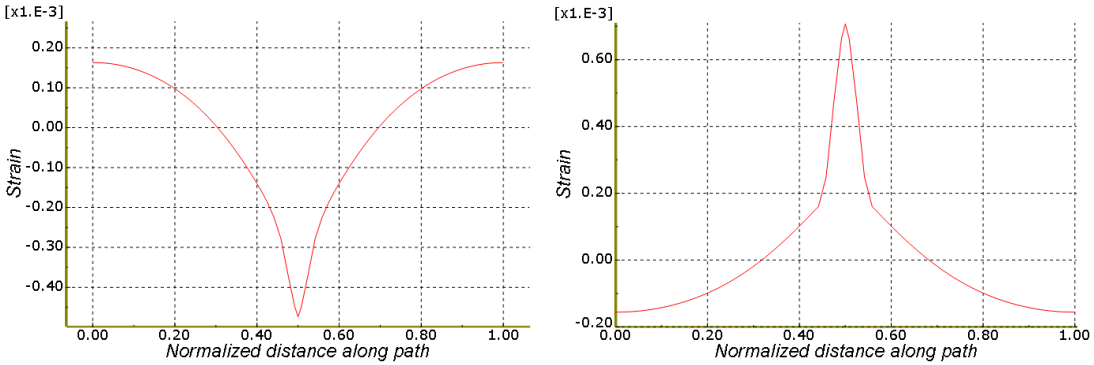

a) At top b) At bottom

Figure 6.63 The strain in longitudinal section of N9 during high moisture level

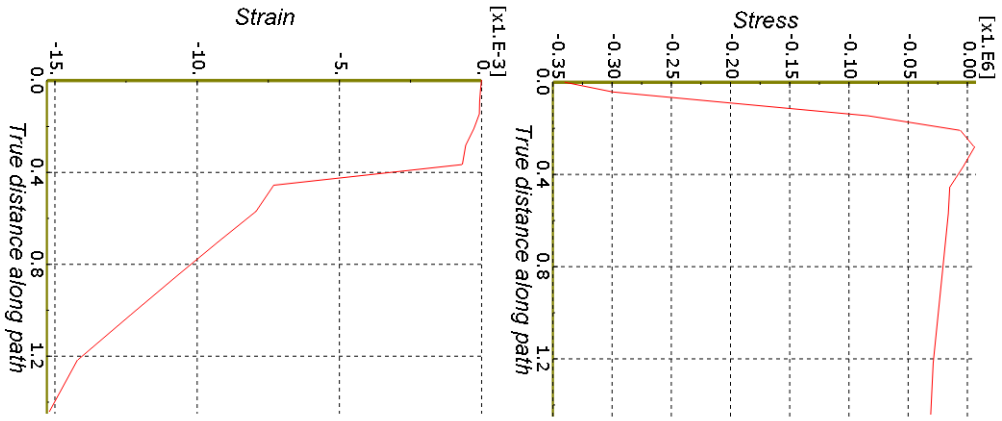

a) Vertical strain b) Vertical stress

Figure 6.64 Vertical strain and stress along depth of pavement of N9 during high moisture level

www.manaraa.com

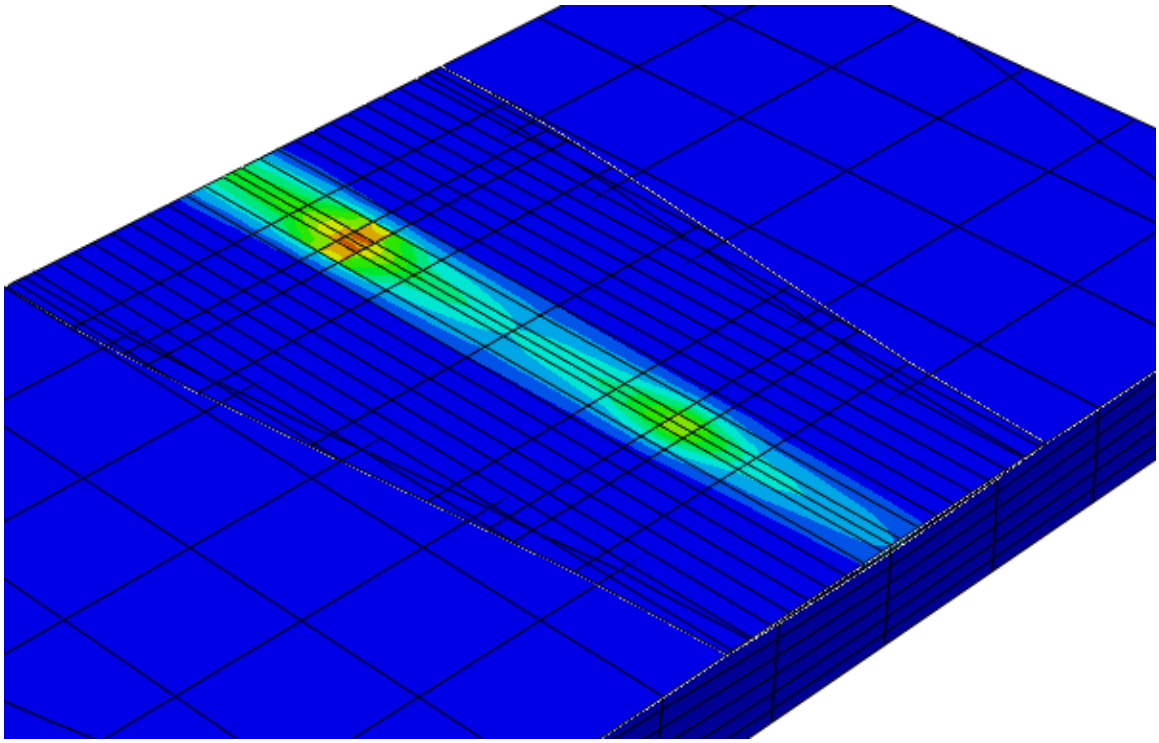

Figure 6.65 Plastic strain at the bottom of the HMA layer

www.manaraa.com

CHAPTER VII

CONCLUSIONS

7.1 Summary

In this dissertation, an analysis has been made of conventional and thicker perpetual HMA pavements. One of the motivations for this work is the unsatisfactory performance of conventional pavements with sub-drainage layers. Perpetual pavements, as the name suggests, are designed for long life. However, this is a relatively new concept and there are still many unknowns concerning responses and performance of this type of pavement. The goal of this work is to determine answers for some of the unknowns. Furthermore, it seeks to understand how and to what degree the perpetual pavements' deterioration and performance could be different from those of conventional pavements.

Instrumentation data from the National Center for Asphalt Technology (NCAT) Test Track study was obtained, analyzed and used as a basis to evaluate FE models. Computational models for both conventional and perpetual pavements were constructed and analyzed using the general purpose FEA software ABAQUS. Geometry, materials and loading are modeled with sufficient accuracy. This research examined several types of pavement responses, such as longitudinal strain, transverse strain, vertical strain and stress, and shear strain. It extends the traditional criteria of pavement distress by suggesting the longitudinal strain at the surface of pavement is an important criterion. Shear strain was studied in detail and provides a reasonable explanation of some distress

www.manaraa.com

in HMA pavements. By studying the FEA results from conventional and perpetual pavements and a thorough investigation of layer thickness, it provides a rationale on why the top of pavements should be a critical location to consider for thick pavements. The effect and range of influence of moving (dynamic) wheel loads are presented. Finally, the effect of environment, specifically temperature and moisture are studied.

The dissertation first summarizes the current development in the research of perpetual pavement testing and modeling. Analytical were combined with empirical concepts of pavement design in the 1990s. During this time, FEA was proven to accurately model pavement responses to moving loads as well as to capture performance (distress). Also, FEA has many advantages over the traditional layered elastic theoretical analysis. The FEA can represent the complex layered geometry and boundary conditions, materials properties, and moving, dynamic loads. In the next chapter, materials and mechanics background for HMA pavements are introduced.

Tests at the NCAT Test Track were studied. Data from two instrumented test sections were used to evaluate the FE models of the two sections, which represent a conventional pavement and a perpetual pavement. The model results show good agreement with the empirical data.

In Chapter 6, there are several findings from the FEA. In the current mechanistic-based design method, horizontal tensile strain at the bottom of HMA layers is used as a criterion to control HMA layers' structural performance. No direction is particularly noted. The layered elastic theory neglects the orientation of strain. This is expected because the semi-infinite space assumption in the theory does not differentiate orientation of structural responses. In the FEA results from this study, the magnitude of longitudinal

www.manaraa.com

strains is over three times the magnitude of the transverse strains. Also, in this particular study, strains in the inner wheel path are larger than the ones for outer wheel path.

The magnitude of longitudinal compressive strains at the surface (where the tires are in contact with the surface) is about two times as large as the magnitude of tensile strains at bottom of the HMA layers. From a dynamic point of view, the pavement surface is also subject to tension and compression repetitively. This work later proposes that a maximum difference between longitudinal compressive and tensile strain at surface could be used to as a criteria for top-down cracking to supplement the current "bottom tensile strain" criteria. A comparison was made of the longitudinal strains at both top and bottom of the pavement HMA layer. There is constant reversal of strain from tension to compression as a wheel passes a point on a pavement. At the surface, the strain in a bow wave in front of a wheel is tension, under the wheel is compression, and in a wake wave behind the wheel the strain is tension again. The strains at the bottom of the HMA layer are opposite of those at the top of the HMA layers.

One important feature of this study is the shear strain, which has not been studied before. Two types of shear strain, i.e., longi-shear strain and trans-shear strain, and their magnitudes could be of potential values to the future studies on pavement performance.

The study of pavement thickness provides a rationale on why the top of pavements should be a critical location to consider for thick pavements.

Moving wheel in the vicinity of the point of loading causes tension at the bottom of the HMA layer. The material is subjected to maximum compression 1 to 2 meters away from the loading. However, the compression rapidly decreases 2 to 3 meters away. This suggests that three meters is sufficient to capture the influence of wheel loading.

www.manaraa.com

Finally, moving, dynamic loading modeled by a discrete, sequential load model captured the strain pattern in the NCAT study.

With high temperature and high moisture, the difference in strain between the two wheel paths is nearly 20%. There are significant increases in strain at both top and bottom of pavements. However, no significant change in vertical stress distribution is observed. Also, under the severe environment, significant plastic strain develops at the bottom of pavement HMA layer and the top of subgrade, which could be a major contribution to pavement rutting.

7.2 Future Work

7.2.1 Field-Based Strain Measurement

Several highway agencies have built long-life pavements (I-90 in Washington, I-80 in Iowa, and Kansas Turnpike). However, research is still going on to identify a fatigue threshold for such pavements. Questions related to establishing the fatigue threshold are:

- What are the dominating surface distresses?
- Did "top-down cracking" happen or not?
- How severe was the top-down cracking if it happened?

The current research indicates the strain distribution for thick pavements is different from thin ones. However, more empirical evidence on critical locations needs to be gathered.

The current strain threshold criteria, 70 microstrain in tension at the bottom of the asphalt layer for fatigue cracking, is from laboratory fatigue tests. This strain threshold criterion may not represent actual field performance of flexible conventional pavements.

www.manaraa.com

Furthermore, different strain thresholds could exist for different types of HMA. This should be investigated further.

7.2.2 Material Characterization and Modeling

Material characterization for HMA and soil in the current pavement engineering practice is still largely for the AASHTO empirical guide. More and comprehensive mechanistic parameters are needed to characterize the properties of geo-materials used in pavements. This could enhance pavement analytical design. Moreover, this work includes very detailed modeling and analysis. To speed up and standardize the experiments for all type of pavements, the mesh numbers for all the thickness of HMA layers in this research were the same. This would definitely cause some error for analysis in thick pavement due to the relative large size of elements at the pavement surface. The future work can refine the mesh sizes to achieve better results.

7.2.3 Reliability

Reliability was introduced to the AASHTO pavement design to account for variability in traffic, materials, environment etc. The reliability method used in AASHTO is based on an empirical design equation and did not consider the concept of perpetual pavements and their possible different distress modes. The potential modes of failure for perpetual pavements should be viewed as a different limit state. The "perpetual and endurance" nature of the pavements deserve a different level of reliability.

www.manaraa.com

REFERENCES

AASHTO. *AASHTO interim guide for design of pavement structures.* Washington, DC: AASHTO, 1972.

Abaqus. *Abaqus 6.9 Analysis User's Manual.* Providence: Dassault System, 2009.

—. *Abaqus Scripting User's Manual.* Providence, RI: Dessault Systemes, 2011.

Ahlvin, Richard. *Origin of developments for structural design of pavements.* Washington, DC: US Army Corps of Engineers, 1991.

Al-Qadi, I L, M Elseifi, and P J Yoo. "In-situ validation of mechanistic pavement finite element modeling." *2nd International Conference on Accelerated Pavement Testing.* Minneapolis, Minnesota, USA, 2004.

APA. *Perpetual pavements: a synthesis.* Lanham, MD: Ashpalt pavement alliance, 2002.

APM. 2012. http://writersalmanac.publicradio.org/index.php?date=2012/06/29.

Asphalt Institute. *Research and development of the asphalt institute's thickness design manual (MS-1) 9th edition.* Lexington, Kentucky: Asphalt Institute, 1982.

Bellis, M. 2013. http://inventors.about.com/od/rstartinventions/a/History-Of-Roads.htm.

Brown, J. "Rocky Road: the story of asphalt pavement." May 2013: 40-43.

Carpenter, S, K Ghuzlan, and S Shen. "A fatigue endurance limit for highway and airport pavements." *Transportation Research Record*, 2003: 131-138.

Das, BM. *Advanced Soil Mechanics.* New York City: Taylor & Francis, 2008.

Dauzats, M, and R Linder. "A method for the evaluation of the structural condition of pavements with thick bituminous road bases." *5th International Conference on the Structural Design of Asphalt Pavements.* Delft, 1982.

de Lille, Alain. *Liber Parabolarum.* 1175.

Desai, CS. *Constitutive laws for engineering materials with emphsis on geologic materials.* Englewood Cliffs, NJ: Prentice-Hall, 1984.

www.manaraa.com

Dunne, F, and N Petrinic. *Introduction to computational plasticity.* New York: Oxford University Press, 2005.

El-Basyouny, M, and M Witczak. "Development of the fatigue crakcing models for the 2002 Design Guide." *TRB.* Washington, DC, 2005.

Fan, S, and CC Kang. *Road Development, Economic Growth, and Poverty Reduction in China.* Washington, DC: International Food Policy Research Institute, 2005.

Ferne, B. "Long-life pavements-a European study by ELLPAG." *International Journal of Pavement Engineering*, 2006: 91-100.

FHWA. 2011. http://www.fhwa.dot.gov/infrastructure/50aasho.cfm.

Galal, K, TD White, and AJ Hand. *Second phase study of changes in in-service asphalt.* West Lafayette, Indiana: IDOT and Purdue Univeristy, 2000.

Grandin, H. *Fundamentals of the finite element method.* NYC: Macmillan, 1986.

Grattan-Guinness, I. *Convolutions in French Mathematics, 1800-1840.* Berlin: Berkhauser Verlag Basel, 1990.

Gudehus, G. *Physical soil mechanics.* Berlin: Springer, 2011.

Haas, R. "Reinventing the pavement management wheel." *5th International Conference On Managing Pavements.* Seattle, 2001.

Helwany, S. *Applied soil mechanics with Abaqus Applications.* Hoboken, NJ: John Wiley & Sons, 2007.

Heukelom, W, and A Klomp. "Dynamic testing as a means of controlling pavements during and after construction." *International Conference on the Structural Design of Asphalt Pavements.* 1962. 667-685.

Hoppen, K. *East meets west.* New York: Rizzoli International, INC, 1997.

Hrennikoff, A. "A solution of problems in elasticity by the framework method." *Journal of applied mechanics*, 1941: 169-175.

Hua, JF. *Finite element modeling and analysis of accelerated pavement testing devices and rutting phenomenon.* Purdue University: PhD Thesis, 2000.

I-37A. *Guide for Mechanistic-Empirical Design.* Washington, DC: NCHRP, 2004.

Imperial. 2012. http://www.britannica.com/EBchecked/topic/283915/Imperial-Highway. (accessed 1 5, 2012).

www.manaraa.com

Kassem, E, Z Grasley, and E Masad. "Viscoelastic Poisson's Ratio of Asphalt Mixtures." *Int. J. Geomech.*, 2013.

Lai, JS, and D Anderson. "Irrecoverable and recoverable nonlinear viscoelatic properties of asphatl concrete." *Transporation Research Record* (TRB), 1973: 73-88.

Lambert, L. 2012. http://www.reuters.com/article/2012/03/26/usa-cities-population-idUSL2E8EQ5AJ20120326.

Lay, MG. *Ways of the world.* New Brunswick, NJ: Rutgers Universtiy Press, 1992.

Local. *Guide for the Local Calibration of the MEPDG.* Washington, DC: AASHTO, 2010.

Maher, A, and B Thomas. *Evaluation of Poisson's Ratio for Use in the Mechanistic Empirical Pavement Design Guide.* Washington, DC: FHWA, 2008.

Mamlouk, M, and J Zaniewski. *Materials for civil and construction engineers.* Menlo Park, CA: Addison Wesley, 1999.

MEPDG. *Mechanistic-Empirical Pavement Design Guide, A Maual of Practice.* Washinton, DC: AASHTO, 2008.

Miravete, EG. *Classical and Computational Solid Mechanics for Materials Engineers.* 2005. http://www.ewp.rpi.edu/hartford/~ernesto/F2005/CINVESTAV/.

Nunn, M, A Brown, D Weston, and J Nicholls. *Design of Long-life flexible pavements for heavy traffic.* Crowthorne, UK: TRL Report 250, 1997.

Perl, M, J Uzan, and A Sides. "Visco-Elasto-Platic Constitutive law for a bituminous mixture under repeated loading." *Transportation Research Record 911*, 1983: 21-27.

Peterson, R, P Turner, M Anderson, and M Buncher. "Determination of threshold strain level for fatigue endurance limit in asphalt mixtures." *International symposium on design and constrution of long lasting pavements.* Auburn, AL, 2004.

Pronk, A, and R Buiter. "Aspects of the interpretation and evaluation of falling weight deflection measurements." *5th International Conference on the Structural Design of Asphalt Pavements.* Delft, 1982.

Prowell, B, R Brown, M Anderson, and etc. *Validating the fatigue endurance limit for hot mix asphalt.* Washington, DC: NCHRP 646, 2010.

Rao Tangella, S, J Craus, J Deacon, and C Monismith. *Summary report on fatigue response of asphalt mixtures.* Washington, DC: SHRP, National Research Council, 1990.

www.manaraa.com

Reddy, J. *An introduction to the finite element method.* New York: Mc Graw-Hill, 2006.

Schwartz, C, and R Carvalho. *Implementation of the NCHRP I-37A Design Guide Volume 2.* Lutherville, MD: Maryland State Highway Administration, 2007.

Strauss, P, V Servas, and J Marais. "Unexpected surface cracking of asphalt wearing courses." *4th Conference on Asphalt Pavements for Southern Africa.* Cape Town, 1984.

Tan, SA, BH Low, and TF Fwa. "Behavior of Asphalt Concrete Mixtures in Triaxial Compression." *Journal of Testing and Evaluation*, 1994.

Taylor, A, and D Timm. *Mechanistic characterization of resilient moduli for unbound pavement layer materials.* Auburn, AL: NCAT 09-06, 2009.

Terzaghi, K. *Theoretical soil mechanics.* New York: John Wiley and Sons, 1943.

Timm, D. *Design, construction and instrumentation of the 2006 test track structural study.* Auburn, AL: NCAT 09-01, 2009.

Timm, D, A Priest, and T McEwen. "Design and instrumentation of the structural pavement experiment at the NCAT Test Track." n.d.

Timm, D, and D Newcomb. "Perpetual pavement design for flexible pavements in the US." *International Journal of Pavement Engineering*, 2006: 111-119.

TXDOT. 2013. http://onlinemanuals.txdot.gov/txdotmanuals/pdm/hot_mix_asphalt_concrete_pavement_mixtures.htm.

Ullidtz, P. "Analytical Tools for Design of Flexible Pavements." *8th ISAP Conference.* Copenhagen: Technical University of Denmark, 2002.

WAPA. 2010. http://www.asphaltwa.com/2010/09/18/welcome-facts/.

Westergaard, H. *Theory of Elasticity and Plasticity.* Boston: Harvard University Press, 1952.

Westrack. 1999. http://www.westrack.com/wt_02.htm.

Willis, JR, and D Timm. *Field-based strain thresholds for flexible perpetual pavement design.* Auburn, AL: NCAT 09-09, 2009.

Willis, JR, D Timm, R West, and B Powell. *Phase III NCAT Test Track findings.* Auburn, AL: NCAT 09-08, 2009.

Wilson, M. 2012. http://www.fastcodesign.com/1669244/by-2050-70-of-the-worlds-population-will-be-urban-is-that-a-good-thing.

www.manaraa.com

Yoder, E, and M Witczak. *Principles of Pavement Design.* New York: John Wiley & Sons, Inc, 1975.

Young, J, S Mindess, R Gray, and A Bentur. *The science and technology of civil engineering materials.* Upper Saddle River, NJ: Prentice-Hall, 1998.

Zaghloul, SM. *Non-linear dynamic analysis of flexible and rigid pavements.* Purdue University: PhD Thesis, 1993.

www.manaraa.com

APPENDIX A

PYTHON SCRIPT

www.manaraa.com

Script for opening .odb files:

```
from abaqus import *
from abaqusConstants import *
session.Viewport(name='Viewport: 1', origin=(0.0, 0.0),
width=248.600006103516,
    height=196.3642578125)
session.viewports['Viewport: 1'].makeCurrent()
session.viewports['Viewport: 1'].maximize()
from viewerModules import *
from driverUtils import executeOnCaeStartup
executeOnCaeStartup()
     o2 = session.openOdb(name='a.odb')
```

Script for creating path for the longitudinal direction:

```
session.viewports['Viewport: 1'].setValues(displayedObject=o2)
session.viewports['Viewport:
1'].view.setProjection(projection=PERSPECTIVE)
session.viewports['Viewport:
1'].odbDisplay.setValues(viewCutNames=('X-Plane',
    ), viewCut=ON)
session.viewports['Viewport: 1'].odbDisplay.viewCuts['X-
Plane'].setValues(
    position=3.85)
session.Path(name='Path-1', type=NODE_LIST,
expression=(('ASPHALT-1', (
    '4689:4029:-11', )), ))
session.Path(name='Path-2', type=NODE_LIST,
expression=(('ASPHALT-1', (
         '663:3:-11', )), ))
```

Script for creating path for the transverse direction:

```
session.viewports['Viewport: 1'].setValues(displayedObject=o2)
session.viewports['Viewport:
1'].view.setProjection(projection=PERSPECTIVE)
session.viewports['Viewport:
1'].odbDisplay.setValues(viewCutNames=('Z-Plane',
    ), viewCut=ON)
session.Path(name='Path-1', type=NODE_LIST,
expression=(('ASPHALT-1', (
    '4357:4367:1', )), ))
session.Path(name='Path-2', type=NODE_LIST,
expression=(('ASPHALT-1', (
         '331:341:1', )), ))
```


www.manaraa.com

Script for plotting strain at a point:

```
session.viewports['Viewport: 1'].setValues(displayedObject=o2)
odbName=session.viewports[session.currentViewportName].odbDisplay
.name
session.odbData[odbName].setValues(activeFrames=(('Wheel', ('0:-
1', )), ))
odb = session.odbs['E:/O/O1-Research/Abaqus Files/6.2-
Perpetual/RPY/a.odb']
xyList = xyPlot.xyDataListFromField(odb=odb,
outputPosition=NODAL, variable=((
    'E', INTEGRATION_POINT, ((COMPONENT, 'E33'), )), ),
nodeLabels=((
    'ASPHALT-1', ('333', )), ))
xyp = session.XYPlot('XYPlot-1')
chartName = xyp.charts.keys()[0]
chart = xyp.charts[chartName]
curveList = session.curveSet(xyData=xyList)
chart.setValues(curvesToPlot=curveList)
     session.viewports['Viewport:

1'].setValues(displayedObject=xyp)
```

Script for plotting strain curve along a path:

```
session.viewports['Viewport: 1'].setValues(displayedObject=o2)
session.viewports['Viewport:
1'].view.setProjection(projection=PERSPECTIVE)
session.Path(name='Path-1', type=NODE_LIST,
expression=(('ASPHALT-1', (
    '663:3:-11', )), ))
session.viewports['Viewport: 1'].odbDisplay.setPrimaryVariable(
    variableLabel='E', outputPosition=INTEGRATION_POINT,
refinement=(COMPONENT,
    'E33'))
xyp = session.XYPlot('XYPlot-1')
chartName = xyp.charts.keys()[0]
chart = xyp.charts[chartName]
pth = session.paths['Path-1']
xy1 = xyPlot.XYDataFromPath(path=pth, includeIntersections=False,
    shape=DEFORMED, labelType=NORM_DISTANCE)
c1 = session.Curve(xyData=xy1)
chart.setValues(curvesToPlot=(c1, ), )
session.viewports['Viewport: 1'].setValues(displayedObject=xyp)
```

Script for plotting strain contour at a section:

```
session.viewports['Viewport: 1'].setValues(displayedObject=o2)
session.viewports['Viewport: 1'].odbDisplay.viewCuts['Z-
Plane'].setValues(
```


www.manaraa.com

```
    showModelBelowCut=False)
session.viewports['Viewport:
1'].odbDisplay.setValues(viewCutNames=('Z-Plane',
    ), viewCut=ON)
session.viewports['Viewport:
1'].odbDisplay.display.setValues(plotState=(
    CONTOURS_ON_DEF, ))
session.viewports['Viewport:
1'].view.setValues(session.views['Front'])
session.viewports['Viewport:
1'].view.setValues(cameraPosition=(4.96, 0.617992,
    13.4828), cameraTarget=(4.96, 0.617992, 3))
session.viewports['Viewport: 1'].odbDisplay.setPrimaryVariable(
    variableLabel='E', outputPosition=INTEGRATION_POINT,
refinement=(COMPONENT,
          'E33'), )
```

Script for plotting multiple strain curves at a point:

```
session.viewports['Viewport: 1'].setValues(displayedObject=o2)
odbName=session.viewports[session.currentViewportName].odbDisplay
.name
session.odbData[odbName].setValues(activeFrames=(('Wheel', ('0:-
1', )), ))
odb = session.odbs['E:/O/O1-Research/Abaqus Files/6.2-
Perpetual/RPY/a.odb']
xyList = xyPlot.xyDataListFromField(odb=odb,
outputPosition=NODAL, variable=(('E', INTEGRATION_POINT,
((COMPONENT, 'E11'), (COMPONENT, 'E22'), (COMPONENT, 'E33'), )),
), nodeLabels=(('ASPHALT-1', ('333', )), ))
xyp = session.XYPlot('XYPlot-1')
chartName = xyp.charts.keys()[0]
chart = xyp.charts[chartName]
curveList = session.curveSet(xyData=xyList)
chart.setValues(curvesToPlot=curveList)
session.viewports['Viewport:1'].setValues(displayedObject=xyp)
```


www.manaraa.com

APPENDIX B

ABAQUS COMMAND AND PARAMETERS

www.manaraa.com

Directory under windows dos environment:

cd /d Drive:\Directory

PREPROCESSING:

Abaqus cae=a.cae

ANALYSIS:

Abaqus job=a input= "a.inp"

POSTPROCESSING:

1. Change the filename of .odb so that the content of .rpy file corresponds to the current .odb file.
2. Abaqus viewer database=a.odb

Abaqus viewer replay=pathVertical.rpy

The .odb file is the binary output file that will be read during post-processing to view graphical results.

Viewcut position:

Transverse cut in the middle: 3

Longitudinal cut in the left wheel path:

for T1, T2 (N9), T3: 3.16+0.69-0.01=3.84

for N1: 7.12+0.69-0.01=7.80

www.manaraa.com

Nodes number along vertical lines:

Asphalt layers: 4359:333:-671

Bottom of asphalt layer: 333

Sugrade: 119:113:-1

Top of subgrade: 119

Nodes numbers for asphalt layers along horizontal lines:

Transverse section, top: 4357:4367:1

Transverse section, bot: 331:341:1

Longitudinal section, top: 4689:4029:-11

Longitudinal section, bot: 663:3:-11

Interpretation of shear strain or shear stress:

E12: first 1 means the shear is @ plane X, 2 means its direction is Y.

E32: first 3 means the shear is @ plane Z, 2 means its direction is Y.

The first is better displayed at the transverse section in this thesis.

www.manaraa.com